“La utopía está en el horizonte.
Camino dos pasos, ella se aleja dos pasos
y el horizonte se corre diez pasos más allá.
¿Entonces para qué sirve la utopía?
Para eso, sirve para caminar.”

Eduardo Galeano

Dedicated to my beloved mother and the memory of my grandfather.

Generation of *in vitro* and *in vivo* models to study pain perception disorders using genome editing

Dissertation

zur Erlangung des akademischen Grades
doctor rerum naturalium (Dr. rer. nat.)

vorgelegt dem Rat der Medizinischen Fakultät
der Friedrich-Schiller-Universität Jena

Lic. Cecilia Soledad Tomni
Born the 11th of May, 1987 in Buenos Aires, Argentina

Gutachter:

1. PD Dr. Ingo Kurth, Aachen
2. Prof. Dr. Aria Baniahmad, Jena
3. Frau Prof. Dr. Angelika Lampert, Aachen

Tag der öffentlichen Verteidigung: 06.02.2018

Table of contents

List of Abbreviations

→	leading to
/	or
+n bp	Insertion of n (number) base pairs
>	nucleotide substitution
Δn bp	deletion of n (number) base pairs
♀	female
♂	male
Akt	protein kinase B
ANOVA	analysis of variance
bp	base pairs
BSA	bovine serum albumin
Cas	CRISPR-associated protein
Cas9	CRISPR-associated protein 9
Cascade	CRISPR-associated complex for antiviral defence
cDNA	complementary cDNA
CIPA	congenital insensitivity to pain with anhidrosis
CMV	cytomegalovirus
CNS	central nervous system
Cpf1	CRISPR from Prevotella and Francisella 1
CRISPR	Clustered Regularly Interspaced Short Palindromic Repeats
crRNA	CRISPR RNA
Cys	cysteine
DAPI	4',6-diamidino-2-phenylindole
DKO	double-knockout
DMEM	Dulbecco´s modified Eagle´s medium
DMSO	dimethyl sulfoxide
DNA	deoxyribonucleic acid
DPBS	Dulbecco's phosphate-buffered saline
DRG	dorsal root ganglion

DSB	double-strand-break
dsDNA	double-stranded DNA
ECL	enhanced chemiluminescence
ER	endoplasmic reticulum
ERK	extracellular signal-regulated kinase
ES	embryonic stem
Ex	exon
FACS	fluorescence-activated cell sorting
FBS	fetal bovine serum
fwr	forward
Gapdh	glyceraldehyde 3-phosphate dehydrogenase
GFP	green fluorescent protein
gRNA	guide RNA
HA	hemagglutinin
HDR	homology-directed repair
HFHR	high-fidelity homologous recombination
HGMD	Human Gene Mutation Database
HM	homozygous
HR	homologous recombination
HS	horse serum
HSAN	hereditary sensory and autonomic neuropathy
HSAN-IV	hereditary sensory and autonomic neuropathy type four
hSpCas9	humanised *Streptococcus pyogenes* CRISPR-associated protein 9
IF	immunofluorescence
Ig1	immunoglobulin 1
Ig2	immunoglobulin 2
IVT	in vitro transcription
JM	juxtamembrane
kDa	kilodaltons
KO	knockout
LRR	leucine reach repeat

M	molecular weight marker
MAPK	mitogen-activated protein kinase
mc	monoclonal
MEK	mitogen-activated protein kinase kinase
MGEs	mobile genetic elements
mTORC	mechanistic target of rapamycin
myc	myc proto-oncogene protein
n	number
Na_V	sodium channel
NCBI	National Center for Biotechnology Information
NGF	nerve growth factor
NGS	next-generation sequencing
NHEJ	non-homologous end-joining
NLS	nuclear localisation sequence
NmeCas9	*Neisseria meningitidis* CRISPR-associated protein 9
nt	nucleotides
NTRK1	Neurotrophic Tyrosine Receptor Kinase type one/ High-Affinity Nerve Growth Factor Receptor
OMIM	Online Mendelian Inheritance in Man
OT	off-target
$p75^{NTR}$	low-affinity nerve growth factor receptor
PAGE	polyacrylamide gel electrophoresis
PAM	protospacer adjacent motif
PBS	phosphate-buffered saline
pc	poyclonal
PCR	polymerase chain reaction
PFA	paraformaldehyde
PI3K	phosphatidylinositol 3-kinase
PKC	protein kinase C
PLC-γ	phospholipase Cγ
PLL	poly-L-lysine

PM	plasma membrane
PNS	peripheral nervous system
pre-crRNA	crRNA precursors
qPCR	quantitative real-time polymerase chain reaction
RAF	rapidly accelerated fibrosarcoma
Rap1	repressor activator protein
RAS	rat sarcoma
RefSeq	reference sequence
rev	reverse
RNA	ribonucleic acid
RT	room temperature
SCN10A	sodium voltage-gated channel alpha subunit 10
SCN11A	sodium voltage-gated channel alpha subunit 11
SCN9A	sodium voltage-gated channel alpha subunit 9
SDS-PAGE	sodium dodecyl sulfate polyacrylamide gel electrophoresis
SEM	standard error of the mean
sgRNA	single guide RNA
SIFT	Sorting Intolerant From Tolerant
SpCas9	*Streptococcus pyogenes* CRISPR-associated protein 9
ssRNA	single stranded RNA
T7	promoter for bacteriophage T7 RNA polymerase
TALEN	transcription activator-like effector nucleases
TBS-T	tris-buffered saline-tween
TK	tyrosine kinase
TM	transmembrane
tracrRNA:	trans-activating crRNA
TTX	tetrodotoxin
TTX-R	tetrodotoxin-resistant
Tyr	tyrosine
U6	U6 promoter
UV	ultraviolet

WB	western blotting
WT	wild type
ZFN	zinc finger nuclease

1. Summary

Several heritable disorders alter an individual's perception of pain. For instance, patients with hereditary sensory and autonomic neuropathies (HSANs) cannot feel pain and do not engage appropriate protective behaviours, while pain-related channelopathies can cause both painful and painless conditions. Moreover, chronic pain affects millions of people worldwide. Elucidation of molecules and signalling pathways that lead to pain sensation is key to understanding the mechanisms underlying these pathologies and to the development of adequate treatments.

The CRISPR/Cas9 technology is a revolutionising approach in genome editing. This versatile system consists of two components: a short guide RNA (gRNA) and a Cas9 nuclease. Recognition of a genomic DNA target is mediated through base-pairing with the gRNA, which recruits Cas9 to the target site and generates a double-strand break. Subsequently, the repair mechanisms of the cell are activated, resulting in deletion or insertion (indel) mutations in the DNA sequence. In the present work, two independent models for *in vitro* and *in vivo* study of pain-related genes were successfully generated using the CRISPR-Cas system for the exploration of pain mechanisms.

First, novel putatively pathogenic mutations in the NTRK1 gene were identified in patients with hereditary sensory and autonomic neuropathy type IV (HSAN-IV). Functional characterization of the mutations was done using CRISPR-Cas-edited PC12 cells in which *Ntrk1* was disrupted. Western blot analysis of cells overexpressing the mutant proteins revealed altered activation of signalling pathways as well as glycosylation defects. Also, neurite outgrowth was impaired in *Ntrk1*-KO PC12 cells expressing the mutant proteins. Localisation studies showed altered expression patterns in one of the mutants. Taken together, this cellular system is a valuable tool to investigate the pathogenicity of NTRK1 variants and suggests that different perturbations of the downstream signalling cascade results in loss of nociceptor function.

Second, a double-knockout (DKO) mouse model disrupting the genetically linked genes *Scn10A* and *Scn11a*, encoding the ion channels $Na_V1.8$ and $Na_V1.9$, respectively, was generated. This mouse model will be used in the near future to address the function of these two sodium channels in pain perception. Moreover, DKO-dorsal root ganglion neurones (DRGs)

can be used as a cellular model for the functional characterization of $Na_V1.8$ and $Na_V1.9$ disease-causing protein variants.

2. Zusammenfassung

Die Schmerzwahrnehmung des Menschen kann durch eine Reihe erblicher Erkrankungen beeinflusst werden. Patienten mit einer erblich-bedingten sensibel-autonomen Neuropathie (HSAN) empfinden beispielsweise keine Schmerzen und weisen in der Folge schwere Verletzungen auf. Von einer Natriumkanalerkrankung betroffene Personen können sowohl unter fehlendem Schmerzempfinden als auch unter einem chronischen Schmerzsyndrom und einer Neuropathie leiden. Neben diesen erblichen Erkrankungen gibt es eine Vielzahl von weiteren Ursachen für chronische Schmerzen, so dass die Entschlüsselung von Molekülen und Signalwegen der Schmerzverarbeitung ein wichtiger Schritt auf dem Weg zur Therapie ist.

Die CRISPR/Cas Technologie stellt einen revolutionären Ansatz dar, der auch zum Studium von Schmerzerkrankungen genutzt werden kann. Dieses breit einsetzbare System besteht aus einer sog. kurzen „guide RNA“ (gRNA) und einer Nuklease, dem Cas9-Protein. Die Komponenten des Systems können so adaptiert werden, dass eine gezielte Manipulation beliebiger Abschnitte der DNA möglich ist. Durch CRISPR/Cas-induzierte Doppelstrangbrüche in der DNA werden so repariert, dass beispielsweise Deletionen oder Insertionen im DNA-Strang resultieren und Gene stillgelegt werden können. Das CRISPR/Cas-System wurde im Rahmen der Arbeit sowohl *in-vitro* als auch *in-vivo* erfolgreich zum Studium von Schmerz-assoziierten Genen und ihren Mechanismen eingesetzt.

Im ersten Abschnitt wurden neue Mutationen im *NTRK1*-Gen untersucht, die bei Patienten mit HSAN Typ 4 identifiziert wurden. NTRK1 gilt als wichtiges Molekül der nozizeptiven Funktion. Die funktionelle Analyse der Patientenmutationen erfolgte in PC12-Zellen, in denen *Ntrk1* zunächst mittels CRISPR/Cas ausgeschaltet wurde. Knockout-Zellen, in denen anschließend entweder das humane NTRK1-Wildtypprotein oder eine der Mutanten exprimiert wurde, zeigten eine veränderte Signaltransduktion oder Defekte der Glykosylierung des NTRK1-Rezeptors. Eine der NTRK1-Mutanten zeigte eine veränderte subzelluläre Lokalisation. Zudem war das Neuritenwachstum mutierter Zellen nach NGF-Stimulation vermindert. Zusammenfassend erwies sich das Modell als wertvolles System, um humane NTRK1-Proteine bezüglich ihrer Fehlfunktion zu untersuchen.

Im zweiten Abschnitt der Arbeit wurde ein Doppel-Knockout Mausmodell mittels CRISPR/Cas generiert. Hierbei wurden die beiden im Genom benachbarten und somit gemeinsam vererbten Gene *Scn10a* und *Scn11a*, die die für Nozizeptoren wichtige Natriumkanäle $Na_V1.8$ und $Na_V1.9$ kodieren, parallel ausgeschaltet. Die Studie zeigte, dass sich die Spinalganglien dieser Mäuse ideal als Expressionssystem für die elektrophysiologische Charakterisierung von $Na_V1.8$ und $Na_V1.9$ Mutationen eignen, die bei Patienten mit verändertem Schmerzempfinden eine wichtige Rolle spielen. Das Mausmodell wird zukünftig auch die gemeinsame Rolle beider Kanäle in der Physiologie des Schmerzempfindens klären können.

3. Introduction

3.1 The pain pathway

Pain is an unpleasant sensory, emotional, and cognitive experience that is usually associated with real or potential tissue damage (*1*). Detection of noxious stimuli alerts us to actual or imminent injury and triggers protective responses that are essential for the organism's survival and wellbeing.

Nociception is the process by which intense chemical, mechanical or thermal stimuli are detected by a subpopulation of specialised peripheral sensory neurones known as nociceptors (*2*). The cell bodies of these neurones reside in the dorsal root ganglia (DRG) and have both a central and peripheral axonal branch that innervates the spinal cord and the target organ, respectively. There are three main types of nociceptors: Aβ large diameter and Aδ medium diameter myelinated fibres, and small diameter unmyelinated C fibres. In contrast to other receptors, nociceptors are normally only activated when the intensity of the stimulus reaches the noxious threshold. On such occasions, stimuli cause several receptors, ion channels, and other cellular machinery to respond and transmit signals to the central nervous system (CNS), where the information is processed and perceived as pain (Figure 1) (*3*).

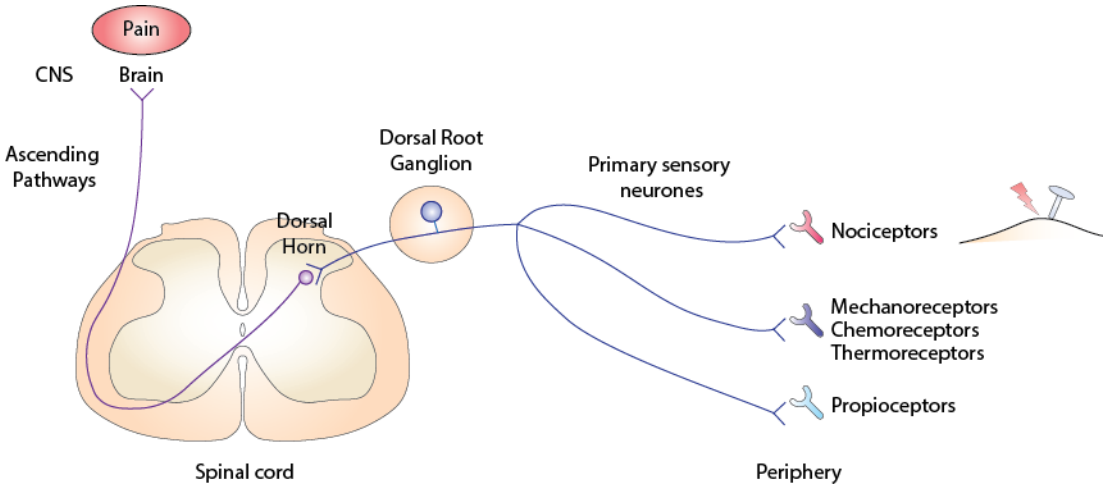

Figure 1. The pain pathway

There are several types of specialised sensory receptors in the peripheral nervous system (PNS), including receptors for temperature (thermoreceptors), mechanical forces (mechanoreceptors), position and movement (proprioceptors), chemical substances (chemoreceptors), and pain (nociceptors). When nociceptors are activated by noxious stimuli, signals travel to the dorsal horn of the spinal cord via the dorsal root ganglion (DRG). From the dorsal horn, signals are carried along the ascending pain pathway or the spinothalamic tract to the brain where the information is processed and perceived as pain (*3*). CNS, central nervous system.

3.2 Hereditary sensory and autonomic neuropathies

The mechanisms that lead to transmission of peripheral information and the generation of an appropriate response are extremely complex. Alterations in the molecular or cellular mechanisms involved at any stage of this process can cause serious diseases. Indeed, peripheral neuropathies affect many people worldwide and are one of the most common neurological disorders (*4*).

Peripheral neuropathies are diseases of the peripheral nervous system (PNS) in which either the axon or the myelin-forming cells surrounding them, the Schwann cells, show dysfunction due to metabolic stress, toxicity, infections, or genetic defects (*5*). Inherited peripheral neuropathies can be classified into three different types according to the nerve fibres affected: hereditary motor neuropathies, hereditary motor and sensory neuropathies, and hereditary sensory and autonomic neuropathies (HSANs) (*6*).

HSANs are a group of genetically and clinically heterogeneous disorders that include phenotypes with pure sensory involvement, others with variable levels of motor involvement and minor autonomic disturbance or virtually pure autonomic neuropathies. Loss of pain and temperature sensation are the most common symptoms of HSANs and usually lead to chronic ulcerations in hands and feet, recurrent unrealized infections, and self-mutilation. Additionally, patients with HSAN show axonal injury in sensory neurones and demyelination might also be present (*6*).

HSANs can be subdivided into autosomal dominant forms that typically show juvenile or adult onset, and autosomal recessive forms, which usually have an early onset (congenital or during childhood). Furthermore, HSAN can be categorised into different subtypes based on age at onset, mode of inheritance, and the predominant clinical features (*7*).

Genetic, electrophysiological, and pharmacological studies during the past decade allowed us a better understanding of the molecular and cellular mechanisms underlying HSAN. Indeed, based on findings from only a small number of families with the disease, it was possible to identify several causal genes and the proteins encoded by them. Some of the altered proteins have clear nerve-specific roles, whereas others are ubiquitously expressed proteins involved in different mechanisms such as transcription regulation, vesicular transport, sphingolipid metabolism, and structural integrity. Even though, to date, only one-third of patients with HSAN have mutations

in the already known causative genes. On the other hand, due to the development of new sequencing and bioinformatics technologies more disease-associated genes will probably be identified in the near future. Consequently, additional insights into the function of the proteins encoded by the HSAN-genes responsible for normal development, differentiation, and maintenance of the sensory and autonomic neurones are needed in order to develop new therapeutic strategies for patients with HSAN (*6*).

3.2.1 Mutations in NTRK1 cause HSAN type IV

Hereditary sensory and autonomic neuropathy type four (HSAN-IV), also known as congenital insensitivity to pain with anhidrosis (CIPA, OMIM 256800), is a rare autosomal recessive disorder caused by a failure of nociceptive and sympathetic neurone development. The complete absence of small-diameter unmyelinated fibres and loss of innervation of eccrine sweat glands by sympathetic neurones can be observed in skin and nerve biopsies from patients suffering from the disease (*8*, *9*). The absence of normal responses to both superficial and deep painful injuries along with the inability to sense temperature is characteristic of HSAN-IV patients. Accordingly, they are susceptible to multiple accidental injuries such as burns, falls, bone and joint fractures, and have a self-mutilating behaviour involving primarily the orofacial region and the fingers of both hands and feet (Figure 2A-B). In addition, patients show variable mental retardation plus a markedly decreased or absent sweating associated with recurrent episodes of fever (*10*).

Over 50 different missense, nonsense, frameshift, splice site mutations as well as alterations in non-coding regions in the neurotrophic tyrosine receptor kinase type 1 (*NTRK1*, OMIM 191315) gene, which encodes the high-affinity nerve growth factor (NGF) receptor 1 (NTRK1), cause HSAN-IV in families of various genetic backgrounds (*10–15*). The *NTRK1* gene consists of 17 exons distributed within a 25-kb region on chromosome 1q21-22 (*16*, *17*). The NTRK1 protein is one of three major tyrosine kinases involved in neurotrophin signalling. Upon NGF binding, NTRK1 is autophosphorylated resulting in the activation of downstream signalling pathways that support neurite outgrowth, survival of sympathetic ganglia and nociceptive sensory neurones, and the development and survival of cholinergic neurones of the basal forebrain (Figure 2C) (*10*). Moreover, NTRK1 is an essential modulator of the expression and sensitization of several neurotransmitters, receptors, and ion channels expressed by adult nociceptors (Figure 3) (*18*).

NTRK1 has an extracellular portion consisting of a leucine rich repeat, flanked on either side by a cysteine-rich and two Ig-like domains, a transmembrane and a juxtamembrane domain, a tyrosine kinase (TK) domain, and a C-terminal end (*19*). Mutations in the TK domain are the most frequent, though a few have been found in the extracellular domain, responsible for binding NGF (*20*). While frameshift, nonsense, and splice-site mutations typically produce aberrant or missing proteins, uncovering the consequences of missense mutations leading to single amino acid substitutions requires more detailed functional studies to demonstrate their involvement in HSAN-IV and discriminate them from rare polymorphisms.

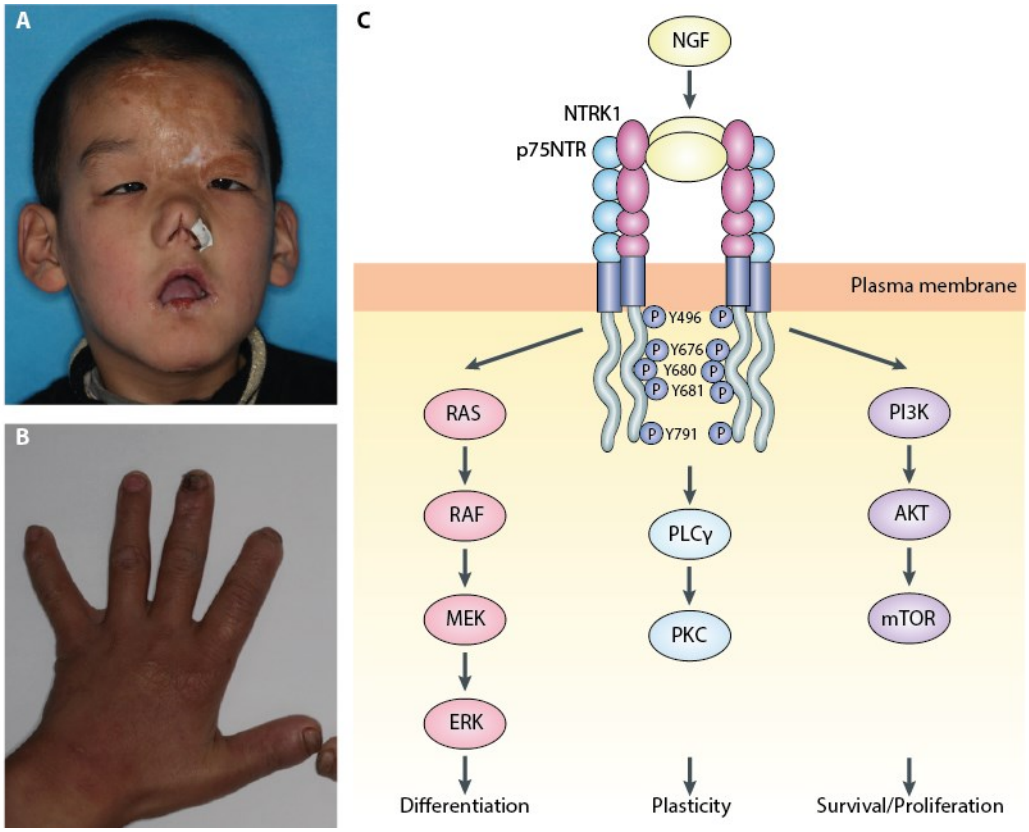

Figure 2. Clinical features of HSAN-IV and the NTRK1-NGF signalling pathway

(A) Scratch marks, erosions, and cicatrization (scars) due to self-inflicted soft tissue trauma, nasal columella defect and keratitis. (B) Lichenification, missing tips of the index finger, dystrophic nails and left digitus minimus extended outward due to old fractures. (C) Binding of Nerve growth factor (NGF) to NTRK1 (high-affinity nerve growth factor receptor 1) causes receptor dimerization and leads to autophosphorylation in five different tyrosine (Tyr) residues resulting in the activation of various signalling cascades that promote cellular differentiation, growth, survival, and synaptic plasticity (*10*). Phosphorylated Tyr496, localised in the juxtamembrane domain, is implicated in the activation of phosphatidylinositol 3-kinase (PI3K) (*21*, *22*) and the ERK (extracellular signal-regulated kinase) signalling pathways (*23*, *24*). Tyr676, Tyr680, and Tyr681 are located in the activation loop of the tyrosine kinase domain and play a pivotal role in receptor activation (*25*). Phosphorylation of Tyr791 on the C-terminal end activates phospholipase Cγ (PLC-γ) (*26*). Signalling is further modulated by the $p75^{NTR}$ receptor (low-affinity nerve growth factor receptor) (*27*). AKT, protein kinase B; mTOR, mechanistic target of rapamycin; MEK, mitogen-activated protein kinase kinase; PKC, protein kinase C; RAF, rapidly accelerated fibrosarcoma; RAS, Rat sarcoma. A and B were published by (*28*). C was adapted from (*29*).

3.2.2 Pain associated disorders: the channelopathies

Ion channels, located in the membranes of all cells and many cellular organelles, have a pivotal role in neuronal function and signalling (Figure 3). Channelopathies are a heterogeneous group of disorders resulting from the dysfunction of ion channels that can be acquired or inherited. Some channelopathies affect the normal functioning of nociceptors. In some individuals, mutations in ion channels can lead to pain insensitivity, whereas in others result in increased pain perception. Moreover, single nucleotide polymorphisms in genes encoding ion channels might affect an individual's sensitivity to pain as well as predisposition to, and severity of chronic pain after tissue inflammation or neural damage and other acquired pain states (*30*).

Voltage-gated sodium channels (Na_V) are crucial determinants of nociceptor excitability. They mediate the influx of sodium ions into the cell in response to local membrane depolarization, which results in the generation of an action potential that will eventually transmit the signal to the CNS (*31*). The channels $Na_V1.7$ (*32*), $Na_V1.8$ (*33*), and $Na_V1.9$ (*34*) are all preferentially expressed in pain-sensing peripheral neurones; however, they have distinct kinetics and show slightly different patterns of expression and sensitivity to the neurotoxin tetrodotoxin (TTX). $Na_V1.7$ channels might be relevant to amplify small sub-threshold stimuli and, therefore, act as a key determinant of threshold in nociceptor terminals (*35*). In DRG neurones, $Na_V1.8$ channels are crucial for transmission of nociceptive information, as they carry most of the current underlying the depolarising phase of the action potential (*36*, *37*), and are essential for repetitive firing. $Na_V1.9$ sodium channels can generate persistent currents at near resting membrane potential, meaning that these channels are key regulators of membrane excitability (*38–40*). Furthermore, $Na_V1.8$ and $Na_V1.9$ channels can be distinguished from $Na_V1.7$ channels by their resistance to TTX (*33*, *41*).

The voltage-gated sodium ion channel $Na_V1.7$ is encoded by the sodium voltage-gated channel alpha subunit 9 (*SCN9A*; OMIM 603415), an 113.5-kb gene comprising 26 exons located on chromosome 2q24 expressed selectively in autonomic and sensory neurones (*32*). The majority of DRG neurones expressing $Na_V1.7$ are pain sensing, suggesting this sodium channel has a vital role in pain pathogenesis (*42*). Gain-of-function missense mutations in $Na_V1.7$ are responsible for primary erythromelalgia (OMIM 133020) (*43–46*), paroxysmal extreme pain disorder (OMIM 613640) (*47–49*), and small-fibre neuropathy (OMIM 133020) (*50*). On the other hand, loss-of-function mutations lead to congenital insensitivity to pain and HSAN (OMIM 243000) (*51*) type IID (OMIM 243000) (*52*), two conditions in which affected individuals are unable to feel physical pain.

The voltage-gated sodium channels $Na_V1.8$ and $Na_V1.9$ are encoded by the sodium voltage-gated channel alpha subunit 10 (*SCN10A*; OMIM 604427) and the sodium voltage-gated channel alpha subunit 11 (*SCN11A*; OMIM 604385) respectively. Both genes are located on chromosome *3p22.2*, one after the other, meaning they are linked genes and, thus, likely to be inherited together. $Na_V1.8$ is expressed in myelinated and unmyelinated axons of DRG neurones, in contrast to $Na_V1.9$ that is only expressed in myelinated fibres (*53*). Painful and painless neuropathies have been recently associated with these genes. Gain-of-function missense mutations in *SCN10A* result in small fibre neuropathy (OMIM 615551) (*54–56*), while in *SCN11A* cause congenital insensitivity to pain (*57–59*), familial episodic pain syndrome type III (*60–62*), painful small fibre neuropathy (*63*, *64*), and cold-aggravated peripheral pain (*65*).

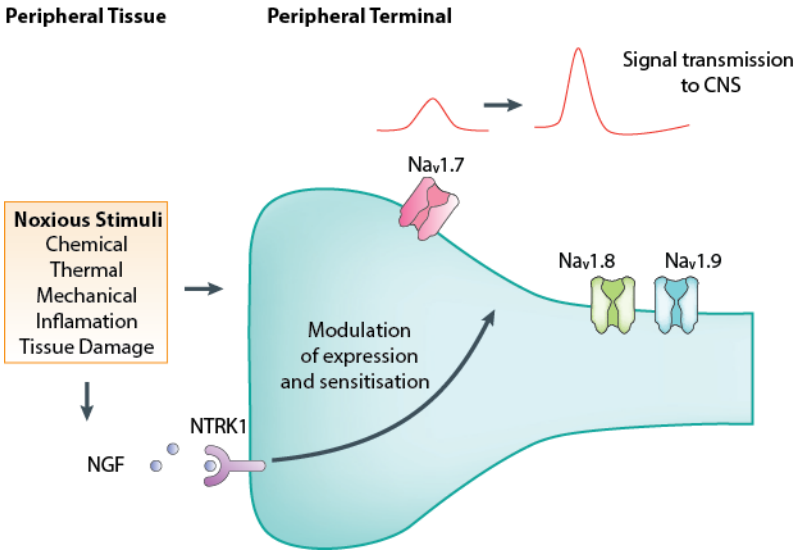

Figure 3. Schematic representation of a nociceptor terminal

Nociceptive signals are transmitted from the periphery by nociceptive sensory neurones. Peripheral nociceptor terminals are clustered with several types of ion channels, including sodium channels (Na_V). Transduction of peripheral noxious stimuli is initiated by membrane depolarization due to the activation of these channels resulting in action potentials that transmit signals to the central nervous system (CNS). The voltage-gated sodium channels $Na_V1.7$, $Na_V1.8$, and $Na_V1.9$, have a fundamental role in responding to small depolarizations and action-potential generation (*30*). During inflammation, injury, or certain diseases, inflammatory, immune, or Schwann cells release nerve growth factor (NGF). NGF binding to the high-affinity nerve growth factor receptor 1 (NTRK1) activates different signalling pathways that directly activate and/or sensitise nociceptors by modulating the expression of several genes, including ion channels (*18*). Adapted from (*30*).

3.3 Peripheral neuropathies: a persisting challenging problem

Solely in the United States, an estimated 15 to 20 million people over age 40 suffer from some type of peripheral neuropathy (*4*). Diagnosis of peripheral neuropathies is often made based on the patient medical history and prevailing symptoms. Physical examinations such as nerve biopsies can be useful to evaluate the presence of nerve fibre damage, while nerve conduction studies might be crucial to confirm severe impairment of sensory/motor nerve conduction

velocities as well as absent or altered sensory/motor nerve action potentials (*5*). Additionally, performing different biochemical tests along with DNA sequencing, which allows identification of potential gene mutations, is crucial for the correct assessment of the disease.

However, management of pain and dysesthesia in these disorders is a challenging task. Though various symptomatic therapies exist which address pain in peripheral neuropathies, these are mostly inefficient. Moreover, to date, there are almost no effective treatments to prevent axonal degeneration or Schwann cell dysfunction characteristic of peripheral neuropathies (*5*).

Establishing cellular or mouse models to study hereditary neuropathies prove to be crucial for understanding the genetic and molecular basis of pain. Indeed, mutations in both NTRK1 and the voltage-gated sodium channel genes SCN10A and SCN11A cause painful and painless neuropathies and are potential analgesic targets (*19*, *66*). Many mutations identified in patients with these conditions are single-base substitutions distributed throughout the coding sequence (*10*, *11*, *67*). Investigating the functional consequences of these mutations will not only enable a deeper understanding of protein function but also shed light on the underlying disease mechanisms causing the variable phenotypes found in patients. Moreover, gaining an in-depth insight into these rare heritable pain disorders may be translated into therapy.

3.4 Genome engineering and programmable nucleases

Generally speaking, genome engineering refers to the process of generating specific modifications to the genome, its contexts, or its outputs. Technologies that can delete, insert, and modify DNA (deoxyribonucleic acid) sequences of cells or organisms allow researchers to elucidate the function of disease-related genes and regulatory elements. Moreover, multiple editing could further enable establishing gene or protein interaction networks that could help to understand complex disease mechanisms. Thus, our ability to manipulate the genome easily and efficiently, particularly in mammalian cells, holds tremendous potential to revolutionise basic research and medicine (*68*).

Eukaryotic genomes contain millions of DNA bases, and their manipulation is challenging. The development of gene targeting by homologous recombination (HR), which allows the integration of exogenous designed DNA flanked by sequences homologous to the donor site (*69*), was a major breakthrough. Thanks to this technique, researchers were able to generate knockin and knockout animal models via manipulation of stem cells, which has led to huge

progress in many areas of biological research. Still, even though HR-mediated gene targeting produces extremely precise modifications, the recombination frequency is very low (*69*), and the procedure is costly and time-consuming (*68*).

In recent years, the development of programmable nuclease-based genome editing technologies has enabled researchers to overcome such challenges, facilitating specific and efficient alteration of several eukaryotic and mammalian genomes (*68*). These enzymes can generate targeted DNA double-strand-breaks (DSBs) that can stimulate editing through HR-mediated recombination events (*70*, *71*) as well as induce insertions or deletions (indels) via the error-prone non-homologous end-joining (NHEJ) repair pathway (*72*).

Of the various genome editing nucleases that have been developed up to date, the most rapidly emerging are the RNA (ribonucleic acid)-guided DNA endonucleases from the bacterial adaptive immune system CRISPR (clustered regularly interspaced short palindromic repeats), known as Cas9 (CRISPR-associated protein 9) (*73*, *74*) which can be easily targeted to practically any genomic region of choice by a short RNA guide (*68*).

3.4.1 CRISPR/Cas, the adaptive immune system of bacteria and archaea

All organisms need to defend themselves against infection by potentially harmful invaders, collectively known as pathogens. The immune system is usually divided into innate and adaptive, though these are not mutually exclusive. In multicellular organisms, innate (non-specific) immune responses act as a first line of defence and include protective barriers, toxic molecules, and phagocytic cells that ingest and destroy invading microorganisms (*75*). Bacteria and archaea possess several innate immunity-like systems such as abortive infection, toxin-antitoxins, receptor mutation, and restriction-modification (*76*). Unlike innate responses, adaptive responses have three essential characteristics: specificity, diversity, and memory. Specificity is crucial to identify exogenous structures and organisms that need to be attacked and distinguished from those that have to be tolerated. Diversity in the immune response is required to defend the host from a large variety of pathogens and malignant elements. Lastly, a memory of past infections allows a more efficient response to recurrent infections and enables the host to react rapidly upon re-exposure (59). Adaptive responses were thought to be exclusively present in higher eukaryotes until the recent discovery of the CRISPR-Cas system, which provides specific and acquired immunisation against invasive mobile genetic elements (MGEs) such as plasmids and viruses in Prokaryotes (*77–81*).

In response to viral and plasmid encounters, bacteria and archaea incorporate small fragments of foreign nucleic acid into the host chromosome at the leader end of a repetitive element, known as the CRISPR array (*77*, *82*). These provide the 'immune memory' and consist of a series of direct repeats of approximately 20 to 50 base pairs separated by unique spacer sequences of a comparable length, which derive from the invading MGEs (*83*). CRISPR arrays are flanked by a large number of highly genetically and functionally diverse *cas* (CRISPR-associated) genes, comprising the CRISPR locus (*79*, *84*). The Cas proteins provide the machinery for defence, and most of them carry functional domains that interact with nucleic acids, for example, DNA binding, RNA binding, helicase, and nuclease motifs (*79*, *85–89*). CRISPR arrays are transcribed into a long primary transcript (pre-crRNA) that is processed into a library of short CRISPR-derived RNAs (crRNAs) complementary to a previously encountered MGE sequence (*90–95*). Each crRNA is wrapped into a large complex, known as the crRNA-guided surveillance complex, which patrols the intracellular environment and mediates detection and specific destruction of the foreign MGEs (*81*, *82*, *90*, *96–99*).

CRISPR-Cas systems are highly diverse among species and can be divided into two main classes, six major types (type I-VI), and multiple subtypes based on the genes encoding the surveillance complex and its architecture (*100*, *101*). Type I and III CRISPR-Cas systems, as well as the putative type IV, are classified as class 1 systems and possess multisubunit surveillance complexes: the CRISPR-associated complex for antiviral defence (Cascade) in type I and Csm or Cmr complex in type III. Class 2 systems, in which all functions of the surveillance complex are carried out by a single protein, include type II (Cas9 protein), the recently established type V (Cpf1, C2c1 or C2c3 proteins), and type VI (C2c2 protein) (*100*, *101*).

CRISPR-Cas systems work in three steps: acquisition (spacer incorporation), expression (crRNA processing and target binding) and interference (target cleavage) (*88*). Moreover, recent studies suggest that CRISPR–Cas systems can also be used for non-defence roles, such as the regulation of collective behaviour and pathogenicity (*102–104*).

Acquisition requires the endonucleases Cas1 and Cas2, which obtain new spacer sequences (protospacers) and integrate it to the CRISPR array (*105*). The CRISPR-repeat sequence is duplicated after each spacer integration, hence maintaining the repeat-spacer-repeat structure (*106*). The *cas1* gene can be found in most CRISPR-*cas* loci while the protein sequence is the

best conserved among all Cas proteins (*88*, *100*, *107*). Cas1 is an integrase that cleaves at specific sites within the repeats of the CRISPR array facilitating the incorporation of spacers. Cas2 substantially increases integration activity, but its role is less well understood (*105*, *108*). Furthermore, in type II systems Cas9 is also involved in acquisition and might provide sequence specificity (*109*, *110*).

Protospacers are not randomly chosen, and in many CRISPR-Cas systems, selection requires recognition of a short protospacer adjacent motif (PAM) in the target DNA (*111–113*). PAM sequences are only a few nucleotides long, and the exact sequence varies depending on the CRISPR system type and the bacterial species. In addition, the PAM is an essential component that facilitates self versus non-self discrimination to avoid the CRISPR locus itself from being targeted (*114*).

During expression, the *cas* genes and the CRISPR array are transcribed. The pre-crRNA is transcribed from the leader sequence (*81*) and further processed into crRNAs containing the MGE-derived spacer sequence and portions of the repeats (*90–95*). Generation of crRNAs differs between the two classes of CRISPR-systems. In class 1 systems, crRNA production usually involves a Cas6 endoribonuclease (*95*) whereas in the class 2 systems the scenario is more diverse. Type II systems require Cas9, RNase III and a non-coding RNA, named transactivating crRNA (tracrRNA), for pre-crRNA processing (*91*). However, in *Neisseria meningitides* (type II-C system) transcription is initiated within each spacer, driven by promoter elements embedded within each repeat and, unexpectedly, pre-crRNA processing is not required (*115*). In type V systems, C2c1 also needs a tracrRNA (*101*) while Cpf1 produces crRNA independently of a tracrRNA (*116*). C2c2 generates mature crRNA without a tracrRNA in type VI systems (*101*).

The crRNAs form a ribonucleoprotein complex with the Cas proteins, and in type II (*91*) and some type V systems (*101*) also with the tracrRNA. During interference, these surveillance complexes recognise and degrade the MGEs. In type I systems, recognition of complementary DNA by Cascade results in the recruitment of the Cas3 helicase-nuclease, which degrades the invasive DNA (*117*, *118*). Type III systems target DNA and RNA in a transcription-dependent manner. Hence, these systems only interfere with transcriptionally active phages (*119*). Finally, type II and type V interference results in DNA degradation, while type VI degrades single-stranded RNA (ssRNA) (*101*, *120*). Remarkably, the large (~950–1,400 amino acids)

multidomain Cas9 protein is necessary for all three steps of CRISPR-based immunity in type II systems and, therefore, concentrating much of the CRISPR-Cas system's function in a single protein (*79*, *100*).

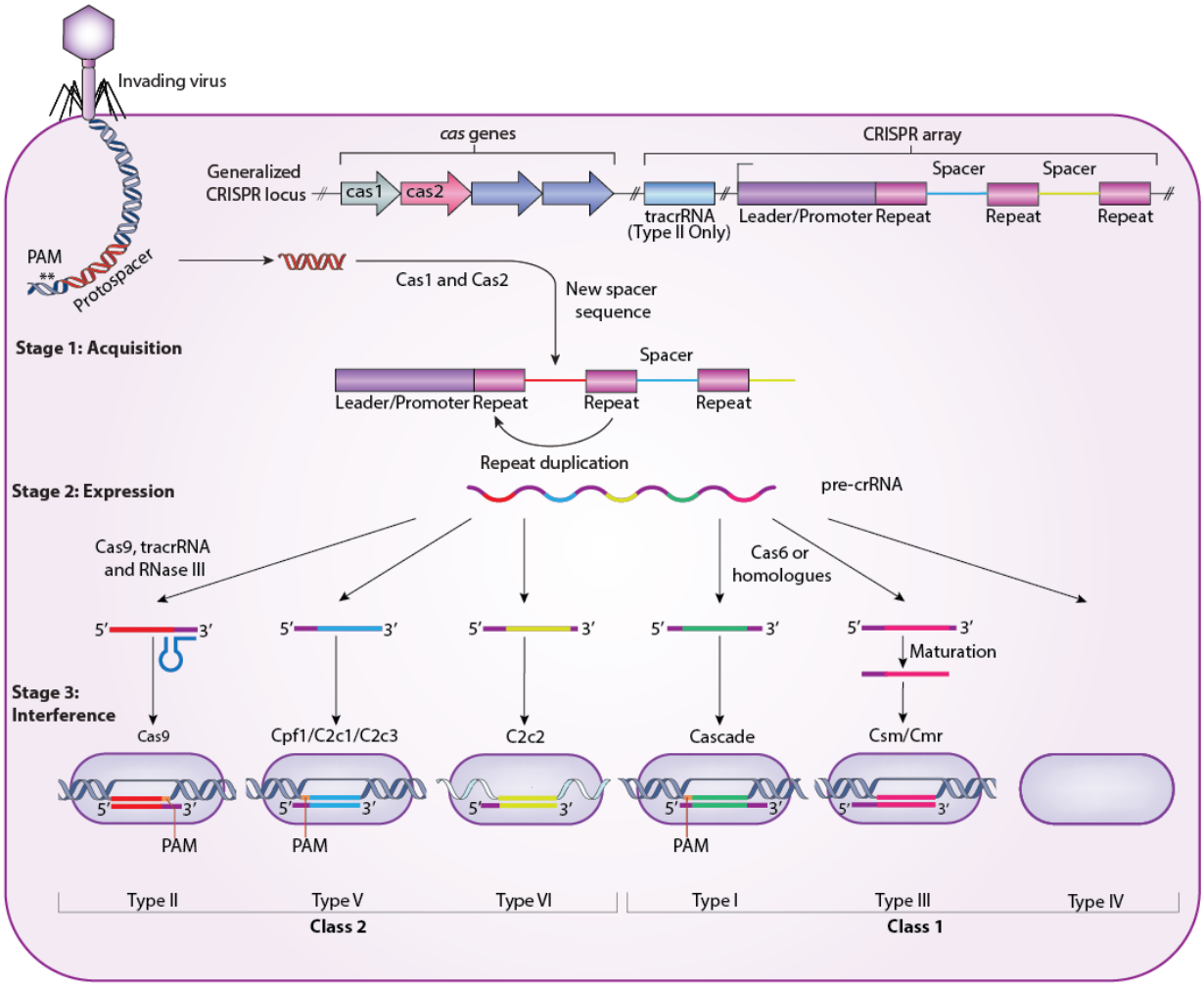

Figure 4. Diversity of CRISPR-Cas mediated adaptive immune systems in prokaryotes

Several CRISPR-associated (*cas*) genes (coloured arrows) encode the proteins needed for spacer sequence acquisition (stage 1), expression (stage 2) and interference (stage 3). CRISPR loci consist of a series of direct repeats followed by unique spacer sequences acquired from invading genetic elements (protospacers). Protospacers are flanked by a short motif known as the protospacer adjacent motif (PAM, **) located on the 5′ or 3′ side of the foreign nucleic acid (*111–114*). Long CRISPR transcripts (pre-crRNA) are processed into short crRNAs by different mechanisms. Multiprotein crRNA–effector complexes (violet ovals) mediate the processing and interference stages in type I and type III CRISPR-Cas systems (*100*). In type I systems, this complex is known as Cascade (CRISPR-associated complex for antiviral defence) (*81*). Cas6, which is part of Cascade, selectively cleaves the pre-crRNA to produce mature crRNAs (*94*) and requires Cas3 for DNA cleavage (*117*, *118*). In type III systems the complexes are named Csm or Cmr, depending on the subtype, and they can cleave DNA or RNA in a transcription-dependent manner (*119*). In this system, the enzyme mediating crRNA processing is unknown, but it is assumed to be Cas6 (*100*). In type II systems, a *trans*-acting antisense RNA (tracrRNA) complementary to the crRNA repeat sequence forms an RNA duplex that is recognised and cleaved by cellular RNase III (*91*). In type V systems, C2c1 also needs a tracrRNA whereas Cpf1 processes crRNA arrays independently of tracrRNA; however, both cut double-stranded DNA (*101*, *116*). In type VI systems, C2c2 produces mature crRNA without a tracrRNA and cleaves RNA (*101*, *120*). Adapted from (*90*, *105*).

3.4.2 Type II systems and their use in genome engineering

The development of the Cas9 nuclease for genome editing is the result of more than a decade of basic research into deciphering the biological function of the CRISPR-Cas system, which is present in more than 40% of sequenced bacteria and 90% of archaea (*122*). Given that the CRISPR arrays and *cas* genes appeared to be well conserved (*123*), interest in such microbial repeat elements began to increase, though it was only in 2007 when the first experimental evidence of the role of CRISPR systems in adaptive immunity was uncovered (*77*).

By 2010, researchers had a clear overview of the building blocks and mechanisms of CRISPR systems, and several groups began to take advantage of this natural system for several biotechnological applications including the production of phage-resistant dairy cultures (*124*). Around the same time, it was reported that in type II CRISPR systems DNA cleavage solely requires Cas 9 (*82*) and this protein, together with RNase III and a tracrRNA-crRNA hybrid, processes the pre-crRNA into mature crRNAs, which then guide Cas9 to its DNA target (*91*). Therefore, theoretically, only three components (Cas9, mature crRNA, and tracrRNA) seemed to be essential for reconstituting the type II CRISPR system in mammalian cells and, due to its simplicity, could be used as an RNA-programmable DNA endonuclease for genome editing.

In 2012, it was demonstrated that crRNAs could guide S*treptococcus thermophilus* or *Streptococcus pyogenes* purified Cas9 to cleave target DNA *in vitro* (*125*, *126*). One year later two groups simultaneously achieved to engineer type II CRISPR systems from *S. thermophilus* (*73*) and *S. pyogenes* (*73*, *74*) and successfully edited mammalian-cell genomes. Both a crRNA-tracrRNA hybrid and a single guide RNA (sgRNA), in which the crRNA 3'and tracrRNA 5' ends are connected by a tetraloop, can direct Cas9 cleavage to a particular sequence of the cellular genome to promote NHEJ or homology-direct repair (HDR)-mediated genome editing (*73*, *74*, *125*). Since these pioneering studies, Cas9, especially *S. pyogenes* Cas9 (SpCas9), has been used by numerous research laboratories for genome editing in a wide range of experimental model systems (*127*).

All Cas9 proteins share a similar structure composed of six domains. The RuvC and HNH nuclease domains are responsible for DNA cleavage, while REC I binds the guide RNA. REC II forms a bridge helix crucial for initiating cleavage, whereas the PAM interacting C-terminal region confers PAM specificity and activates the nuclease domains (*128–130*). The guide RNA functions as a scaffold around which Cas9 can fold and organise its various domains (*128*).

To direct Cas9 to a particular DNA sequence, SpCas9 requires twenty nucleotides (nt) at the 5′ end of the crRNA (or sgRNA) directly matching the target site along with a 5′-NGG PAM sequence, where N can be any nucleotide, immediately downstream of the target sequence (*125*). Type II systems from other bacterial species that recognise other PAM sequences and differ in the tracrRNA and crRNA sequences have also been used for genome editing, such as *Neisseria meningitides* Cas9 (NmeCas9). While both Cas9 proteins produce DSBs three base pairs (bp) upstream of the PAM sequence, in contrast to SpCas9, NmeCas9 requires a twenty-four nucleotide target guide sequence followed by a 5'-NNNGATT PAM to cleave DNA (Figure 5) (*131*, *132*). In this thesis, I will exploit these nucleases for generating mouse and cellular models to study pain-related-gene mutations.

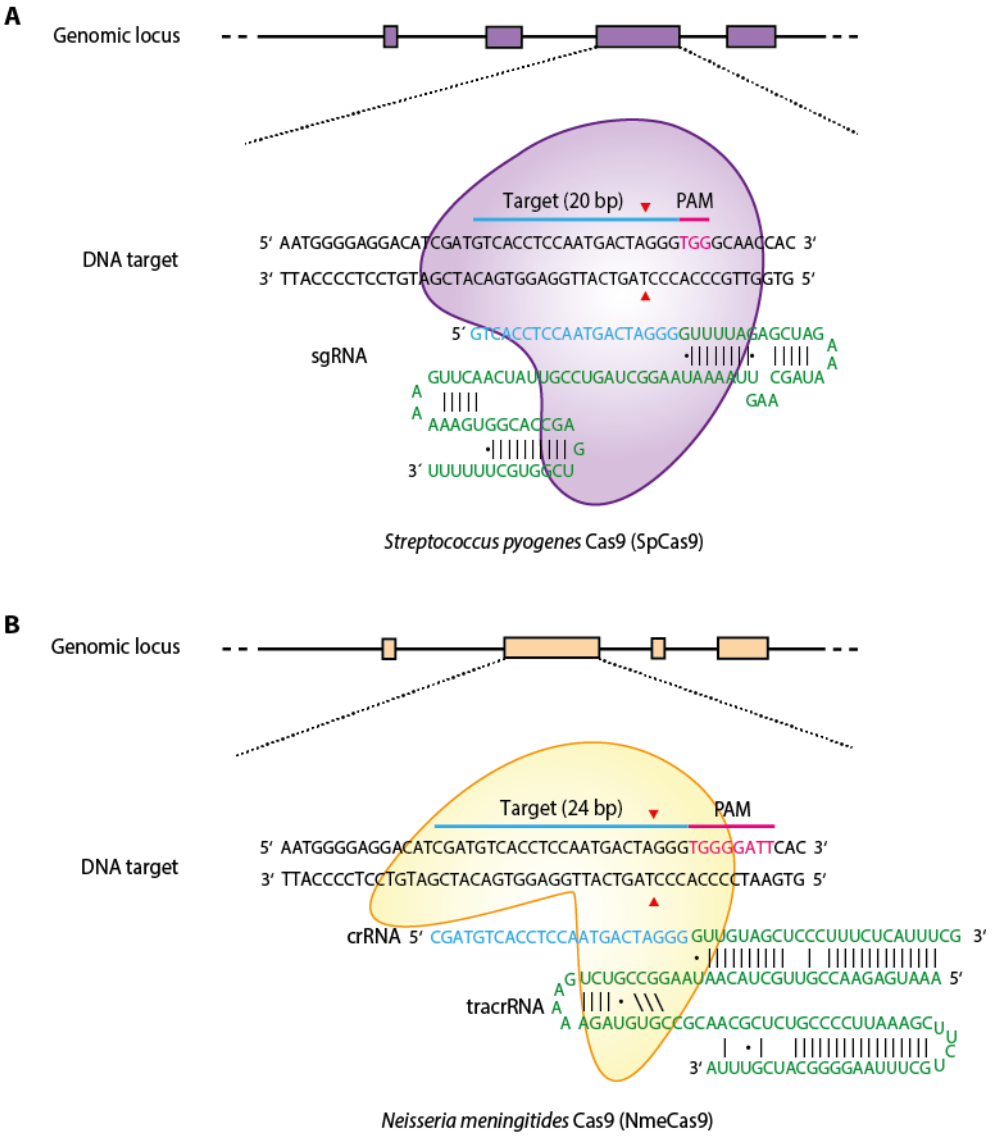

Figure 5. Type II RNA-guided Cas9 nucleases from *S. pyogenes* and *N. meningitides*

(A) The Cas9 nuclease from *S. pyogenes* (SpCas9; in violet) is targeted to genomic DNA by a single guide RNA (sgRNA) consisting of a 20-nt sequence (in blue) and a scaffold (in green). The guide sequence pairs with the target DNA (blue bar on top strand), directly upstream of the 5′-NGG protospacer adjacent motif (PAM; pink) (*73*). (B) The Cas9 nuclease from *N. meningitides* (NmeCas9; in yellow) is directed to genomic DNA by a CRISPR-RNA (crRNA) consisting of a 24-nt guide sequence (in blue) and part of the repeat sequence hybridised to the transactivating crRNA (tracrRNA). The guide sequence pairs with the target DNA (blue bar on top strand) upstream of a 5′-NNNNGATT PAM (pink) (*131*). Both SpCas9 and NmeCas9 produce a double strand break three base pairs (bp) upstream of the PAM (cleavage site: red triangles) (*73*, *131*). The figure was adapted from Ran et al. 2013.

3.5 Objectives

Studying gene function in a biological context proves to be essential to understanding the genetic and molecular basis of pain and might eventually lead to improved diagnosis and novel therapeutic strategies for patients with peripheral neuropathies. Therefore, the main aim of this thesis was the generation of models that would enable a faster characterization of unreported putative disease-causing mutations in genes involved in pain perception using the recently developed genome engineering method CRISPR-Cas, in particular:

- Generation of a cellular knockout model for functional characterization of missense mutations in the *NTRK1* gene.

- Validation of the model by functional characterization of recently identified *NTRK1* mutations of unclear clinical significance.

- Comparing different CRISPR/Cas-based approaches to disrupt genetically linked genes in mice simultaneously, and generating *Scn10a* and *Scn11a* double-knockout mice.

4. Materials and Methods

4.1 Materials

4.1.1 Bacteria

For amplification of DNA plasmids, the bacterial strain *Escherichia coli* XL-1-Blue was used.

4.1.2 Cell lines

PC12, HEK293T and HeLa cells were used. PC12 is a rat cell line that was derived from a pheochromocytoma of the adrenal medulla (*133*). PC12 cells cease to proliferate and undergo terminal differentiation into a neuronal phenotype when treated with nerve growth factor (NGF) (*134*). HEK293T is a highly transfectable cell line derivative of human embryonic kidney 293 cells and contains the SV40 T-antigen (*135*), while HeLa cells derived from an epidermoid carcinoma of the human cervix (*136*). Cell lines were a gift from Prof. Dr. rer. nat. Aria Baniahmad.

4.1.3 Antibodies

Table 1. List of primary commercial antibodies

Antibody	*Host, clonality: polyclonal (pc); monoclonal (mc)*	*Company*	*ID number*	*Working dilution for Western Blot (WB); Immunofluorescence (IF)*
Akt (pan)	rabbit, mc	Cell Signaling Technology (CST)	4601	WB: 1:1000
Phospho-Akt (Ser473)	rabbit, pc	CST	9271S	WB: 1:1000
P44/42 MAPK (Erk 1/2)	mouse, mc	CST	9107	WB: 1:2000
Phospho-p42/44 MAPK (Erk1/2) (T202/204)	mouse, mc	CST	9106	WB 1:1000
Anti-β-actin	mouse, mc	Abcam	ab6276	WB 1:5000
Anti-TrkA (NTRK1)	rabbit, pc	CST	2505	WB 1:1000
Anti-Acetylated Tubulin	mouse, mc	Sigma	T7451	IF: 1:1000
Alexa Fluor® 546 anti-mouse	goat, pc	Life Technologies	A11003	IF: 1:2000
Alexa Fluor® 488 anti-rabbit	goat, pc	Life Technologies	A11003	IF: 1:2000
Mouse or Rabbit IgG (H+L) - HRP	goat, pc	Kirkegaard & Perry Laboratories	0741806 /1506	WB 1:5000
Anti-myc	rabbit, pc	Millipore	06-549	IF: 1:1000

4.1.4 DNA Plasmids

Table 2. List of DNA Plasmids

Protein/RNA expressed by vector DNA	*Plasmid Name*	*Vector backbone*	*Source*
GFP	GPF	peGFP_N1	Clonetech
NmeCas9 +trRNA + crRNA	pSimpleII-U6-tracr-U6-BsmBI-NLS-NmCas9-HA-NLS(s)	pSimpleII	Gift from Erik Sontheimer & James Thomson (Addgene #47868)
NmeCas9 + trRNA + crRNA +GFP	pSimpleII-U6-tracr-U6-BsmBI-NLS-NmCas9-HA-NLS(s)-CMV-GFP	pSimpleII	
NmeCas9 + trRNA + crRNA(Exon 5 *Ntrk1*) +GFP	pSimpleII-U6-tracr-U6-crRNA(Exon 5 *Ntrk1*)-NLS-NmCas9-HA-NLS(s)-CMV-GFP	pSimpleII	
Wild Type NTRK1	pCI-neo- NTRK1	pCI-neo	GenScript
Wild Type NTRK1-myc	pCI-neo-NTRK1-myc	pCI-neo	
Mutant I NTRK1-myc	pCI-neo- NTRK1-myc-I	pCI-neo	
Mutant II NTRK1-myc	pCI-neo- NTRK1-myc-II	pCI-neo	
Mutant III NTRK1-myc	pCI-neo- NTRK1-myc-III	pCI-neo	
K-RAS (HRV)-mCherry	K-RAS (HRV)-mCherry		Gift from Dr. rer. nat. Ignacio Rubio
hSpCas9	pX330-U6-Chimeric_BB-CBh-hSpCas9	pUC ori vector	Gift from Feng Zhang (Addgene plasmid # 42230)
hSpCas9 + sgRNA-*Scn10a*-Ex6	pX330-U6-Chimeric_BB-CBh-hSpCas9_sgRNA-*Scn10a*-Ex6	pUC ori vector	
hSpCas9 + sgRNA-*Scn10a*-Ex11	pX330-U6-Chimeric_BB-CBh-hSpCas9_sgRNA-*Scn10a*-Ex11	pUC ori vector	
hSpCas9 + sgRNA-*Scn11a*-Ex9	pX330-U6-Chimeric_BB-CBh-hSpCas9_sgRNA-*Scn11a*-Ex9	pUC ori vector	
hSpCas9 + sgRNA-*Scn11a*-Ex10	pX330-U6-Chimeric_BB-CBh-hSpCas9_sgRNA-*Scn11a*-Ex10	pUC ori vector	
Scn10a-Ex6	pCR2.1TOPO-Ex6	pCR2.1TOPO	
Scn10a-Ex11	pCR2.1TOPO-Ex11	pCR2.1TOPO	
Scn11a-Ex9	pCR2.1TOPO-Ex9	pCR2.1TOPO	
Scn11a-Ex10	pCR2.1TOPO-Ex10	pCR2.1TOPO	

4.1.5 Kits

Amaxa SF cell line 4D-Nucleofector X Kit S and L	Lonza
BigDye® Terminator v1.1 Cycle Sequencing Kit	Applied Biosystems
Clarity™ Western ECL Substrate	Bio-RAD
DNA Clean & Concentrator™	Zymoclean
Gel DNA Recovery Kit - Uncapped columns	Zymoclean
MEGAclear™ Transcription Clean-Up Kit	Thermo Scientific
MEGAshortscript™ T7 Transcription Kit	Thermo Scientific
NucleoBond® Xtra Midi / Maxi	Macherey-Nagel
Pierce™ BCA Protein Assay Kit	Thermo Scientific
Plasmid Miniprep Kit I, peqGOLD	VWR Peqlab
Quick-RNA™MiniPrep	Zymoclean
TOPO® TA Cloning® Kit with pCR®2.1 TOPO®	Invitrogen

4.1.6 Chemicals and Reagents

1-kb Plus DNA ladder	Life Technologies
5× Herculase II Reaction Buffer	Aligent Technologies
50 mM $MgCl_2$	Thermo Scientific
5X First-Strand Buffer	Thermo Scientific
5X Phusion HF Buffer	Thermo Scientific
Acrylamide/bisacrylamide mixture, Rotiphorese® Gel 40	Roth
Bovine serum albumin (BSA), pH 7.0	PAA
BsmbI	Thermo Scientific
CoralLoad PCR Buffer	QIAGEN
CoralLoad PCR Buffer, 10X	QIAGEN
Dimethyl sulfoxide (DMSO)	Sigma-Aldrich
DMEM, high glucose, GlutaMAX™ Supplement, pyruvate	Thermo Scientific
DPBS, no calcium, no magnesium	Thermo Scientific
DTT	Thermo Scientific

EcoRV	Thermo Scientific
Exonuclease I	Thermo Scientific
FastAP™ Thermosensitive Alkaline Phosphatase or Shrimp	Thermo Scientific
FastDigest *BbsI* (BpiI)	Thermo Scientific
FastDigest buffer, 10X	Thermo Scientific
Fetal bovine serum (FBS)	Biowest
Fluoromount-G	Southern Biotech
GlutaMAX™ Supplement	Gibco
Herculase II Fusion DNA Polymerase	Aligent Technologies
Herculase II 5X reaction buffer	Agilent Technologies
Hi-Di™ Formamide	Thermo Scientific
Hoechst 33258	Invitrogen
Horse serum (HS)	Sigma
HotStarTaq *Plus* DNA Polymerase	QIAGEN
Krebs-Ringer Bicarbonate Buffer	Sigma
Lipofectamine® 2000 Reagent	Invitrogen
Laminin (from mouse Engelbreth-Holm-Swarm sarcoma)	Roche
M16 medium	Sigma
M2 medium	Sigma
MluI	Thermo Scientific
Nerve Growth Factor 2.5S subunit (NGF)	Invitrogen
Opti-MEM I reduced-serum medium	Gibco
PageRuler	Thermo Scientific
PageRuler Plus Prestained Protein Ladder	Thermo Scientific
Penicillin-Streptomycin (P/S), 5,000 U/mL	Gibco
Phusion High-Fidelity DNA Polymerase	Thermo Scientific
Poly-L-lysine hydrobromide (PLL)	Sigma
PrecisionX™ Cas9 SmartNuclease mRNA (Eukaryotic version)	System Biosciences
Protease Inhibitor Cocktail Tablets	Roche
PscI	Thermo Scientific
PVDF membrane (0.45 µm)	Amersham Hybond™

QIAGEN PCR Buffer, 10X	QIAGEN
QuickExtract DNA extraction solution	Epicentre
Random Primers	Thermo Scientific
RNaseOUT™	Thermo Scientific
Roswell Park Memorial Institute 1640 Medium	Gibco
SuperScript ® III Reverse Transcriptase	Thermo Scientific
SmaI	Thermo Scientific
T4 DNA Ligase	Thermo Scientific
T4 DNA Ligase Buffer (10X)	Thermo Scientific
TRIzol® reagent	Thermo Scientific
UltraPure DNase/RNase-free distilled water	Gibco
SsoAdvanced™ Universal SYBR® Green Supermix	Bio-Rad
XcmI	Thermo Scientific

4.2. Methods

4.2.1 General molecular biology methods

4.2.1.1 Preparation of competent bacteria

The prerequisite for bacteria to undergo transformation is their ability to take up free, extracellular genetic material. Such bacteria are termed competent cells and are needed for the amplification of plasmid DNA. For the preparation of competent bacteria, a preculture of *E. coli* XL1 Blue was grown overnight at 37°C in 2 ml LB broth medium (4 mM $MgSO_4$, 10 mM KCl, 3 µg/ml tetracycline, pH 7.0). The following morning, 1 ml of the preculture was inoculated with 500 ml broth medium and grown at 37°C in a shaking incubator until an optical density at 600 nm (OD600) of 0.3-0.6 was reached. Bacteria were cooled on ice and then centrifuged at 3000 rpm for 5 minutes at 4°C. The pellet was resuspended in 150 ml ice-cold TFB1 buffer (15% glycerol, 10 mM $CaCl_2$, 30 mM potassium acetate, 100 mM RbCl, 50 mM $MnCl_2$, pH 5.8) and incubated on ice for 60 minutes. Afterwards, the bacterial suspension was centrifuged again at 3000 rpm for 5 minutes at 4°C, and the pellet was resuspended in ice-cold TFB2 buffer (15% glycerol, 10 mM MOPS, 75 mM $CaCl_2$, 10 mM RbCl). The competent cells were quickly aliquoted, frozen in liquid nitrogen, and stored at -80°C.

4.2.1.2 Bacterial transformation

An aliquot of competent bacteria was thawed on ice for 30 min. Transformation was performed by adding 1 µg of plasmid DNA to 50 µl of competent *E.coli* XL-1 Blue bacteria followed by incubation on ice for 5 min. For the heat shock, tubes were placed into a 42°C water bath for 60 seconds and placed back on ice for 2 min. Afterwards, 250 µl of SOC medium (0.5% yeast extract, 2% tryptone, 10 mM NaCl, 2.5 mM KCl, 10 mM MgCl2, 10 mM MgSO4, 20 mM Glucose, pH 7.0) were added and bacteria were grown at 37°C for 1 hr in a shaking incubator at 300 rpm. Then, cells were centrifuged at 3000 rpm for 10 min. 200 ul of supernatant fraction were removed, and cells were resuspended and plated on LB agar (1% NaCl, 1% tryptone, 0.5% yeast extract, 1.5% agar, pH 7.0) containing antibiotics according to the resistance marker encoded by the plasmid DNA to be amplified. LB agar plates were incubated at 37°C overnight.

4.2.1.3 Midi preparation of plasmid DNA

Applications like mammalian cell transfection require large amounts of highly pure DNA. To achieve high-quality DNA, a single bacterial colony was inoculated in 200 ml LB medium (1% NaCl, 1% tryptone, 0.5% yeast extract, pH 7.0) supplemented with the respective antibiotic. Bacteria were grown at 37°C in a shaking incubator overnight. Purification of plasmid DNA was done using the NucleoBond® Xtra Midi/Maxi Kit following the manufacturer's instructions. Following alkaline lysis of bacteria, the plasmid DNA was purified on an anion-exchange column. Eluted plasmid DNA was precipitated with isopropanol, washed with 70% ethanol, dried, and resolved in an appropriate volume of TE buffer (10 mM Tris-HCl pH 7.5, 1 mM EDTA). DNA concentration and purity were assessed by absorbance at 260 nm and 280 nm (NanoDrop 2000©, Thermo Scientific).

4.2.1.4 Minipreparation of plasmid DNA

A single bacterial colony was inoculated in 2 ml of LB medium supplemented with the respective antibiotic. Bacteria were grown at 37°C in a shaking incubator overnight. Purification of plasmid DNA was done using the peqGOLD Plasmid Miniprep Kit I following the manufacturer's instructions. In brief, after alkaline lysis of bacteria, the plasmid DNA was purified on an anion-exchange column and further eluted in 50 µl of distilled water. DNA concentration and purity were assessed by absorbance at 260 nm and 280 nm.

4.2.1.5 Agarose gel electrophoresis

Separation of DNA fragments from PCR reactions or restriction digests was achieved by horizontal gel electrophoresis in agarose gel chambers. Agarose gel concentration was 1-2 % depending on the purpose and size of the DNA fragments to be separated. Agarose was boiled in 1X TAE buffer (40 mM Tris-acetate, 1 mM EDTA). Before casting the gel, 0.5 µg/ml ethidium bromide was added. To assist gel loading and monitor DNA separation, DNA samples were mixed with 5X DNA loading buffer (30% glycerine, 0.25% bromophenol blue, and 0.25% xylene cyanol). DNA fragments were separated by applying a constant voltage between 30-150 V depending on the desired separation time. After separation, DNA was visualised under UV light.

4.2.1.6 Non-denaturating polyacrylamide gel electrophoresis (PAGE)

In the absence of denaturants, double-stranded DNA (dsDNA) retains its double helical structure and can be separated (fragments of up to 1000 bp) on non-denaturating polyacrylamide gels (native PAGE). In this type of gel, the mobility of dsDNA is affected not only by its size but also by its sequence composition, as certain sequences may cause bending of the helical structure leading to slow migration of the fragment hampering the determination of molecular weight.

This principle can be used for the identification of genome-modified mice or cells carrying CRISPR/Cas9-mediated indel mutations with high sensitivity and accuracy. After DNA isolation from mouse tails or cells, the genomic region spanning the sgRNA binding site was amplified by PCR using CoralLoad PCR Buffer. This buffer can be used to directly load the PCR reaction onto a gel as it contains two marker dyes - an orange dye and a red dye - that facilitate estimation of DNA migration distance. PCR fragments from genetically modified animals or cells, which contain a mixture of indel mutations and wild-type alleles, form both heteroduplex and homoduplex DNA (Figure 6A). Due to the existence of an open angle between matched and mismatched DNA strands caused by indel mutations, heteroduplex DNA migrates at a significantly slower pace than homoduplex DNA during native PAGE. Therefore, one can assess the number and even the type of indel mutations simply based on their heteroduplex mobility pattern. Hence, Non-denaturating gels are a useful tool to screen mice or cells harbouring indel mutations (Figure 6B) as it provides additional information to standard denaturating gels (*137*).

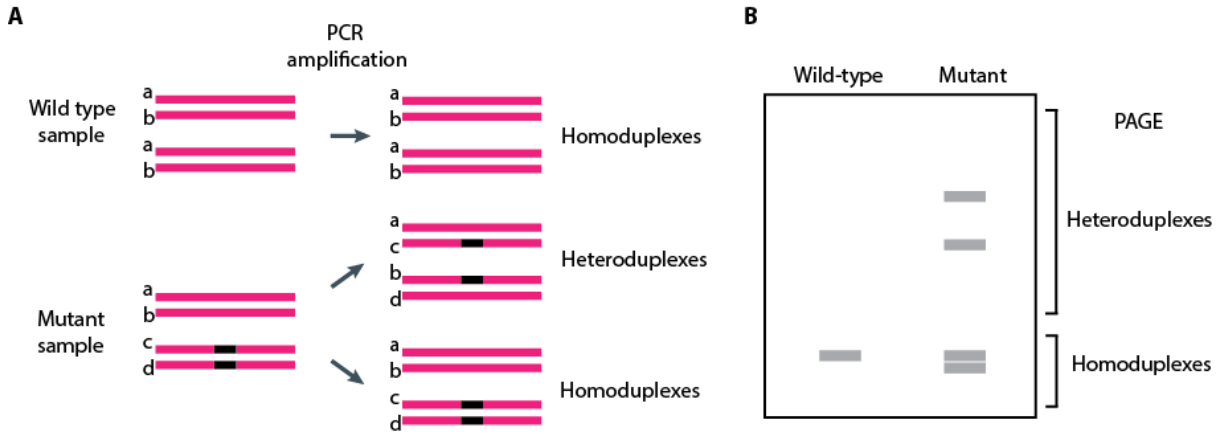

Figure 6. Schematic overview of PAGE-based genotyping protocol

(A) Diagram of heteroduplex DNA formation during denaturation and annealing. Pink bars represent four DNA strands (a–d) in mice or cells harbouring monoallelic mutations (black bars). Following denaturation and annealing produced during PCR amplification, heteroduplex DNA, as well as two different types of homoduplex DNA, are formed in samples with mutations. (B) Detection of heteroduplex DNA fragments by 5% PAGE assay. Since heteroduplex DNA migrates slower due to formation of an open angle between matched and unmatched genomic regions, homoduplex and heteroduplex DNA can be easily identified according to their mobility rate (*137*). Figure adapted from Zhu et al. 2014 (*137*).

Washed plates were assembled with a 0.75 mm spacer for casting acrylamide gels. The PCR products were resolved by electrophoresis in a gel containing 5% acrylamide-bisacrylamide, 10X TBE buffer (1 M Tris base, 1 M Boric Acid, 0.02 M EDTA), Ammonium Persulfate and TMED. After 1 hr electrophoresis at 100 V in 1X TBE buffer run in a Mini-PROTEAN®3 System (Biorad), polyacrylamide gels were immersed in 0.5% ethidium bromide solution for 10 min before visualisation under UV light.

As it is not possible to identify homozygous indel mutations unless PCR products from wild-type and mutant alleles are mixed, following the standard genotyping analysis by loading PCR samples directly onto the 5% gels, 10 µl of each mutant and wild-type PCR products were mixed. A drop of paraffin oil was added on top of the solution and placed in boiling water for denaturation. The PCR products were allowed to reanneal by leaving the solution in the water and let it cool at room temperature (RT) for at least 3 hr before loading onto the gel.

4.2.1.7 Digestion of plasmids and PCR Fragments

All DNA digestions were carried out using a final volume of 30 µl. In general, 3 µg of plasmid DNA or 5 µl of purified PCR product were mixed with 1 µl of enzyme plus 3 µl of the corresponding buffer. The digestion mixture was incubated for 3 hr or overnight at 37°C or 30°C, depending on the enzyme. After enzyme inactivation, the DNA was gel-purified.

4.2.1.8 DNA purification from agarose gels

Under UV light, DNA bands were excised quickly from the agarose gel using a sharp scalpel and placed into a 1.5 ml tube. DNA was purified using the Gel DNA Recovery Kit. Following addition of 500 µl of agarose dissolving buffer to the agarose gel slice and incubation at 56°C for 10 min, the melted agarose solution was transferred to a Zymo-Spin™ Column in a collection tube and centrifuged for 60 seconds. The flow-through was discarded, and 200 µl of DNA Wash Buffer were added to the column and centrifuged for 30 seconds two times. An appropriate volume of distilled water ranging from 5 to 20 µl was directly added to the column matrix and centrifuged for 2 min at full speed to elute DNA.

4.2.1.9 DNA ligation

To clone plasmid constructs, insert, and vector fragments with compatible ends were ligated. A typical ligation mixture was performed in a total volume of 20 µl containing 1 µl of T4 DNA Ligase, 2 µl of T4 DNA Ligase Buffer, 1 µl of vector DNA, and different amounts of insert ranging from 1 to 6 µl. The ligation mixture was incubated overnight at 4°C, and 5 µl of the ligation reaction were used to transform chemo-competent bacteria.

4.2.1.10 Colony PCR

To sequence independent alleles, Taq polymerase-amplified PCR products were cloned into pCR®2.1 TOPO® vector using the TOPO® TA Cloning® Kit. The plasmid is supplied linearized with 3′-deoxythymidine (T) overhangs and Topoisomerase I covalently bound to the vector. Taq polymerases have a nontemplate-dependent terminal transferase activity that adds a single deoxyadenosine (A) to the 3′ ends of PCR products. This allows PCR inserts to ligate efficiently with the vector. A reaction mix containing 1 µl of Salt Solution, 1 µl of TOPO vector, 4 µl of PCR product and 4 µl of water was prepared. Following incubation at RT (22–23°C) for 10 min, 5 µl of the reaction mixture were used to transform competent bacteria. The following day, DNA was extracted from 10 colonies using the QuickExtract™ DNA Extraction Solution, which can be used to rapidly and efficiently extract PCR-ready genomic DNA. Each bacterial colony was resuspended in 5 µl of this solution and incubated for 6 min at 65˚C followed by 2 min at 98˚C. The resulting DNA was used as a template for PCR amplification of inserts using the M13 forward (fwr; 5′-GTAAAACGACGGCCAG-3′) and reverse (rev; 5′-CAGGAAACAGCTATGAC-3′) primers provided with the kit. 2.5 µl DNA were used in a single PCR mix containing 0,1 µl of HotStarTaq *Plus* DNA Polymerase, 0.5 µl dNTPs, 2 µl of 10X QIAGEN PCR Buffer, and 1 µl of each primer. The amplification was carried out in a

PCR thermal cycler using the following program: 5 min at 95˚C, 40 cycles of 20s at 95˚C, 20s at 50˚C, 40s at 72˚C followed by a final 10 min extension step at 72˚C. The amplified DNA fragments were mixed with 5 µl of 5x DNA loading buffer and separated on a 2% agarose gel. Only the colonies containing an insert were sequenced.

4.2.1.11 DNA Sequencing

Sequencing of plasmids and PCR products was carried out using the BigDye Terminator v1.1 Cycle Sequencing Kit. Briefly, 3 µl of PCR product was cleaned in a reaction volume of 10 µl containing 1 µl of ExoSAP (1 Exonuclease I: 2 FastAP™ Thermosensitive Alkaline Phosphatase or Shrimp Alkaline Phosphatase) that removes unincorporated primers and degrades unincorporated nucleotides. The mixture was incubated at 37˚C for 15 min followed by 15 min at 80˚C. Sequencing PCR was performed in a reaction volume of 10 µl containing 5 µl of purified PCR product or 1 µl of plasmid, 1 µl Ready Reaction Mix, 2 µl BigDye Terminator v1.1 Sequencing Buffer and 0.5 µl of a 10 pmol/µl solution of the corresponding primer. The amplification was carried out in a PCR thermal cycler using the following program: 15s at 96˚C, 27 cycles of 15s at 96˚C, 15s at 55˚C, 4 min at 60˚C. Purification of this PCR product was done by adding 2 µl of sodium acetate (3 M, pH 5.2) and 50µl of 100% ethanol, incubated at RT for 15 min and then centrifuged for 30 min at 14000 rpm. The pellet was washed two times by adding 50 µl of 70% ethanol and centrifugation for at 14000 rpm. The supernatant fraction was removed, and the sample was dried for 15 min at RT, and 10 µl of Hi-Di™ Formamide were later added to each sample. Automated electrophoreses were performed on a capillary electrophoretic ABI 3130 genetic analyser (Applied Biosystems). Sequences were aligned and analysed with Benchling (www.benchling.com) or SnapGene® software (from GSL Biotech; available at www.snapgene.com).

4.2.1.12 Isolation of RNA from cells

For the isolation of RNA from cells, the *Quick-RNA*™ MiniPrep Kit was used following the manufacturer's instructions. Briefly, cells were plated in 10 cm dishes and grown at 37 ˚C. When confluent, cells were washed two times with DPBS and lysed by adding 600 µl RNA Lysis Buffer directly to the monolayer. Afterwards, the RNA was purified on an anion-exchange column and further eluted in 30 µl of UltraPure DNase/RNase-free distilled water. RNA concentration and purity were assessed by absorbance at 260 nm and 280 nm.

4.2.1.13 Isolation of RNA from tissue samples

Mice were sacrificed via cervical dislocation and tissue was collected, frozen in liquid nitrogen, and stored at -80°C. The following day, the tissue was ground with a mortar and pestle into powder using liquid nitrogen and transferred to a 50 ml falcon. 1 ml TRIzol® reagent was added per 100 mg tissue. Samples were thoroughly vortexed and incubated for 5 min at RT and centrifuged for 5 minutes at 4,000 g at 20°C. The supernatant fraction was transferred to a new tube. 200 µl of chloroform per 1 ml TRIzol® was added. Samples were shaken by hand for 30 seconds followed by 2 min incubation at RT and subsequently centrifuged at 14,000 rpm at 4°C for 15 minutes. The aqueous phase (upper) was transferred to a new tube, and the RNA was precipitated by adding 1 volume of isopropanol followed by 10 minutes incubation at RT and centrifuged at 13000 rpm at 4°C for 10 minutes. The resulting RNA pellet was washed with 75% ethanol, dried, carefully solved in UltraPure DNase/RNase-free distilled water, and stored at-80°C until further use.

4.2.1.14 Reverse transcription

To analyse the expression of the different genes, RNA was extracted from cells or tissue, and complementary DNA (cDNA) was generated using SuperScript ® III Reverse Transcriptase. For each reaction, 5 µg of total RNA were mixed with 1 µl Random Primers, 1 µl 10 mM dNTP mix completed to a final volume of 13 µl with UltraPure DNase/RNase-free distilled water. The reaction was incubated at 65°C for 5 min, then placed on ice for at least 1 min. Afterwards, 4 µl of 5X First-Strand Buffer, 1 µl 0.1 M DTT, 1 µl RNaseOUT™, and 1 µl SuperScript® III were added. The reaction mixture was incubated for 5 min at 25°C followed by 60 min at 50°C, and 70°C for 15 min. cDNA synthesis reactions were stored at −20°C.

4.2.2 Generation of *Ntrk1*-KO PC12 cells and functional characterization of NTRK1 mutants

4.2.2.1 Maintenance of PC12 cells

Rat PC12 cells were grown at 37°C (5 % CO2) in supplemented RPMI medium (Roswell Park Memorial Institute 1640, containing high glucose, 1 % GlutaMAX™ Supplement, 1 % pyruvate, plus 10% FBS, 1 % P/S). Cells were seeded onto T-75 cm^2 flasks coated with 0.1 mg/ml poly-D-lysine hydrobromide and split every 3 to 4 days at a ratio of about 1:2. For splitting, cell culture medium was removed, and the cell layer was gently rinsed with phosphate-buffered saline (PBS) to remove traces of serum. Fresh medium was pipetted onto

the cells that were detached by pipetting up and down extensively and by slightly hitting the flask. Cells were collected into a falcon and centrifuged at 1500 rpm for 5 min. The cell pellet was resuspended in 1 ml of fresh medium, and a syringe was used to de-aggregate cell clusters. Appropriate aliquots of cell suspension were transferred into flasks according to the required split ratio.

For storage, cells were suspended in freezing medium (90% FBS, 10% DMSO) and aliquotted into freezing phials at a density of about 2 x 10^6 cells/ml. For a slow cooling process, freezing phials were placed in an isopropanol freezing container and placed to -80°C for 24 h. The following day, phials were transferred into a nitrogen tank for long-term storage. Thawing of cells was performed rapidly by incubation in a water bath at 37°C for 5 min. Afterwards, cells were washed immediately and resuspended in fresh prewarmed cell culture medium.

4.2.2.2 Generation of GFP-expressing NmeCas9 targeting DNA constructs

For the selection of transfected cells by cell sorting, a GFP cassette was introduced into the pSimpleII-U6-tracrRNA-U6-BsmBI-NLSNmCas9-HA-NLS(s) (Addgene #47868, Plasmid map 1), which expresses NmeCas9, tracrRNA and a U6-BsmBI cassette for the generation of the crRNA. The GFP cassette was amplified from the peGFP-N1 plasmid using primers containing *EcoRV* restriction sites on the 5' (Table 3) in a reaction mix containing 15 ng of plasmid DNA, 1 µl of Phusion High-Fidelity DNA Polymerase, 1 µl dNTPs, 2 µl of 5X Phusion HF Buffer. The amplification was carried out in a PCR thermal cycler using the following program: 30s at 98°C, 5 cycles of 10s at 98°C, 20 s at 59°C, 30s at 72°C, followed by 23 cycles of 10s at 98°C, 20 s at 56°C, 30s at 72°C following a final 10 min extension step at 72°C. The amplified DNA fragment was gel purified and digested with *EcoRV*. The pSimpleII-U6-tracrRNA-U6-BsmBI-NLSNmCas9-HA-NLS plasmid was digested with *SmaI. B*oth fragments were ligated to generate the pSimpleII-U6-tracrRNA-U6-BsmBI-NLSNmCas9-HA-NLS-CMV-GFP plasmid (Plasmid map 2).

A 24-nt-guide RNA (gRNA) was designed to target Exon 5 of *Ntrk1* with the design tool available at Benchling (www.benchling.com) using the rat genome assembly rn6 (*Rattus norvegicus,* Rnor_6.0). This online based tool takes an input sequence, identifies and ranks suitable target sites, and computationally predicts off-target (OT) sites for each intended target based on the specificity analysis performed in Hsu et al, 2013 (*138*) as well as an activity score for each sgRNA based on Doench et al. 2014 (*139*) (high scores reflect higher specificity).

Afterwards, the pSimpleII-U6-tracrRNA-U6-BsmBI-NLSNmCas9-HA-NLS-CMV-GFP plasmid was digested with *BsmbI,* and the linearized vector was gel purified. A pair of partially complementary DNA oligos containing the 24-nt-gRNA and the processed crRNA sequence with four nucleotide overhangs compatible with those generated by *BsmbI* was ordered. As the U6 promoter requires a 5' guanine (G) to start transcription, the first nucleotide of the gRNA sequence was replaced by a G (Table 3). To be cloned into the vector, partially complementary oligos were annealed. First, stock solutions of the oligos were prepared to a final concentration of 100 pmol/µl. Next, 200 µl of paraffin oil were added on top of a solution containing 30 µl of each forward and reverse oligos, placed in boiling water, and let cool for at least 3 hr. The annealed oligos were then used for ligation with the linearized plasmid. The construct was further sequenced to check for correct insertion.

Table 3. List of DNA oligos used for cloning GFP and gRNA into pSimpleII-U6-tracrRNA-U6-BsmBI-NLSNmCas9-HA-NLS(s)

Primer name	*Sequence (5'to 3')*	*Expected size (bp)*
eGFP_F	GGGGATATCCGTTACATAACTTACGGTAAATGG	1600
eGFP_R	GGGGATATCTAAGATACATTGATGAGTTTGGACAAAC	
g*Ntrk1*-Ex5_F	CACCGTTGTGGCTCCAGCGCTGGGAGCAGTTGTAGCTCCCTTTCTCATTTCG	
g*Ntrk1*-Ex5_R	AAAACGAAATGAGAAAGGGAGCTACAACTGCTCCCAGCGCTGGAGCCACAAC	

4.2.2.3 Transfection of NmeCas9, trRNA, and crRNA expressing plasmid into PC12 cells

For transient protein overexpression, cells were transfected with pSimpleII-U6-tracrRNA-U6-crRNA (Exon 5 *Ntrk1*) NLSNmCas9-HA-NLS-eGFP using Lipofectamine®2000 transfection reagent. Cells were seeded in 10-cm-culture-dish and allowed to reach about 80% confluence while maintained in cell culture medium. On the day of transfection, cells were washed three times with Opti-MEM®. After 2 hr incubation in Opti-MEM® containing 1 % P/S, cells were transfected with a solution of 10 µg of DNA and 10 µl of Lipofectamine®2000 prepared in Opti-MEM®. Following incubation for 4 hr with the transfection mixture, the medium was replaced with fresh medium.

4.2.2.4 Cell sorting

48 hr post-transfection cells were harvested, washed three times in DPBS, and incubated on ice. Before sorting, cells were incubated for 5 min in DPBS with 2% FBS containing 4,6-

Diamidino-2-phenylindole (DAPI; 0,1µg/ml) to exclude dead cells. Cells were sorted in a BD FACS ARIAIII flow cytometer (BD Biosciences, USA). GFP-positive cells were collected on culture media, and serial dilutions were made to reach a concentration of 10 cells per ml. Afterwards, cells were seeded on ten 96-well-plates coated with 0.1 mg/ml poly-D-lysine hydrobromide for clonal isolation.

4.2.2.5 CRISPR-genome-edited-PC12-cells genotyping

For DNA extraction, 96-well-plate replica plates were generated containing single clones. Cells were washed two times with DPBS and 10 µl QuickExtract™ DNA Extraction Solution was used to extract DNA by pipetting up and down. The DNA was incubated for 6 min at 65˚C followed by 2 min at 98˚C, and the concentration and purity were assessed by absorbance at 260 nm and 280 nm. Samples were diluted in low TE buffer (10 mM Tris-HCl, 0.1 mM EDTA) to reach a concentration of 200-400 ng/µl. The resulting DNA was used as a template for PCR amplification using two primers spanning the gRNA cut site (*Ntrk1*_Exon5_F: 5´-TTCTGCC TAGACCCCTTGGT-3´; *Ntrk1*_Exon5_R:5'-ATCTAAGTGTGGGCTGGTGAG-3'; product size: 409 bp). 2.5 µl DNA were used in a single PCR mix containing 0,1 µl of HotStarTaq *Plus* DNA Polymerase, 0.5 µl dNTPs, 2 µl of 10X QIAGEN PCR Buffer, and 1 µl of each primer. The amplification was carried out in a PCR thermal cycler using the following program: 5 min at 95˚C, 40 cycles of 20s at 95˚C, 20s at 64˚C, 35s at 72 ˚C followed by a final 10 min extension step at 72˚C. 15 µl of the amplified DNA was mixed with 5 µl of 5x DNA loading buffer and separated on a 2% agarose gel and 5 µl were used for sequencing. PCR amplified products were also analysed by non-denaturating polyacrylamide gel electrophoresis (PAGE) as described in section 4.2.1.6.

4.2.2.6 Off-target analysis

Potential off-target (OT) sites in the rat genome (*Rattus norvegicus,* Rnor_6.0) were identified and ranked using the design tool from Benchling (www.benchling.com), which allows for up to four mismatches in the target gRNA sequence. Also, COSMID (https://crispr.bme.gatech.edu/) (*140*), which enables the identification of OTs with up to three base mismatches without insertions or deletions and two base mismatches with either an inserted or deleted base (bulge), was used. Specific primers for each OT were designed (Table 4), and PCR amplification was carried out from DNA of the two clones presenting a homozygous deletion to determine if any mutations or changes occurred in these sites. For each PCR reaction, 2.5 µl DNA were used in a single PCR mix containing 0,1 µl of HotStarTaq *Plus* DNA Polymerase, 0.5 µl dNTPs, 2 µl of

buffer and 2 µl of each primer pair mix. The amplification was carried out in a PCR thermal cycler using the following program: 5 min at 95°C, 40 cycles of 30s at 95°C, 30 s at 57°C (for OT-1) or 59°C (for OT-2), 30s at 72°C, followed by a final 10 min extension step at 72°C. 15 µl of the amplified DNA was mixed with 5 µl of 5x DNA loading buffer and separated on a 2% agarose gel and 5 µl were used for sequencing (see section 4.2.1.11).

Table 4. Primers used for off-target-site amplification

Primer name	*Sequence (5' to 3')*	*Expected size (bp)*
OT1_F	AATGCCGAATGCCGTGGTAA	461
OT1_R	TAGGAAATAACTAAGGGCCTAAG	
OT2_F	CCTCTGAAGAAGTGACTGAGG	470
OT2_R	ATGGGGAGGCTCAGTGGC	

4.2.2.7 Gene expression analysis

To compare the expression of *Ntrk1* between wild-type and genetically modified clones, RNA was extracted from cells, and complementary DNA (cDNA) was generated according to section 4.2.1.12 and 4.2.1.14 respectively. To have a quantitative estimation of gene expression, quantitative real-time PCR (qPCR) amplification of WT and KO-PC12-cells cDNA was performed using a Bio-Rad C1000 Thermal Cycler-CFX96 Real-Time system (Bio-Rad). All samples were run in triplicate in a final volume of 5 µl containing 1 µl of cDNA, 1 µM of primers and SsoAdvanced™ Universal SYBR® Green Supermix (BioRad). Before qPCR, a 5 min enzyme activation step was done at 95°C. The qPCR protocol consisted of 10s denaturation at 95 °C, 15s at annealing temperature at 60 °C, 30 s elongation at 72 °C for 45 cycles. The annealing temperature was confirmed by the melting curve.

Table 5. Primers used for cDNA amplification

Primer name	*Sequence (5' to 3')*	*Expected size (bp)*
cDNA_*Ntrk1*_F	GTTGAGAAGCCTAACCATCGTG	163
cDNA_*Ntrk1*_R	TGACAGGGTCAAGTCCTGTAG	
*Gapdh*_F	AGGTCGGTGTGAACGGATTTG	355
*Gapdh*_R	GCGGAGATGATGACCCTTTTG	

4.2.2.8 Sequencing and segregation studies

All patients analysed presented the minimal clinical features of HSAN-IV. Written informed consent was given by the patients and the parents. Genomic DNA was extracted from peripheral blood samples of the affected individuals and their parents (when available). Next-generation sequencing (NGS-panel analysis) was performed and included the exons and intron–exon boundaries of transcript variant 2 of *NTRK1* (RefSeq ID NM 002529.3), which is the full-length isoform and thought to be the main variant expressed in neuronal tissue (*141*). Direct bidirectional Sanger sequencing of the amplified DNA fragments harbouring putatively pathogenic mutations was performed. The resulting sequences were analysed using the multiple sequence alignment tool included in SnapGene® software (from GSL Biotech; available at www.snapgene.com) and compared with the current reference sequence for *NTRK1* in the NCBI database (NM_002529.3), corresponding to the amino sequence NP_002520.2. Sequencing reactions and alignments to the reference human transcriptome were repeated twice. The level of evolutionary conservation of the affected residues was analysed using Protein Blast (https://blast.ncbi.nlm.nih.gov/Blast.cgi?PAGE=Proteins) (*142*). The relevance of identified variants was evaluated by online prediction tools including the Human Gene Mutation Database (HGMD, http://www.biobase-international.com/) and in-silico pathogenicity programs Mutation Taster (http://www.mutationtaster.org/) (*143*), PolyPhen-2 (*144*) (http://genetics.bwh.harvard.edu /pph2/) and by SIFT (*145*) (http://sift.jcvi.org/www/SIFT_enst_submit.html). Allele frequency of the variants was determined using ExAC, dbSNP, EVS, 1000genomes.

4.2.2.9 Cloning of *NTRK1* expression constructs

The wild-type full-length human *NTRK1* (RefSeq ID NM 002529.3) construct was obtained from GenScript (Plasmid map 3). A C-terminal myc-tag was introduced into this plasmid by site directed mutagenesis using the *NTRK1*-myc forward and reverse primers (Table 6). Briefly, 20 ng of pCI-neo-*NTRK1* plasmid were used as template for PCR amplification of a 471 bp fragment using Herculase II fusion Polymerase. The amplification was carried out in a PCR thermal cycler using the following program: 2 min at 95°C, 40 cycles of 20 s at 95°C, 30 s at 62°C, 30s at 72°C followed by a final 3 min extension step at 72°C. The PCR product and the pCI-neo-*NTRK1* were digested with *MluI* and *EcoRV* and gel-purified. A ligation was performed to generate the pCI-neo-*NTRK1*-myc (Plasmid map 4) plasmid.

To produce the mutant constructs, the pCI-neo-*NTRK1*-myc was used as template for the amplification of two smaller fragments to introduce the desired mutations. The reaction was performed in a 50 µl final volume containing 15 µg plasmid, 10 µl 5× Herculase II Reaction Buffer, 0.5 µl 100 mM dNTPs, 1.25 µl of each primer (Table 6) and 0.5 µl of Herculase II Fusion DNA Polymerase. The amplification was carried out in a PCR thermal cycler using the following program: 2 min at 95°C, 40 cycles of 20s at 95°C, 30s at 62 or 61°C, 30s or 45s at 72°C followed by a final 3 min extension step at 72°C. The PCR products were gel-purified and used as template for a second PCR with similar conditions to generate a longer fragment. These fragments as well as the pCI-neo-*NTRK1*-myc plasmid were digested with *XcmI* and *EcoRV* and ligated to generate three mutant pCI-neo-*NTRK1*-myc plasmids termed: pCI-neo-*NTRK1*-myc-I, pCI-neo-*NTRK1*-myc-II, pCI-neo-*NTRK1*-myc-III, according to the respective mutation.

Table 6. Primers used for the generation of *NTRK1* constructs

Primer name	*Sequence (5' to 3')*	*Purpose*
NTRK1-Myc-F	CCAGGGACTGGTGGTCAAGA	Myc tag
NTRK1-Myc-R	ACGCGTTCACAGATCCTCTTCAGAGATGAGTTTCTGCTCGCCCAGGAC ATCCAGGTAGAC	
NTRK1-I-myc_F	CGTGGCTAGCCGGGTCGCT	Mutation C to A (I)
NTRK1-I-myc_F	AGCGACCCGGCTAGCCACGGC	
NTRK1-II-myc_F	GTGTTCACCACAACAAGCGCCGG	Mutation T to A (II)
NTRK1-II-myc_R	TCCCGGCGCTTGTTGTGGTGAAC	
NTRK1-III-myc_F	TGCTGGCTGCCAAACCCTTC	Mutation A to G (III)
NTRK1-III-myc_F	GAAGGGTTTGGCAGCCAGCA	
NTRK1-Mut-Myc-F	GTGTGCCCACGCTGAAGGT	
NTRK1-Mut-Myc-R	CGGCCTCCCACACGGTAATAGT	

4.2.2.10 Transfection of NTRK1 expression constructs into PC12 cells

In order to achieve a high transfection efficiency, PC12 cells were transfected using the Amaxa SF cell line 4D-Nucleofector X Kit in a 4D-Nucleofector™ X-Unit (Lonza). Cells were seeded onto T-75 cm^2 flasks coated with 0.1 mg/ml poly-D-lysine hydrobromide. On the day of transfection, cells were detached, collected into a falcon and centrifuged at 1500 rpm for 5 min. The cell pellet was resuspended in 1 ml of DPBS, and a syringe was used to de-aggregate cell clusters. For each 20 µl transfection reaction, 4 x 10^5 cells were centrifuged in 1.5 ml tubes and

resuspended in a solution containing 2 µg (1 µg/µl) of plasmid DNA, 16.4 µl of SF Nucleofector® Solution plus 3.6 µl of Supplement 1. The cell suspension was transferred into a cuvette and placed inside the Nucleofector® Cuvette Holder, and the Nucleofector® Program EO-100 was applied. Once the program finished, 100 µl of warm culture medium was added to the cuvette followed by incubation for 5 min at RT. Afterwards, the cells were transferred into 12 or 6 well plates, and fresh medium was added. For a 100 µl reaction, 10 µg (1 µg/µl) of plasmid DNA, 82 µl of SF Nucleofector® Solution plus 18 µl of Supplement 1 were used to transfect 2 x 10^6 cells.

4.2.2.11 Neurite outgrowth assay

PC12 cells were seeded on coverslips coated with 0.1 mg/ml poly-D-lysine hydrobromide and 5 ug/ml laminin to promote adhesion. Cells were treated with 100 ng/ml NGF in RPMI supplemented with 1% HS for 3 or 7 days, with media being replaced every 3 days. Cells were then washed in DPBS and fixed in warm 4% paraformaldehyde, permeabilised (PBS, 0.25% Triton-X at RT for 20 min), blocked (DPBS, 0.25% Triton-X and 5% normal goat serum at RT for 1 hr) and stained overnight at 4°C with α-Acetylated tubulin and anti-myc antibodies. The following day cells were stained with secondary antibody (diluted 1:2000 in blocking solution, 2 hr at RT) and nuclei were stained with Hoechst-33258 (1:10000 in DPBS, 10 min at RT) and slightly washed. Cells were imaged with a Leica TCS SP5 confocal scanning fluorescence microscope using a 20X or 40X objective. Cells were analysed using the ImageJ software. A neurite was identified as being more than twice the cell body diameter. Neurite length per cell was quantified as the longest neurite measured for each cell (*146*). Percentage of cells bearing neurites was calculated from the same data as the number of cells with neurites divided the total number of cells in that field of view (for WT vs KO cells).

4.2.2.12 Immunocytochemistry

48 hr post-transfection, HeLa cells were fixed with fixative solution (4% paraformaldehyde (PFA) in DPBS, pH 7.4) at RT for 20 min and rinsed three times with DPBS for 5 min. For permeabilization, cells were incubated with PBS, 0.25% Triton-X at RT for 20 min. Next, cells were incubated with blocking solution (DPBS, 0.25% Triton-X and 5% normal goat serum) at RT for 1 hr and incubated with primary antibody (see Table 1) diluted in blocking solution at 4°C overnight. For co-stainings, a mixture of primary antibodies was applied. The following day, cells were washed three times with DPBS for 10 min each. Afterwards, secondary antibodies (see Table 1) diluted 1:2000 in blocking solution were incubated at RT for 1 hr

followed by a washing step with DPBS. Following nuclei staining with Hoechst-33258 (1:10000 in DPBS) for 10 min at RT, cells were washed three times with DPBS. Finally, coverslips with stained cells were mounted with Fluoromount-G (Southern Biotech) on microscope slides and analysed with a Leica TCS SP5 confocal scanning fluorescence microscope equipped with a 63x objective.

4.2.2.13 Cell stimulation with NGF

Upon stimulation with Nerve Growth Factor (NGF), wild-type PC12 differentiate into neurone-like cells due to the activation of diverse signalling pathways. For short-term stimulation of up to 30 min, the cells were starved for four hours in serum-free medium (RPMI containing 0.25% BSA). 30 min before stimulation with NGF (100 ng/ml), the medium was substituted with HEPES-buffered solution containing 0.25% BSA and cells were incubated at 37 ˚C without CO_2. NGF was added to this medium to a final concentration of 100 ng/ml. After 0, 5, 10 or 30 min, the cells were washed with ice-cold wash-lysis buffer (50 mM Tris base, 2 mM EDTA, 1mM EGTA, 50 mM NaF, 100mM $Na_4P_2O_7$, 1 mM Na_3VO_4, 1mM DTT, pH 7,4) and were incubated with lysis buffer (50 mM Tris base, 2 mM EDTA, 1mM EGTA, 50 mM NaF, 100mM $Na_4P_2O_7$, 1 mM Na_3VO_4, 1mM DTT, 1% Triton-X-100, 0,1 % SDS, 0.2 M PMSF, 10 µl/ml Protease Cocktail inhibitor) on ice for 15 min. The cells were then scraped off the plastic surface, and the collected cell lysates were centrifuged (700 *g*, 6 min, 4°C). The supernatant fraction was transferred to a new tube and stored at -20 C.

4.2.2.14 SDS-PAGE and Western blotting

Western blot analysis was performed together with Dr Katrin Spengler. Protein concentration was determined using the Lowry method and analysed spectrophotometrically. Afterwards, 3x Laemmli buffer (186 mM Tris pH 6.8, 10 mM EDTA, 15 % Glycerol, 9 % SDS, 6 % 2-Mercaptoethanol, 0.03 % Bromophenol blue) was added and proteins were denaturated for 5 min at 95 °C under gentle shaking. The proteins were separated by SDS-polyacrylamide gel electrophoresis (SDS-PAGE) according to their size together with a molecular size marker. SDS-gels consisting of stacking and a 7.5 % separating gel were run with electrode buffer (25 mM Tris, 192 mM Glycine, 1 % SDS) at 45 mA per gel for 2 hr. After electrophoresis, the separated proteins were transferred to a PVDF membrane by a wet-blot system in transfer buffer (25 mM Tris base, 192 mM glycine, 20 % methanol). The Western blot sandwich contained three pieces of Whatman filter paper overlaid by a methanol-activated PVDF membrane, the SDS-gel and another three pieces of Whatman filter paper. The transfer was

performed at 750 mA per gel for 100 min. Afterwards, the membranes were blocked by incubation in blocking solution containing 5 % milk in Tris-buffer saline (10 mM Tris pH 7.6, 1.5 m NaCl) supplemented with 0.1 % Tween-20 (TBS-T) at RT for 1 hr. Next, membranes were incubated in primary antibody solution (5 % BSA in TBS-T and primary antibody according to Table 2) under gentle agitation at 4 °C overnight. The next day, the membrane was washed four times with TBS-T for 5 min each followed by incubation in secondary antibody solution (5 % milk in TBS-T and secondary antibody according to Table 2) at RT with agitation for 60 min. After three more washing steps in TBS-T for 5 min each and two washing steps in TBS, immunodetection was performed by enhanced chemiluminescence (ECL). The membrane was incubated with ECL substrate for 1 min. The horseradish peroxidase enzyme linked to the secondary antibody cleaves the chemiluminescent agent producing luminescence. The luminescence was detected by a photosensitive film (Fujifilm). For reprobing, the membranes were washed and incubated in stripping buffer (62.5 Tris pH 6.7, 2 % SDS, 100 mM 2-Mercaptoethanol) for 35 min at 54°C under gentle shaking. Afterwards, membranes were washed and blocked again as described followed by incubation in another primary antibody solution. Finally, the films were scanned, and the protein bands were quantified with ImageJ software.

4.2.3 Generation of *Scn10a/Scn11a* double-knockout mice with CRISPR

4.2.3.1 Cloning of targeting sequences into pX330 plasmids and generation of sgRNAs by in vitro transcription

The bicistronic expression vector pX330-U6-chimeric_BB-CBh-hSpCas9 (Addgene #42230, Plasmid map 5) expressing human codon-optimized Cas9 (hSpCas9) and an sgRNA cloning site (*73*) was digested with *BbsI,* and the linearized vector was gel purified. A pair of partially complementary DNA oligos, containing the 20-nt-sgRNA sequence and 4-nt-overhangs compatible for cloning into the vector, was designed for each targeting site using CRISPR Design Tool (www.crispr.mit.edu) (*138*) or Benchling (www.benchling.com) (Table 7). Both online based tools take an input sequence, identify and rank suitable target sites, and computationally predict OT sites for each intended target based on the specificity analysis performed in Hsu et al., 2013 (*138*). Benchling also provides an activity score for each sgRNA based on Doench et al. 2014 (*139*). As the U6 promoter driving the expression of the sgRNA requires a 5' guanine (G) to start transcription, an additional G was added to the front of the sgRNA sequence in cases in which the target did not start with a G (Figure 7).

To be cloned into the pX330 vector, partially complementary oligos need to be annealed. First, stock solutions of the oligos were prepared to a final concentration of 100 pmol/µl. Next, 200 µl of paraffin oil was added on top of a solution containing 30 µl of each forward and reverse oligos, placed in boiling water, and let cool for at least 3 hr. The annealed oligos were then used for ligation with the digested pX330 plasmid. The respective construct was further sequenced to check for correct insertion.

For injection into zygotes, the sgRNA needs to be in vitro transcribed. *In vitro* transcription requires a purified linear DNA template containing a promoter, a buffer system that includes DTT and magnesium ions, ribonucleotide triphosphates, and an appropriate phage RNA polymerase. pX330 plasmids lack a T7 promoter site, which is needed by the T7 RNA Polymerase to start transcription; thus, a 120-bp PCR product containing T7 promoter, target and scaffold sequence is used as template for the in vitro transcription (IVT). The fwr primer (Table 7) introduces the T7 promoter sequence plus 2 G nucleotides (or only one in case the sgRNA sequence starts with G), needed for transcription initiation, into the sgRNA DNA template while the rev primer binds to the sgRNA scaffold (Figure 7) (*147*).

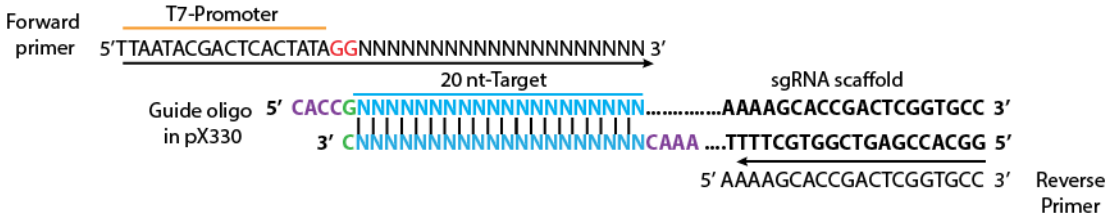

Figure 7. Schematic representation of annealed guide-oligos needed for cloning into pX330 vector and primers for IVT template amplification

The top strand guide oligo must contain a 5′-CACC while the bottom oligo a 5′-AAAC overhang (in violet). The top oligo is the one containing the 20-bp target sequence (blue bar on top strand) preceding the 5′-NGG PAM in the genomic DNA. A G-C base pair (in green) is added to the 5′ end of the guide sequence to enable U6 transcription (*148*). Moreover, for the production of a 120-bp PCR product to be used as template for in vitro transcription (IVT), a T7 promoter sequence (orange bar) followed by two G nt (or only one in case the sgRNA sequence starts with G) needs to be added to the forward primer, while the reverse primer anneals to the end of the sgRNA scaffold. N can be any nucleotide (*147*).

Therefore, the pX330 plasmid was diluted to a final concentration of 15 ng/µl and used as template for the amplification of the sgRNA-containing PCR fragment. The reaction was performed in a 50 µl final volume containing 1 µl of the diluted plasmid, 10 µl 5× Herculase II Reaction Buffer, 0.5 µl 100 mM dNTPs, 1.25 µl T7-sgRNA fwr primer and 1.25 µl T7-sgRNA Rev primer and 0.5 µl of Herculase II Fusion DNA Polymerase. The amplification was carried

out in a PCR thermal cycler using the following program: 2 min at 95°C, 40 cycles of 20s at 95°C, 30s at (Annealing Temp of the T7-sgRNA fwr primer, see Table 7) °C, 30s at 72°C followed by a final 3 min extension step at 72°C. The PCR product was gel purified and concentrated with DNA Clean & Concentrator™ Kit following the manufacturer' s instructions and eluted into UltraPure DNase/RNase-free distilled water.

The IVT was done using the MEGAshortscript™ T7 Transcription Kit following the manufacturers' instructions. The reaction was performed in a 20 µl volume containing 8 µl dNTPs mix, 2 µl T7 10X Reaction Buffer, 2 µl T7 Enzyme Mix, 8 µl of PCR template (200 ng total) and 2 µl of UltraPure DNase/RNase-free distilled water. The mixture was incubated at 37°C for at least 4 hr. To remove the DNA template, 1 µl of TURBO DNase was added to the reaction mix and incubated for 15 more minutes at 37°C. The RNA was purified using the MEGAclear™ Transcription Clean-Up Kit. Briefly, 80 µl of Elution Solution was added to the RNA, followed by 350 µl of Binding Solution Concentrate and 250 µl of 100% ethanol. The mixture was added onto the Filter Cartridge and centrifuged for 1 min at full speed. Washing was done by adding two times 500 µl Wash Solution. For elution, 50 µl of pre-heated Elution Solution at 95° C was applied to the centre of the Filter Cartridge, centrifuged for 1 min at RT at max speed. The concentration of RNA was assessed by UV Absorbance at 260 nm. Around 500 ng of denaturated RNA (10 min at 75°C) were loaded on a 2 % gel to confirm integrity before injection.

Table 7. List of DNA oligos used for cloning the sgRNA into pX330 and for in vitro transcription PCR template amplification

Oligo	*Sequence (5' to 3')*	*Annealing Temperature (°C)*
sg*Scn10a*-Ex6_F	CACCGTGAGAACTCGGAATGTCCGC	
sg*Scn10a*-Ex6_R	AAACGCGGACATTCCGAGTTCTCAC	
T7-sg*Scn10a*-Ex6_F	TTAATACGACTCACTATAGGTGAGAACTCGGAATGTCCGC	59.4
sg*Scn10a*-Ex11_F	CACCGTCCGTTGTGGGAATAGAGCG	
sg*Scn10a*-Ex11_R	AAACCGCTCTATTCCCACAACGGAC	
T7-sg*Scn10a*-Ex11_F	TTAATACGACTCACTATAGGTCCGTTGTGGGAATAGAGCG	59.4
sg*Scn11a*-Ex9_F	CACCGTATTGCACGTGGAACCATCG	
sg*Scn11a*-Ex9_R	AAACCGATGGTTCCACGTGCAATAC	

Oligo	*Sequence (5′ to 3′)*	*Annealing Temperature (°C)*
T7-sg*Scn11a*-Ex9_F	TTAATACGACTCACTATAGGTATTGCACGTGGAACCATCG	57.3
sg*Scn10a*-Ex10_F	CACCGAAGACAAAGTAGATCCCGG	
sg*Scn10a*-Ex10_R	AAACCCGGGATCTACTTTGTCTTC	
T7-sg*Scn10a*-Ex10_F	TTAATACGACTCACTATAGGAAGACAAAGTAGATCCCGG	57.3
Sequencing Primer_F	GATACAAGGCTGTTAGAGAGA	
Sequencing Primer_R	CCAAGTAGGAAAGTCCCATAA	

4.2.3.2 Plasmid DNA *in vitro* cleavage assay

To avoid delivery of ineffective single guide RNAs (sgRNAs) to the mouse zygotes for Cas9-mediated genome editing, a simple assay to test the efficacy of the different sgRNAs *in vitro* based on Jinek et al. 2013 was performed. Initially, a PCR fragment containing the target sequence was amplified with the designed genotyping primers (Table 10) and cloned into pCR®2.1 TOPO® vector as described in section 4.2.1.10. A minipreparation of plasmid DNA was performed for five colonies, checked for the incorporation of insert by restriction digestion and further sequenced. Afterwards, the plasmid was linearized with *PscI* and gel purified. The DNA concentration was set to a minimum of 100 ng/µl. In order to get the SpCas9 protein, HEK293T cells were seeded in a 10 cm-culture-dish and allowed to reach about 80% confluence and maintained in DMEM (Dulbecco's Modified Eagle Medium containing high glucose, GlutaMAX™ Supplement, pyruvate, plus 10% FBS, 1 % P/S). Then, cells were transfected with 10 µg of empty pX330-U6-chimeric_BB-CBh-hSpCas9 plasmid expressing hSpCas9 using Lipofectamine® 2000 Reagent. First, the DNA and 15 µl Lipofectamine were diluted in 500 µl Opti-MEM® (Minimum Essential Medium) in separate tubes. After 5 min incubation, both solutions were mixed and further incubated for 20 min at RT allowing the formation of liposomes that entrap the DNA. Following addition of fresh medium to the cells, the transfection mixture was added drop-wise on top of the cells and incubated for 48 h at 37˚C. On the day of the assay, cells were washed three times with DPBS and collected on ice with a cell scraper in 1 ml of DPBS containing 100 µl of Protease Inhibitor Cocktail. Cells were homogenised by passing the solution ten times through a sterile 1 ml syringe with a 22 G x 1 ¼ needle, centrifuged 1 min at 14,000 rpm at 4°C for 1 min. The supernatant fraction was used to prepare four reaction tubes as described in Table 4. The tubes were incubated for 4 hr at 37°C in a shaking incubator with 10 mM $MgCl_2$, as Cas9 is a Mg^{2+}-dependent endonuclease with 3'-5' exonuclease activity. The reactions were stopped by adding 10 µl of 5X DNA loading buffer,

purified with the Gel DNA Recovery Kit and further loaded on a 1% agarose gel. Only in tube number 3, where all the components needed by SpCas9 to produce a DSB in the DNA are present (SpCas9, sgRNA, $MgCl_2$, and the target sequence), we expect to see two bands as result of an efficient cut. The other tubes are the respective negative controls.

Table 8. Reactions prepared for the plasmid DNA in vitro cleavage assay

Tube N°	*1*	*2*	*3*	*4*
Cell Lysate containing SpCas9 (µl)	20	-	20	-
IVT sgRNA (µl)	-	1	1	-
50 mM $MgCl_2$ (µl)	10	10	10	10
Linearized plasmid (µl)	5	5	5	5
DPBS (µl)	15	34	14	35
Total volume (µl)	50	50	50	50

4.2.3.3 One-cell embryo injection

For the injection of CRISPR constructs, a large number of zygotes is needed. Through the administration of gonadotropins, female mice can be induced to ovulate a greater number of eggs than normal, a process called superovulation. For this purpose, approximately ten C57BL/6 female mice of 21-28 days (body weight of 12-14 grammes) were injected intraperitoneally (i.p.) with a dose of 5.0 international units (IU) of pregnant mare's serum gonadotropin (PMSG) between 1:00 and 3:00 PM of day 1 to give the best yield of fertilised eggs. On day 3, the mice received an IP injection of human chorionic gonadotropin (hCG). Immediately following injection, superovulated females were mated to C57BL/6 males. Ovulation takes place approximately 12 hours after the HCG injection, at which time the eggs can be fertilised (*149*). On day 4, fertilised eggs were collected from oviducts and kept in Krebs-Ringer Bicarbonate Buffer at 37°C until both female and male pronuclei are visible. At this point, zygotes were then transferred to Krebs-Ringer Bicarbonate Buffer, 20 mM HEPES, and the pX330-U6-chimeric_BB-CBh-hSpCas9 expressing hSpCas9 and sgRNA or PrecisionX™ Cas9 SmartNuclease mRNA (Eukaryotic version) plus the IV transcribed sgRNA mixture was injected into the pronucleus or cytoplasm respectively (Table 9). All the injected zygotes were cultured in M16 medium covered with mineral oil overnight, and only two-cell-stage embryos were transferred into the oviduct of pseudopregnant foster mothers (0.5 days post coitus) (*150*).

Table 9. DNA/RNA mixtures used for zygote injection

Scn11/10a DKO	*Cas 9 mRNA (ng)*	*sgRNA (ng)*	*pX330 DNA (ng/µl)*	*Final concentration (ng/µl)*
Attempt 1			25 ng of each plasmid (100 ng total)	5
Attempt 2			25 ng of each plasmid (100 ng total)	10
Attempt 3	100	25 ng of each (100 ng total)		50

4.2.3.4 Mouse genotyping

DNA was extracted from tail biopsies using the HotSHOT method (*151*). Briefly, a 0.2 mm-tail biopsy was incubated with 50 µl of alkaline lysis buffer (25 mM NaOH, 0.2 mM EDTA) for 60 min at 98°C while shaking. Samples were neutralised with 50 µl of neutralisation buffer (40 mM Tris-HCl). For genotyping PCR, 2.5 µl DNA were used in a single PCR mix containing 0,1 µl of HotStarTaq *Plus* DNA Polymerase, 0.5 µl dNTPs, 2 µl of buffer and two exon-specific primers with the respective sequence (Table 10). The amplification was carried out in a PCR thermal cycler using the following program: 5 min at 95°C, 40 cycles of 30s at 95°C, 30 s at 59°C, 30s at 72°C, followed by a final 10 min extension step at 72°C. 15 µl of the amplified DNA was mixed with 5 µl of 5x DNA loading buffer and separated on a 2% agarose gel and 5 µl were used for sequencing (see section 4.2.1.11). PCR amplified products were also analysed by non-denaturating polyacrylamide gel electrophoresis (PAGE) as described in section 4.2.1.6. In addition, large fragment PCR amplification was performed using Herculase II fusion Polymerase as outlined in section 4.2.2.10.

Table 10. Genotyping primers

Primer name	*Sequence (5' to 3')*	*Expected size (bp)*
Scn10a-Exon 6_F	GTAGATGGCAATGCTGCTGG	301
Scn10a-Exon 6_R	GTGTGCATATCAAAGAAGAGCTG	
Scn11a-Exon 9_F	ATCCCTTAGGAGGGTCAGTGA	516
Scn11a-Exon 9_R	GCTCTTATTTCCAGCATGGTGC	
Scn11a-Exon 10_F	TCAGCTCATTCGTAGTTGCCCT	513
Scn11a-Exon 10_R	TGCGTCCAGACCCATTTGAGA	
Scn10a-Exon 11_F	GTTCTGCCATGCCCAATCC	480
Scn10a-Exon 11_R	CAACTGCTGCCAACCTAGC	

Primer name	*Sequence (5' to 3')*	*Expected size (bp)*
Scn10a-Exon 6_F2	GATTTGTCCTATGCCCATGGG	990
Scn10a-Exon 6_R2	GGGATGATCTGAGGAGATCAG	
Scn11a-Exon 9_F2	GGCGACCACTAACTGTCAGTC	900
Scn11a-Exon 9_R2	TCCCTGAGCTGACGGTCCA	
Scn11a-Exon 10_F2	GGTATTCACTTGCGCTTGCAG	1068
Scn11a-Exon 10_R2	GAGGAGAATGCCTTCGGCTTT	
Scn10a-Exon 11_F2	GAGTCATTAGGACCCAAGGGA	1088
Scn10a-Exon 11_R2	GCAGATAGACCCTTAGCTGTG	

4.2.3.5 Off-target analysis

Off-target (OT) sequences were computationally identified and ranked using the online design tool from Benchling (www.benchling.com), which allows for up to four mismatches in the target gRNA sequence (*138*). For each sgRNA, primers for the top five OT sequences and OT coding regions, if detected, were designed (Table 11). PCR amplification was carried out from DNA of the founder chimaera and the two F_1 founder animals to determine if any mutations or changes occurred in OT sites. For each PCR reaction, 2.5 µl DNA were used in a single PCR mix containing 0,1 µl of HotStarTaq *Plus* DNA Polymerase, 0.5 µl dNTPs, 2 µl of buffer and 1 µl of each specific primer pair. The amplification was carried out in a PCR thermal cycler using the following program: 5 min at 95°C, 40 cycles of 30s at 95°C, 30 s at (Annealing Temperature of the primers), 30s at 72°C, followed by a final 10 min extension step at 72°C. 15 µl of the amplified DNA was mixed with 5 µl of 5x DNA loading buffer and separated on a 2% agarose gel and 5 µl were used for sequencing (see section 4.2.1.11).

Table 11. Primers used for amplification of off-target sites

SgRNA	*Primer name*	*Sequence (5' to 3')*	*Expected size (bp)*
sg*Scn10a*-Ex6	OT-1 F	GACTTACCAAGCAGTGAGTC	470
	OT-1 R	CTTTTGCGATGTAGACAATGAGA	
	OT-2 F	ATCTGCATTGCTCATCAGTGC	431
	OT-2 R	TTTAAGTGTCCACTATGGGGG	
	OT-3 F	CTTAAAAACCTCCCTGCAATGC	419
	OT-3 R	AAGAGCAGCTAGTACTCTAGTTC	

SgRNA	*Primer name*	*Sequence (5' to 3')*	*Expected size (bp)*
sg*Scn10a*-Ex6	OT-4 F	AAGGCATAACCCAACCTATGCTC	404
	OT-4 R	ATGTGAGTTCCACCGCTGTCTA	
	OT-5 F	TTGTCCCTAGCAACACTCAC	245
	OT-5 R	ACATACATACAATGGGGAAAAGC	
sg*Scn10a*-Ex11	OT-1 F	GTCCATGCCTCTCCCTAGG	391
	OT-1 R	TTGGACGCTTAGAGAGGAACTAGT	
	OT-2 F	CTCTTTAAGGAGTGAGCTATACT	378
	OT-2 R	AAGCCTCACATAGTCTGCAC	
	OT-3 F	GATGTAATGATAGTGTCATCTGG	406
	OT-3 R	GCCTTCAGTTCCAAGACTAG	
	OT-4 F	TACAATGATCAGAGAGAGCTGTAT	347
	OT-4 R	GATCGAAGGGCATACAACATC	
	OT-5 F	GAGGGACTGCCTTGATATTAG	462
	OT-5 R	CCAACTGGGTAACAGGTACAT	
	OT-45 F	CCCTAACTTCTTGCTCCGCT	334
	OT-45 R	GGAACCCAATAACAGCGTCG	
sg*Scn11a*-Ex9	OT-1 F	TGTACCTATGACAGCCGCTG	423
	OT-1 R	CCTGGTTGATGGTGTTGGCA	
	OT-2 F	ATCCAATCCAAGTCACGGCAC	375
	OT-2 R	GCAAGTCCTGGATACACGATC	
	OT-3 F	TATCTATGTATGGTGCACTTCCA	311
	OT-3 R	GTTGCTACTGAGATGGGGTA	
	OT-4 F	AAGGTGCAGGTGTTTGGGAT	376
	OT-4 R	CTATGGTCCACTAAGAAGGG	
	OT-5 F	TCTGTTCTCACTTAGACCGC	380
	OT-5 R	GGACTGACTCTGAAGGTACA	
	OT-37 F	CACCACATGCCAAGAATGAG	456
	OT-37 R	CGATTCTGCACACCACTCAT	

SgRNA	*Primer name*	*Sequence (5' to 3')*	*Expected size (bp)*
sg*Scn11a*-Ex10	OT-1 F	AGGCAACCTGCTCTTGGGA	403
	OT-1 R	GGTGATGGTGTCGCTACTC	
	OT-2 F	CTCACATGCCAGCCCAGAAA	478
	OT-2 R	TCCCATGATCGCTCCGTGAT	
	OT-3 F	GAACACAAGAGATGTGGTGC	306
	OT-3 R	ATACAGGAGCGTATACAGCC	
	OT-4 F	GCTCTGGGCCACACGAGT	468
	OT-4 R	AACCTGTCATTACTGAGGTCGG	
	OT-5 F	CTCCTTACACAAGCAGTTTGC	353
	OT-5 R	TTTCTCTAACACGGCTGGCT	
	OT-10 F	CTGCCAGCAGGCTTTAAGTTG	374
	OT-10 R	GCTGGAAGTTCCTGGTGAAC	

4.2.3.6 Gene expression analysis

To analyse the expression of *Scn10a* and *Scn11a* in mouse tissue, RNA was extracted from DRGs tissue, and complementary DNA (cDNA) was generated according to section 4.2.1.13 and 4.2.1.14 respectively. In order to have a quantitative estimation of gene expression, quantitative real-time PCR (qPCR) amplification of WT and KO cDNA was performed using a Bio-Rad C1000 Thermal Cycler-CFX96 Real-Time system (Bio-Rad). All samples were run in triplicate in a final volume of 5 µl containing 1 µl of cDNA, 1 µM of primers and SsoAdvanced™ Universal SYBR® Green Supermix (BioRad). Prior to qPCR, a 5 min enzyme activation step was done at 95 °C. The qPCR protocol consisted of 10s denaturation at 95 °C, 15s at annealing temperature at 58 °C, 30 s elongation at 72 °C for 45 cycles. The annealing temperature was confirmed by the melting curve.

Table 12. Primers used for amplification of cDNA

Primer name	*Sequence (5' to 3')*	*Expected size (bp)*
cDNA_*Scn10a*-Exon 11_F	GTGTGCATGACCCGAACTGAT	101
cDNA_*Scn10a*-Exon 11_R	CAAAACCCTCTTGCCAGTATCT	
cDNA_*Scn11a*-Exon 9_F	CCCTTGTGAGTCTCGCTGAC	143
cDNA_*Scn11a*-Exon 9_R	GGAGTGGCCGATGATCTTAAT	
*Gapdh*_F	AGGTCGGTGTGAACGGATTTG	355
*Gapdh*_R	GCGGAGATGATGACCCTTTTG	

4.2.4 Electrophysiological studies of *SCN10A* and *SCN11A* wild-type and mutant constructs.

Electrophysiological studies were carried out by Dr Enrico Leipold. Cell culture and transfection of ND7/23 cells, isolation and transfection of mouse DRG neurones, as well as electrophysiological methods, are described in Leipold et al. 2015. (*65*)

4.2.5 Mouse studies

All animal experiments were approved by the local administrative institution (Thüringer Landesamt für Verbraucherschutz, Bad Langensalza, Germany) and the experimental procedures were performed in accordance with the guidelines established by the animal welfare committee of the State of Thuringia.

4.2.6 Statistical analysis

Data are presented as mean ± SEM in the figures. The statistical test applied for p-value calculation is noted in the legends of the respective figures. One- or Two-way ANOVA or parametric two-tailed Student's t-test were applied after confirming a parametric distribution by Normal Q-Q-Plots. For non-parametric distributed data, the Mann-Whitney-U-test was applied. Levels of significance were set as following: *** $p < 0.001$; ** $p < 0.01$, * $p < 0.05$.

5. Results

The results section is divided into two parts. The first part is dedicated to the creation of a cellular model for the functional characterization of novel missense mutations in the *NTRK1* gene whereas in the second part the generation of an *SCN10A* and *SCN11A* double-knockout mouse model is described.

5.1 Generation of a cellular model for the functional characterization of novel missense mutations in the *NTRK1* gene

5.1.1 Putative newly identified mutations in *NTRK1* causing HSAN-IV

In the present study, three cases with a typical hereditary sensory and autonomic neuropathy type IV (HSAN-IV) phenotype, in which parents had no features of the disease, are reported. All patients exhibited the characteristic symptoms of HSAN-IV (*8–10*), including congenital insensitivity to noxious stimuli and temperature, anhidrosis (inability to sweat), muscular hypotonia, global cognitive delay, self-mutilations of the tongue and fingertips accompanied by painless fractures, and episodes of unexplained high fever. All patients were from India. Using next-generation sequencing panel analysis including the full-length *NTRK1* (RefSeq ID NM 002529.3) isoform expressed in neuronal tissue (*141*), novel homozygous missense mutations were identified in affected individuals. Additionally, sequencing of both parents confirmed that the mutations segregated as expected for an autosomal recessive disorder. However, for patient one no parental data was available. Of note, no mutation was detected in the *NGF* gene (RefSeq ID NM 002506.2), which may cause a similar phenotype (*6*). The putative missense mutations were c.1095C>A, c.1514T>A, and c.1898A>G (RefSeq ID NM 002529.3), leading to the NTRK1 protein changes p.N365K, p.I505N, and p.Q633R respectively. Nucleotide numbering uses +1 as the first nucleotide of the ATG translation initiation codon (codon #1) in the reference sequence. To date, no variation at these positions is reported in the Exome Variant Server (http://evs.gs.washington.edu/EVS/), the 1000 Genomes Server, dbSNP (http://www.ncbi.nlm.nih.gov/SNP/), or the ExAC database (http://exac.broadinstitute.org). The mutation in patient one causes a single amino acid change in the second immunoglobulin –like domain of NTRK1, while in patients two and three the missense mutations localise within the juxtamembrane domain and the tyrosine kinase domain respectively (Figure 8B). All mutations affect evolutionarily conserved residues and were predicted to be pathogenic by Mutation Taster, Polyphen and SIFT (Figure S1).

However, further evaluation of missense mutations requires functional studies to prove their pathogenicity.

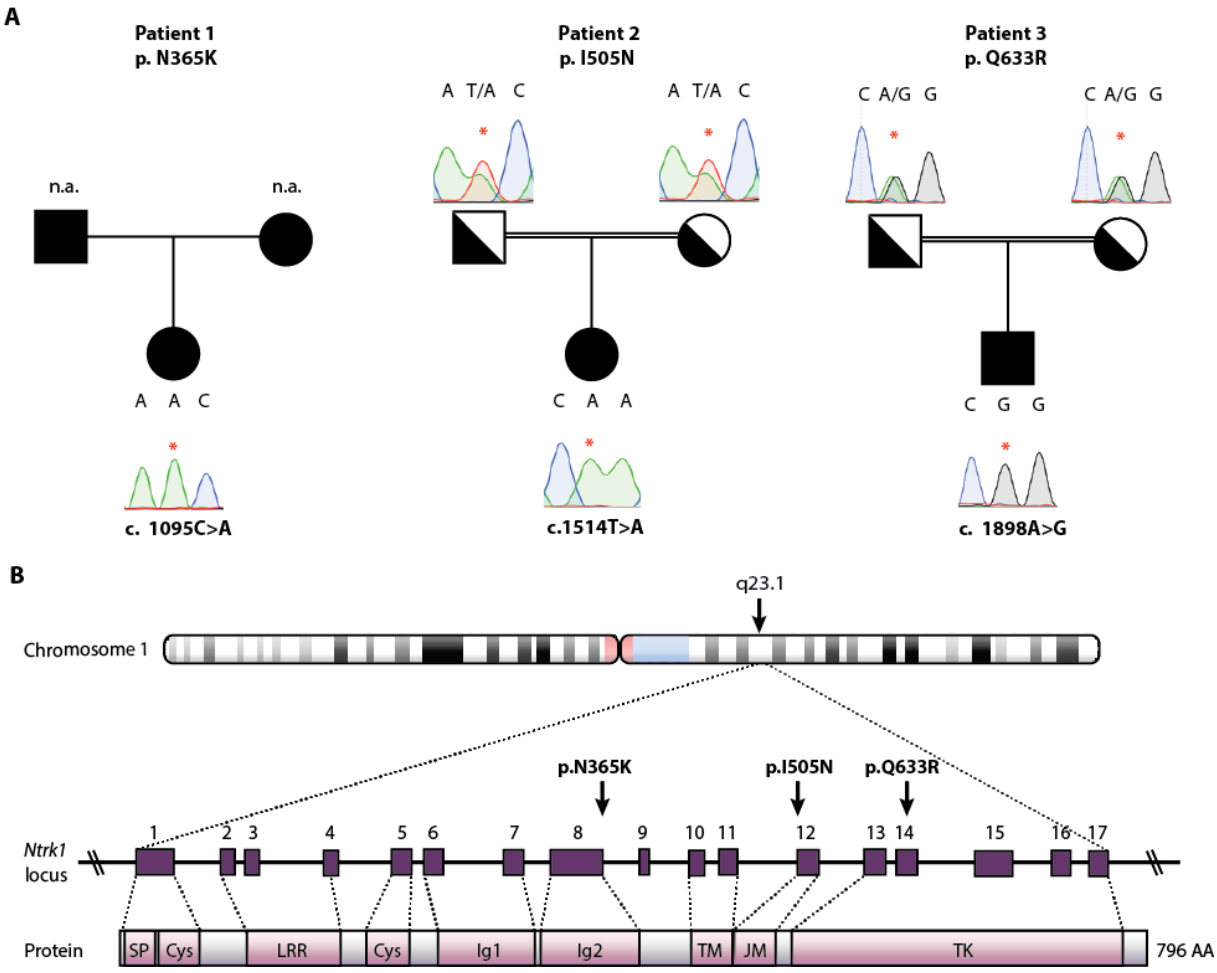

Figure 8. Identification of novel *NTRK1* mutations in patients with HSAN-IV

(A) Sequencing of NTRK1 (RefSeq ID NM 002529.3) revealed different homozygous missense mutations in three individuals diagnosed with HSAN-IV. For patient 1 (c.1095C>A) no parental samples were available (n.a., not available). Patient 2 (c.1514T>A) and 3 (c.1898A>G) originated from consanguineous Indian families. Sequencing of both parents confirmed that the mutations segregated as expected for an autosomal recessive disorder. The mutations identified in these patients correspond to the NTRK1 protein changes p.N365K, p.I505N, p.Q633R, respectively. (B) NTRK1 is located on chromosome 1q21-q22 and consists of 17 exons. The NTRK1 protein has an extracellular portion consisting of a leucine-rich repeat (LRR), flanked on either side by a cysteine-rich (Cys) and two Ig-like domains (Ig1 and Ig2), a transmembrane (TM) and a juxtamembrane domain (JM), a tyrosine kinase (TK) domain, and a C-terminal end (*19*). The mutation p.I505N is located in exon 12 which codes part of the juxtamembrane domain, while the p.Q633R mutation is located in exon 14, which codes part of the TK domain. Mutation p.N365K localises to the second immunoglobulin domain.

5.1.2 Efficient generation of *Ntrk1*-KO PC12 cells via CRISPR genome editing

To study the effect of the NTRK1 mutants in a physiologically relevant cellular context, *Ntrk1* was disrupted in PC12 cells using the CRISPR (clustered regularly interspaced short palindromic repeats)-Cas (CRISPR-associated protein) system. PC12 cells are derived from a

rat pheochromocytoma and can recapitulate neurite differentiation and neuronal signalling upon stimulation with NGF (*134*). In contrast, as illustrated in Figure 9A, in an *Ntrk1*-KO PC12 cell line, one should not expect neurite outgrowth or activation of signalling cascades upon NGF treatment, thus making it a good model for testing the NTRK1 mutants, which can be heterologously expressed in the system.

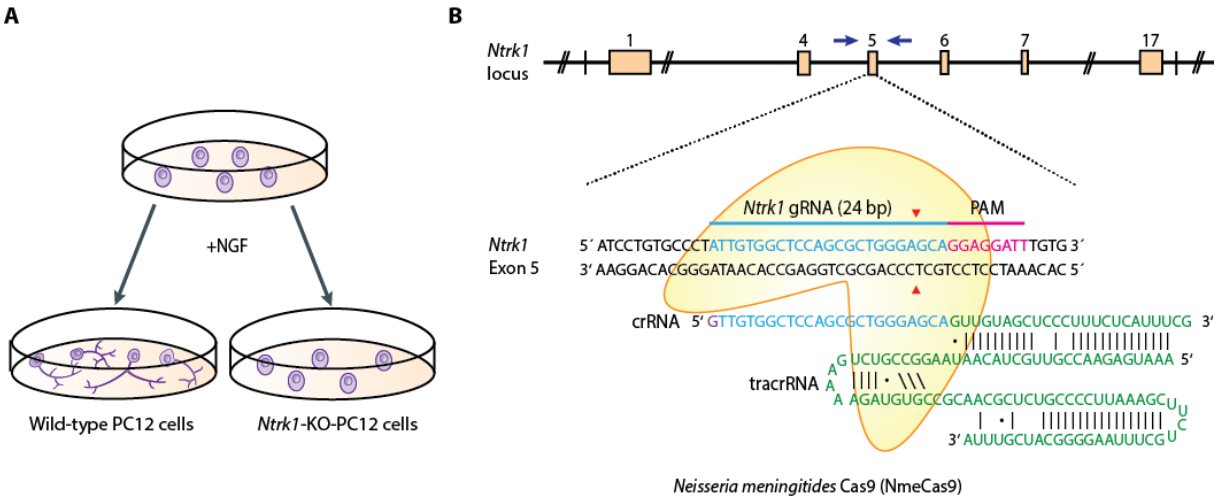

Figure 9. Generation of an *Ntrk1*-KO PC12 cell line using the *Neisseria meningitides* Cas9.
(A) Schematic representation of the cellular system. PC12 cells differentiate into neurone-like cells upon stimulation with NGF (nerve growth factor) (*134*). In contrast, *Ntrk1*-KO PC12 cells should not develop neurites or activate downstream signalling cascades upon NGF treatment. (B) Schematic representation of the *Ntrk1* gene and the target site. The guide RNA (gRNA) target site is located in the middle of *Ntrk1*-Exon 5. The 24-nt guide sequence (light blue bar on top strand) comprising the 5′-end of the crRNA is shown. As the U6 promoter requires a 5′ guanine to start transcription, the first nucleotide of the guide RNA was replaced (G in violet). The gRNA sequence pairs with the DNA target site. 3′ of the target sequence is the protospacer adjacent motif (PAM; 5′-NNNNGATT-3′; pink) of the *Neisseria meningitides* Cas9 (in yellow). The NmeCas9 enzyme introduces a double-strand-break three nucleotides upstream of the PAM (red triangles), triggering imperfect non-homologous end-joining repair pathways. Genotyping primers spanning the cleavage site are indicated by dark blue arrows.

The CRISPR-associated protein 9 (Cas9) nuclease catalyses a site-specific double-strand-brake (DSB) in a desired target DNA sequence. Targeting of Cas9 to specific genomic loci is mediated by a short guide RNA (gRNA) sequence. Recognition of cleavage sites is determined by gRNA-DNA base pairing, and cleavage only occurs if the target site is followed by a protospacer-adjacent-motif (PAM), a three-nucleotide sequence juxtaposed to the DNA complementary region. The DSB activates DNA repair enzymes that often disrupt the DNA sequence by generating insertions or deletions (indels) as well as substitutions near the cleavage site via the error-prone non-homologous end-joining (NHEJ) repair pathway (*73*, *125*). However, Cas9 can tolerate single-base mismatches, DNA insertions (DNA bulges) or deletions (RNA bulges) between the gRNA and the genomic target site, which have

significant implications to the targeting specificity of the enzyme as they can lead to undesired mutations (off-targets) (*132*, *152*).

In order to generate indels in the *Ntrk1* gene, the *Neisseria meningitides* Cas9 (NmeCas9) was used, as it has been reported that it produces less off-target (OT) cleavage while achieving similar on-target activities than the *Streptococcus pyogenes* Cas9 in mammalian cells (*131*, *132*). In addition, the optimal SpCas9 PAM (5'-NGG) can be found approximately every eight bases in a random DNA sequence, while the optimal NmeCas9 PAM (5'-NNNNGATT) is present every 128 bases, thus reducing the number of potential OT sites (*131*).

Therefore, a 24-nt-guide RNA was designed using the online design tool from Benchling (www.benchling.com) to target exon 5 of *Ntrk1* (g*Ntrk1*-Ex5; Figure 9B). As shown in Figure 10A, wild-type PC12 (wtPC12) cells were transfected with a plasmid expressing NmeCas9, tracrRNA (transactivating crRNA), a cassette for the expression of the crRNA (CRISPR-RNA), where the gRNA was cloned, and GFP to enable selection of NmeCas9-expressing cells (*131*). Subsequently, cells were FACS-sorted 48 hr post-transfection (Figure 10B). GFP-positive cells were initially seeded in a small dish to let them recover and later seeded on 96-well-plates for single clone selection.

To confirm that NmeCas9 introduced a DSB in the intended genomic locus, DNA was extracted from each clone and the genomic region flanking the cleavage site was PCR-amplified and analysed by standard 2 % agarose gel electrophoresis (Figure 10C) as well as by non-denaturating polyacrylamide gel electrophoresis (PAGE; Figure S2). Surprisingly, none of the clones exhibited formation of heteroduplex DNA bands. However, as by this methods 1 bp indels cannot be detected, all clones were sequenced. Sequencing results showed that only 6 of the 30 PC12 clones analysed were genetically modified. As depicted in Figure 10D, all indels were found at the NmeCas9 cleavage site, indicating that the DSB occurred at the intended position, but at a relatively low frequency (20%). Clone #7 contained a 1 bp insertion (+1 bp; Figure S3). As shown in Figure 10E, two clones (#3 and #16) contained a homozygous 1 bp deletion (Δ1 bp), which was also found in heterozygosity in the remaining modified clones (Figure S3). Interstingly, all the genetically-engineered clones had a similar rearrangement. A possible explanation for this observation is that cells were plated before clonal isolation, allowing cell proliferation and thereby causing clonal drifts. Still, this does not explain why the same Δ1 bp was found in both heterozygosity and homozygosity.

Thus, these results suggest that the genome context influences the repair mechanisms in favour of similar rearrangements.

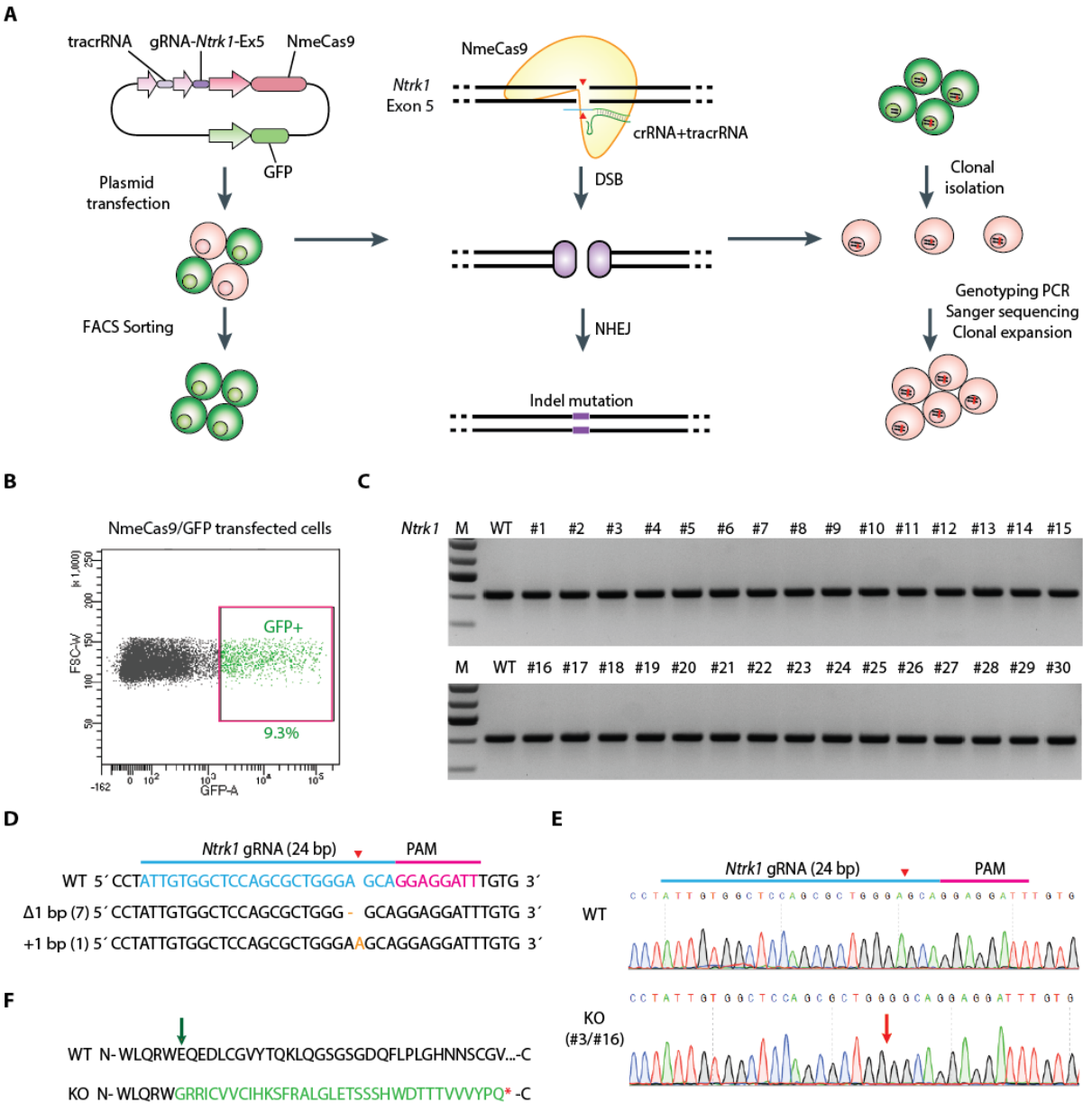

Figure 10. Targeted deletion of *Ntrk1* in PC12 cells with CRISPR-NmeCas9.

(A) Schematic representation of the targeting strategy. PC12 cells were transfected with a plasmid expressing NmeCas9, tracrRNA, a cassette for the expression of the crRNA, where the 24-nt gRNA was cloned, and GFP to enable selection of NmeCas9-expressing cells. NmeCas9 produces a double-strand break (DSB), triggering the non-homologous end joining (NHEJ) repair pathways, which often results in indel mutations (violet box). (B) Cells were FACS-sorted 48 hr post-transfection resulting in 9.3 % GFP-positive cells. (C) Identification of genome-engineered cells by 2% agarose gel electrophoresis. (D) Direct sequencing of the PCR products showing indels introduced by NmeCas9 in *Ntrk1*. The 24-nt guide sequence (blue bar) followed by the protospacer adjacent motif (PAM; 5'-GGAGGATT-3'; pink) is shown. A red triangle indicates the cleavage site. The numbers in parenthesis indicate the number of sequenced clones containing that particular deletion (Δ) or insertion (+). (E) Chromatogram of the *Ntrk1* targeted site of wild-type (WT) and knockout (KO) clones (#3, #16). (F) Predicted protein sequence in WT and KO clones. M, Molecular weight marker; bp, base pairs.

5.1.2.1 Off-target analysis in CRISPR/Cas-mediated *Ntrk1*-KO PC12 cells

OT cleavage can cause unwanted mutations and chromosomal rearrangements due to nonspecific hybridization of the guide strand to genomic DNA sequences. Therefore, potential OT-sites were predicted and ranked using the web-based tool COSMID (*140*) (Table S1) as well as the design tool available in Benchling (Table S2) and further analysed. Though other potential OTs than the predicted ones cannot be excluded, no mutation was found in undesired target sites in neither clone (Figure S4).

5.1.2.2 Functional characterization of *Ntrk1*-KO PC12 cells

The homozygous Δ1 bp found in clone #3 and #16 produces a frameshift in the coding sequence of *Ntrk1* and is predicted to result in a premature stop codon in exon 6 (Figure 10F). To investigate whether Ntrk1 expression is absent in *Ntrk1*-KO PC12 clones, mRNA and protein expression levels were analysed under normal culture conditions (10% serum in the medium) and compared to wtPC12 cells. As expected, the high mRNA levels of *Ntrk1* in wtPC12 cells were diminished in both *Ntrk1*-KO PC12 clones (qPCR), as shown in Figure 11A. Ntrk1 gives rise to two different bands in western blot analysis. It is proposed that the lower band at ~110 kDa corresponds to the immature Ntrk1 that has not completed Golgi-mediated processing of high-mannose N-glycans (*153*) while the upper band of ~140 kDa represents the fully glycosylated mature form present in the plasma membrane (PM). Moreover, it is known that intracellular Ntrk1 can spontaneously dimerize (*154*). As can be seen in Figure 11B, the upper band corresponding to the fully functional glycosylated isoform is absent in the KO cells (clone#3), suggesting that Ntrk1 is not functionally expressed in these cells (data shown for clone#3 only, see Figure 11C). However, a lower band was detected in both WT and KO cells, which may be unspecific.

Next, the two major Ntrk1-signalling cascades triggered by NGF stimulation were investigated. Specifically, the phosphatidylinositol 3-kinase (PI3K) and the mitogen-activated protein kinase (MAPK) signalling pathways were analysed by detecting the specific phosphorylation of Erk 1/2 (extracellular signal-regulated kinase one and two) and Akt kinase (protein kinase B). As shown in Figure 11B, Western blot analysis revealed that both the expression levels of Erk 1/2 and Akt were comparable between wtPC12 and *Ntrk1*-KO-PC12 cells clones. However, NGF-induced phosphorylation at the T202/Y204 sites of Erk 1/2 and T308 of Akt was not detected in the *Ntrk1*-KO PC12 clones.

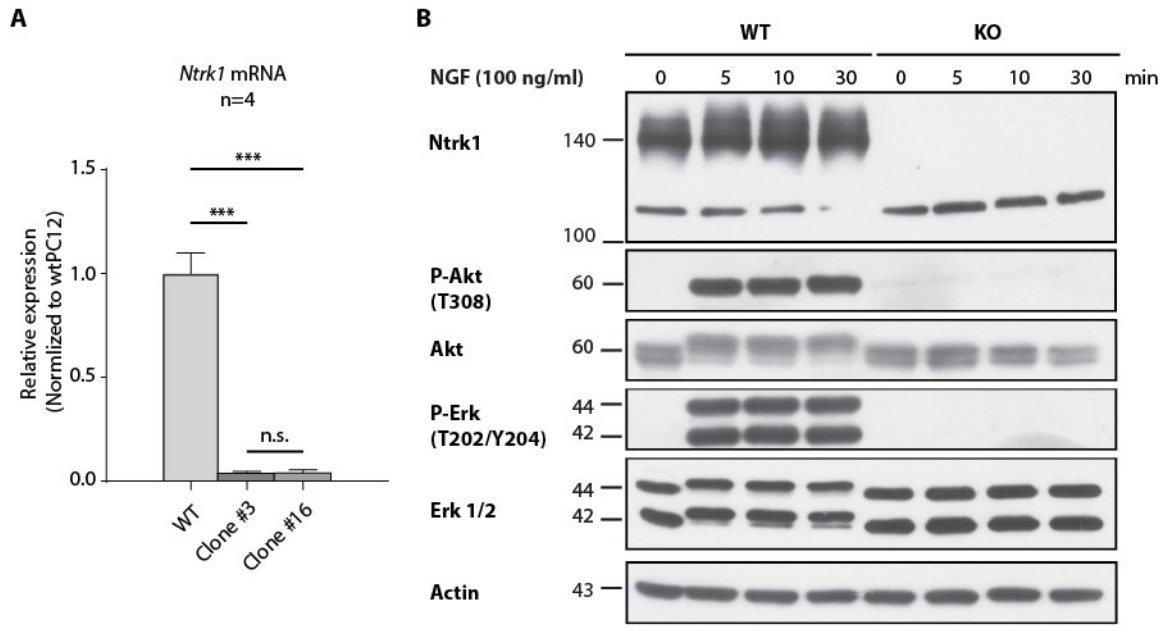

Figure 11. Expression of *Ntrk1* and NGF-induced phosphorylation of Erk and Akt in wtPC12 and *Ntrk1*-KO PC12 cells.

(A) Decreased levels of *Ntrk1* mRNA in clone #3 and #16 revealed by qPCR. Data representative of four independent experiments shown as mean ± SEM calculated using the two-tailed unpaired t-test; ***p<0.001. (B) Time-course of Erk and Akt phosphorylation induced by NGF (100 ng/ml) in wtPC12 cells and *Ntrk1*-KO PC12 cells (clone #3 is shown) analysed by western blot. Expression levels of Erk 1/2 and Akt were close in wtPC12 and *Ntrk1*-KO-PC12. After 5 min of NGF stimulation, phosphorylation of Erk 1/2 at the T2020/Y204 sites and Akt at the T308 site can be observed in wtPC12 cells, remaining constant up to 30 min after stimulation. However, NGF-induced phosphorylation of Erk 1/2 and Akt was not detected in the *Ntrk1*-KO PC12 clones. Y-axis: molecular weight in kilodaltons (kDa).

To address neurite outgrowth of the *Ntrk1*-KO-PC12 line, cells were treated with NGF for 7 days and compared to wtPC12 cells. As can be observed in Figure 12, the *Ntrk1*-KO cells do not show any sign of neurite outgrowth (only clone #3 is shown). Taken together, the data suggest that these cells are a good model for evaluating the effects of the NTRK1 missense mutations.

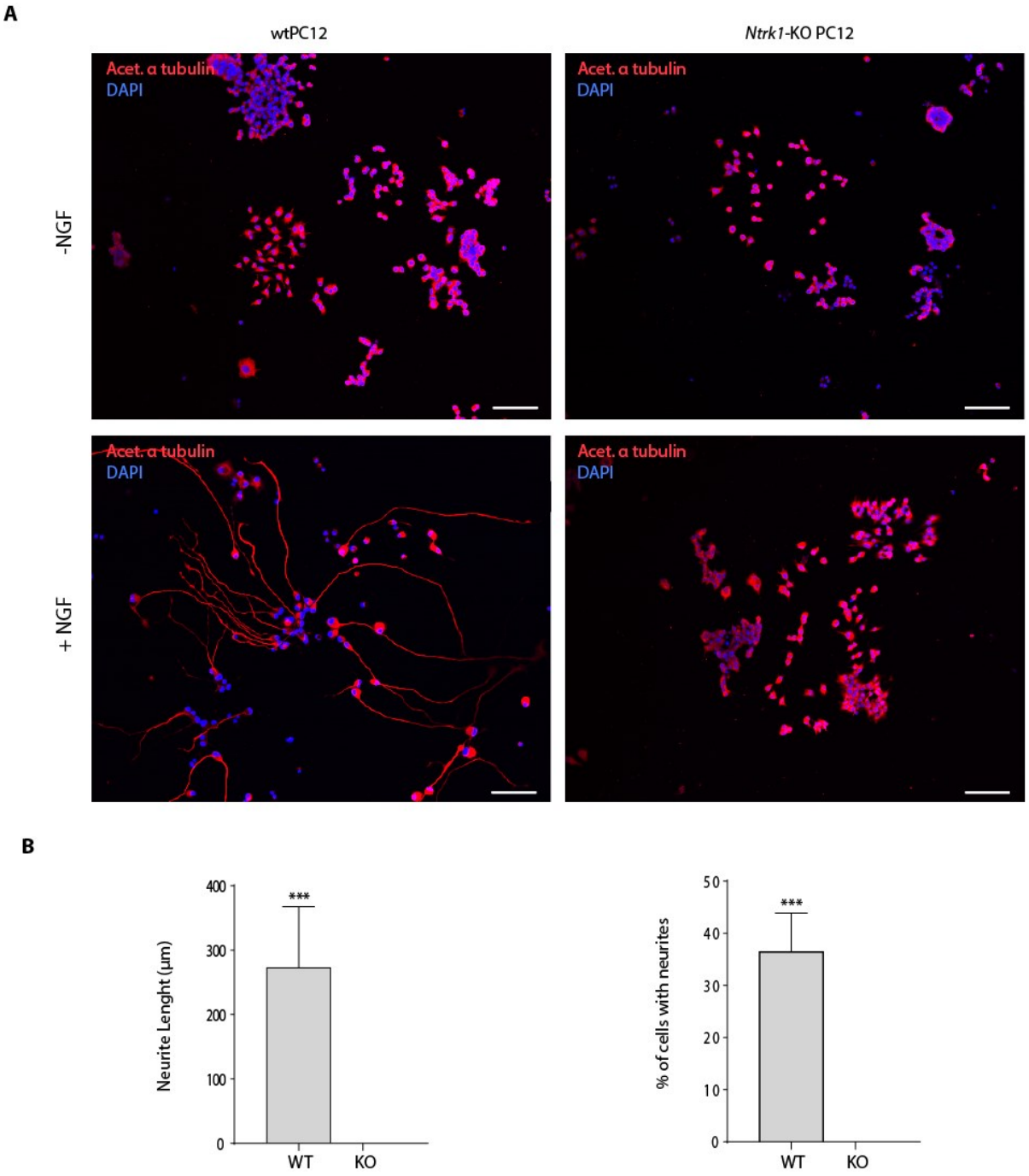

Figure 12. *Ntrk1*-KO PC12 cells do not develop neurites after NGF treatment.
(A) wtPC12 and *Ntrk1*-KO PC12 cells were grown in differentiation media (RPMI, 1 % horse serum) for 7 days, in the presence of absence of NGF (100 ng/ul). Neurites can be observed in wtPC12 cells treated with NGF, while KO cells do not differentiate. Scale bar: 75 µm. (B) Total neurite length was calculated from a total of 50 cells and percentage of neurites counted from a total of 200 cells from three independent experiments. Data are shown as mean ± SEM calculated using the two-tailed unpaired t-test; ***p<0.001.

5.1.3 Glycosylation changes and downstream activation of MAPK and PI3K signalling pathways by NTRK1 mutants

Next, the effects of the patient-related missense mutations on NTRK1 expression and activation of the PI3K and MAPK signalling pathways were analysed. *Ntrk1*-KO-PC12 cells

were transiently nucleofected with the respective wild-type and mutant NTRK1-cDNA constructs, and 24 hr post transfection cells were treated with NGF for different time points and subjected to protein extraction. As can be seen in Figure 13A, Western blot analysis of NTRK1 expression showed that similarly to the wtNTRK1, mutants p.I505N and p.Q633R had a functional membrane-bound NTRK1 isoform, as can be assessed by the presence of a band of ~140 kDa. In addition, all constructs, except p.I505N, showed increased expression of the ~110 kDa band that was previously proposed to be unspecific. Thus, it can be presumed that this band, expected to be the intracellular immature form of NTRK1, is overlapping with an unspecific band. Interestingly, mutant p.N365K showed a two-fold increase of intracellular NTRK1 compared to mock-treated cells but significantly reduced levels of the mature fully glycosylated form compared to wtNTRK1, indicating that this mutation might cause HSAN-IV due to defective processing or trafficking to the PM (Figure 13B).

Expression of the heterologous wtNTRK1 construct in *Ntrk1*-KO PC12 cells showed a similar ability to activate the PI3K and MAPK pathways than mock-transfected wtPC12 cells upon NGF stimulation (Figure S5). As shown in Figure 13, basal phosphorylation was detectable in untreated transfected cells due to NTRK1 self-activation caused by overexpression. In cells transfected with the wtNTRK1 construct, the level of Erk phosphorylation increased approximately 3-fold upon NGF stimulation, reaching a peak after 5 min and declined slightly after 30 min of treatment, while Akt phosphorylation increased with time of exposure to NGF, reaching ~3-fold increased at 30 min. In contrast, no Erk phosphorylation was detected upon NGF stimulation in cells transfected with mutant p.N365K. Additionally, Akt phosphorylation remained constant over time in these cells, indicating Akt is not activated in an NGF-dependent manner. These results support the hypothesis that this mutant is not able to mature and traffic correctly to the PM.

In cells transfected with mutant p.I505N or p.Q633R, Akt signalling is activated similarly to wtNTRK1, suggesting this is not the main reason by which these mutants cause HSAN-IV. However, Erk phosphorylation decreases abruptly to basal levels at 30 min in both mutants. Upon NGF binding, NTRK1 interacts with $p75^{NTR}$ and several adaptor proteins to facilitate signalling events (*20*). Additionally, NTRK1 is ubiquitinated and subsequently internalised into endocytic vesicles (*155*) and can be either sorted to lysosomes or recycled back to the PM (*156*, *157*). The degradative pathway to lysosomes is characterised by down-regulation of the total number of receptors at the cell surface and decreased responsiveness to the ligand.

Recycling to the PM promotes functional resensitization and prolongation of cell surface–specific signalling events (*156*). Most NTRK1 receptors at the cell surface are internalised by 30 min of NGF treatment (*158*). In PC12 cells, internalisation of activated NTRK1-NGF complexes is required for the induction of neurite outgrowth but not for NGF-mediated survival. Indeed, activated NTRK1 receptors located at the cell surface promote cell survival via PI3K/Akt activation whereas NTRK1 receptors from internalised endosomes promote cell differentiation by preferential activation of Erk (*159*). Furthermore, persistent activation of the MAPK pathway is essential for NGF-induced morphological and biochemical differentiation of PC12 cells into a neuronal phenotype (*160*)**.** Chen et al. reported that this effect is promoted by the activation of Rap1 (Repressor Activator Protein 1), a member of the Ras superfamily. They showed that after NGF treatment Ras activation is transient, while Rap1, which localises to endosomes together with the NTRK1-NGF receptor complex, activated Erk 1/2 from endosomes for prolonged periods of time (*160*). As both mutant receptors do not exhibit prolonged activation of Erk, it can be speculated that either NTRK1 internalisation or its interaction with other proteins needed for persistent activation of the MAPK pathway is impaired in mutants p.I505N and p.Q633R (Figure 13 C).

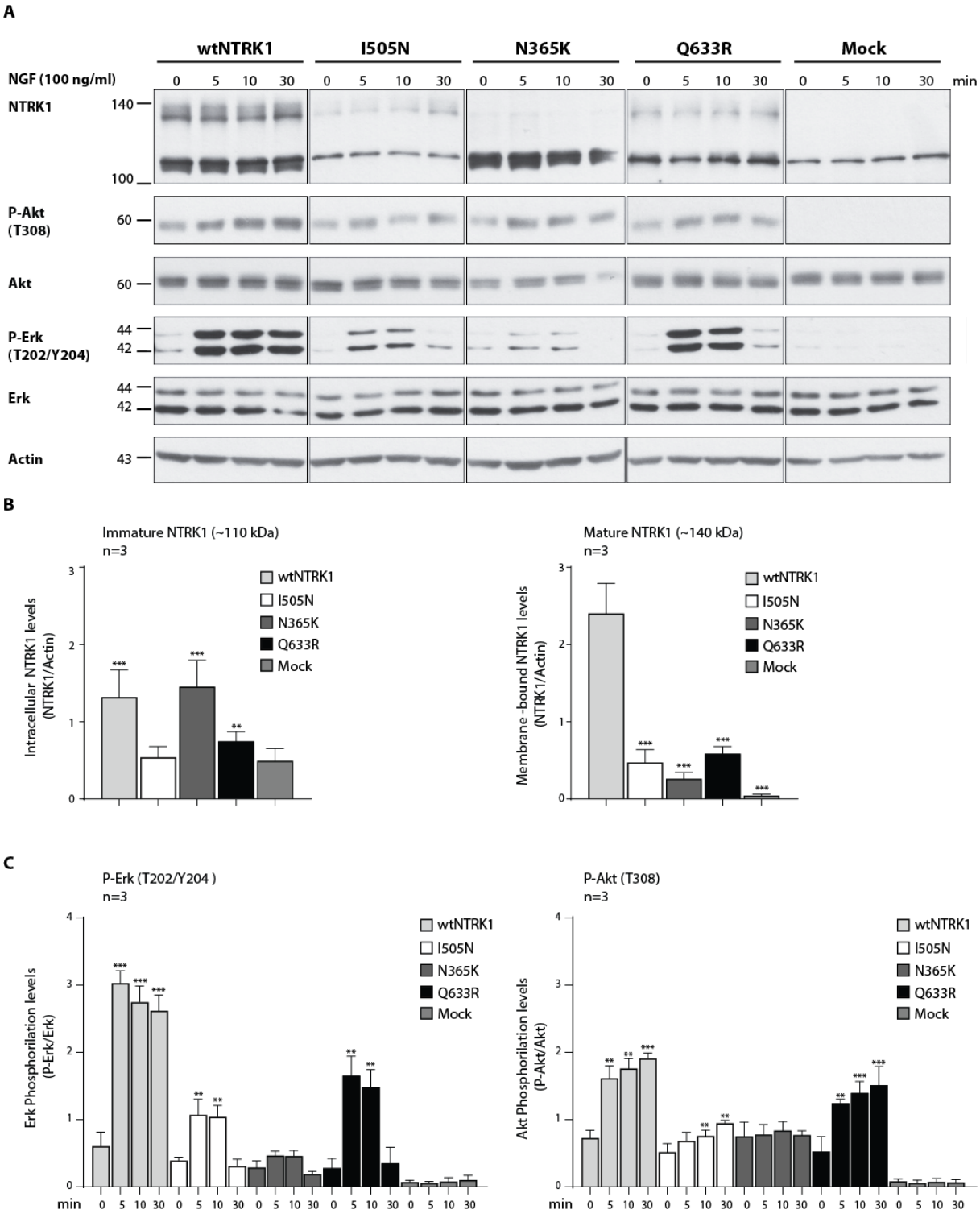

Figure 13. Expression of NTRK1 constructs and NGF-induced Erk/Akt phosphorylation

Ntrk1-KO PC12 cells were transfected with the respective NTRK1 cDNA construct. (A) NGF-induced Erk and Akt phosphorylation levels were analysed by western blotting. Y-axis: molecular weight in kilodaltons (kDa) (B) Quantification of intracellular (lower band ~110 kDa) and membrane-bound (upper band ~140 kDa) receptor levels. Intracellular NTRK1 levels are compared to the mock sample. Membrane-bound NTRK1 levels are compared to the WT sample. (C) Quantification of the time course data of NGF-induced Erk and Akt phosphorylation of panel A. Relative Erk or Akt phosphorylation levels were calculated by dividing phosphorylated values (P-Erk or P-Akt) by total Erk or Akt expression, respectively. Phosphorylation levels are compared to time point 0 in each cell population. The number of gels analysed quantitatively is given by "n". Data calculated by a two-tailed unpaired t-test, given as mean ± SEM; *p<0.05: **p<0.01; ***p<0.001.

Although all four constructs were nucleofected with the same amount of plasmid DNA, the different receptors seemed to be differentially expressed. Since the amount of receptor may influence activation of signalling pathways, Erk and Akt phosphorylation was first standardised to the endogenous Erk and Akt, respectively, and further normalised to the average of the standardised ratios (NTRK1/Actin) of both NTRK1 bands. As can be seen in Figure 14, the results are similar than the ones obtained by normalising phosphorylated Erk and Akt to the endogenous Erk and Akt, suggesting total receptor levels do not substantially influence the activation or the kinetics of the signalling pathways.

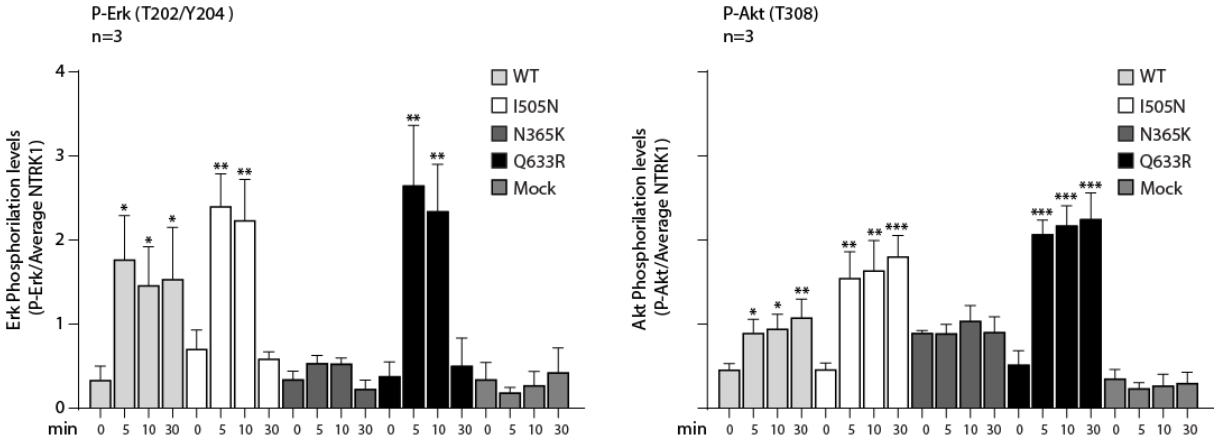

Figure 14. Normalization of NGF-induced Erk/Akt phosphorylation to total NTRK1

Quantification of the time course data of Figure 13A. Relative Erk or Akt phosphorylation levels (P-Erk) were calculated by dividing phosphorylated values by total Erk or Akt expression, respectively, and further divided by a mean of intracellular and membrane-bound NTRK1 levels. Phosphorylation levels are compared to time point 0 in each cell population. The number of gels analysed quantitatively is given by "n". Data calculated by a two-tailed unpaired t-test, are given as mean ± SEM; *p<0.05: **p<0.01; ***p<0.001.

5.1.4 Cellular localisation of NTRK1

As noted above, Western blot analysis showed that mutant p.N365K predominantly migrated as a ~110 kDa protein band, suggesting an improper processing or trafficking to the PM. Thus, the next step was to address the subcellular localisation of the wild-type and mutant NTRK1 proteins. HeLa cells were co-transfected with a fusion protein of K-Ras (HVR)-mCherry and the different NTRK1 receptors and further analysed by confocal microscopy. K-Ras was used as a membrane marker as it is activated by cell surface receptors and localises predominantly to the PM. As can be seen in Figure 15, wtNTRK1 and mutants p.I505N and p.Q633R show membrane localisation, while mutant p.N365K is not colocalizing with K-Ras (HVR)-mCherry and shows a perinuclear reticular pattern, indicating that this mutant is retained either in the Golgi apparatus or the endoplasmic reticulum (ER).

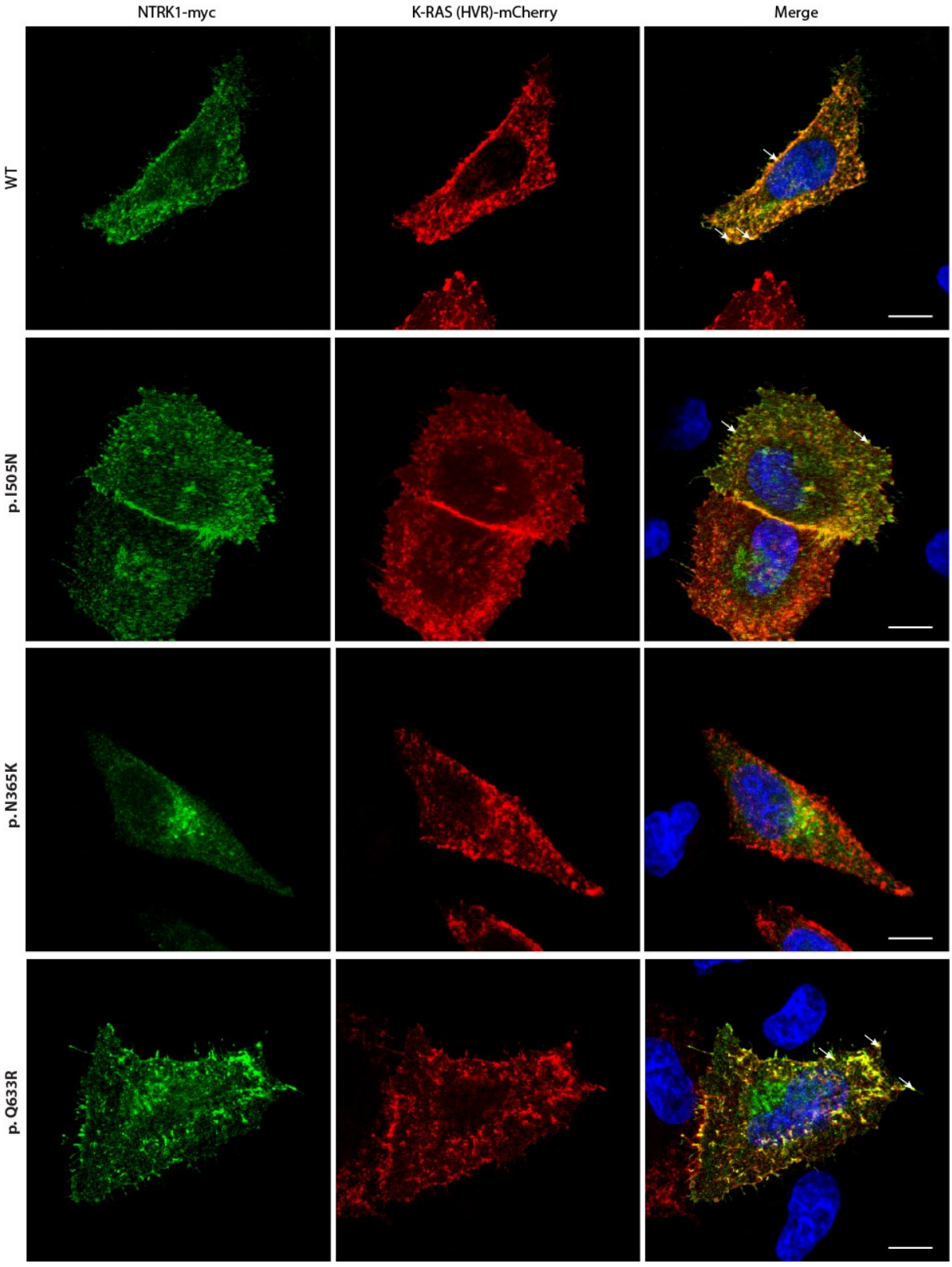

Figure 15. Co-localization of NTRK1-myc constructs with K-Ras (HVR)-mCherry

HeLa cells transiently expressing NTRK1-myc and K-Ras(HVR)-mCherry. 48 hr post-transfection, cells were fixed and co-stained for myc (green channel). Images were taken with a confocal laser scanning microscope. The left panel shows NTRK1-myc stained with anti-myc antibodies. In the middle panel K-Ras (HVR)-mCherry shows both an intracellular and a plasma membrane distribution. In the right panel the merged images are shown (Scale bars: 10 µm). Nuclei were stained with Hoechst 33258. Co-staining is illustrated by the yellow colour in overlay images. Arrows indicate co-localization of NTRK1-myc and K-Ras(HVR)-mCherry on the plasma membrane.

5.1.5 Neurite outgrowth

Activation of the Akt and Erk signalling pathways triggered by NTRK1 upon NGF stimulation results in morphological and biochemical differentiation of wild-type PC12 cells into a neuronal phenotype (*160*). Accordingly, the ability of the NTRK1 mutants to induce these changes was addressed. For this purpose, *Ntrk1*-KO PC12 cells were transiently transfected with the wtNTRK1, the three mutant constructs and GFP, and treated with NGF (100 ng/ml) for three days.

As expected, 25 % of *Ntrk1*-KO PC12 cells transfected with wtNTRK1 differentiated into a neuronal phenotype (Figure 16). However, cells transfected with mutants p.I505N and p.Q633R presented a strong reduction in the percentage of differentiated cells. The p.N365K mutation led to a significant decline in the proportion of differentiated cells to 9 %. In the GFP control, only 2% of transfected cells could be classified as having neurites two times longer than the cell body, which represents the percentage of spontaneously differentiated cells.

Altogether, the biochemical and biological data indicate a loss of function for all three NTRK1 mutants.

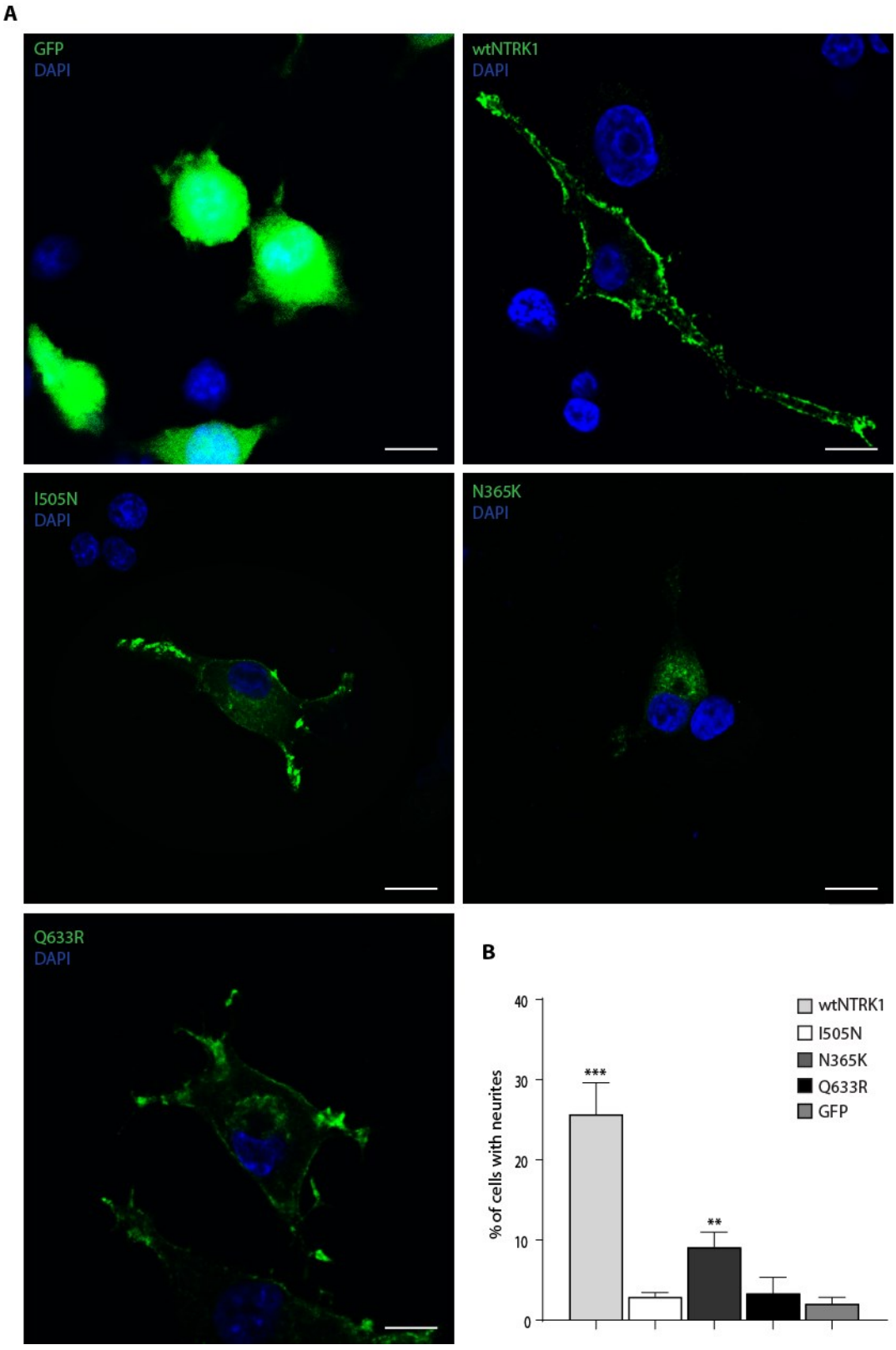

Figure 16. Differentiation capacity of wild-type and mutant NTRK1 variants of *Ntrk1*-KO PC12 cells
(A) Representative images of *Ntrk1*-KO PC12 cells transfected with the indicated NTRK1 cDNA-constructs after stimulation with NGF (100 ng/ml) for 72 hr. The presence of neurites is observed in wtNTRK1-transfected cells (B). Percentage of *Ntrk1*-KO cells transfected with the indicated NTRK1 cNDA-construct having neurites two times longer than the cell body diameter (Scale bars: 10 µm). The percentage was calculated from a total of 300 cells from three independent experiments (100 cells per experiment), and compared to GFP-transfected cells. Data are shown as mean ± SEM calculated using the two-tailed unpaired t-test; **p<0.01; ***p<0.001.

5.2 Generation of double-knockout mice by simultaneous targeting of the genetically linked genes *Scn10a* and *Scn11a* using the CRISPR/Cas9 system.

The alpha-subunits of the voltage-gated sodium channels $Na_V1.8$ and $Na_V1.9$ are encoded by *Scn10a* and *Scn11a*, respectively. Both ion channels are highly expressed in pain-sensing (nociceptive) neurones and have been involved in pain-related disorders in humans (*51*, *52*, *54*, *57*, *60*). Both channels are essential for the excitability of peripheral nociceptors. However, the single knockout of each gene only results in minor pain-related phenotypes. Thus, the generation of a *Scn10a/Scn11a*$^{-/-}$ double-knockout (DKO) mouse will be a valuable model to study the combined effect of both ion channels on pain-sensing pathways. Second, DKO DRG neurones are an ideal tool to investigate heterologously expressed $Na_V1.8$ and $Na_V1.9$ mutants and their role in human diseases.

Both *Scn10a* and *Scn11a* are located in close proximity on chromosome 9 and arose from gene duplication of an ancestral gene (*161*). Due to the short physical distance between them, these genes are genetically linked and inherited together, precluding that DKO animals can be generated by breeding of single knockout mice (*Scn10a* $^{-/-}$ x *Scn11a* $^{-/-}$). Therefore, the generation of the DKO mice was envisioned using the CRISPR-Cas system, targeting both genes simultaneously.

5.2.1 Generation of a double-knockout *Scn10a* and *Scn11a* mouse model via CRISPR genome editing: targeting strategy design.

The CRISPR-associated protein 9 (Cas9) nuclease generates an RNA-guided blunt double-strand-brake (DSB) at a targeted genomic sequence immediately upstream of the protospacer-adjacent-motif (PAM). Consequently, the non-homologous end-joining (NHEJ) repair pathway is activated. This error-prone repair mechanism frequently results in deletions and insertions (indels), inversions, duplications, as well as base substitutions near the cleavage site that might disrupt the gene-coding sequence (*73*, *125*). Simultaneous targeting two genes residing next to each other adds another layer of complexity regarding the possible rearrangements produced by the repair mechanisms of cells, including inversions and fusions between exons. Moreover, editing can occur on alleles of the two different homologous chromosomes (in *trans*) or the same chromosome (in *cis*). Only the latter event is useful to produce a *Scn10a/Scn11a* double-knockout line. Accordingly, the targeting and genotyping strategy had to take into account the different outcomes of CRISPR-aided-mutagenesis.

Consequently, the selected approach involved targeting independent exons in each gene to avoid novel transcripts from gene fusion. Hence, it was expected that at least one cut would occur in the same chromosome resulting in a frameshift mutation in both consecutive genes. Each gene was screened for potential single guide RNAs (sgRNAs) that minimised off-target cleavage in order to reduce detrimental effects of mutations and chromosomal rearrangements using the online design tool from Benchling (www.benchling.com). Two 20-nt-sgRNAs were designed per gene. For *Scn10a,* sgRNAs targeting exon 6 (Ex6) and exon 11 (Ex11) were selected, while sgRNAs targeting exon 9 (Ex9) and exon 10 (Ex10) were chosen for *Scn11a* (Figure 17). The cleavage sites in exon 6 and 11 are separated by 6650 bp, while in exon 9 and 10 they are separated by 1234 bp. A precise deletion of the region between both cuts in each respective gene would lead to a frameshift mutation.

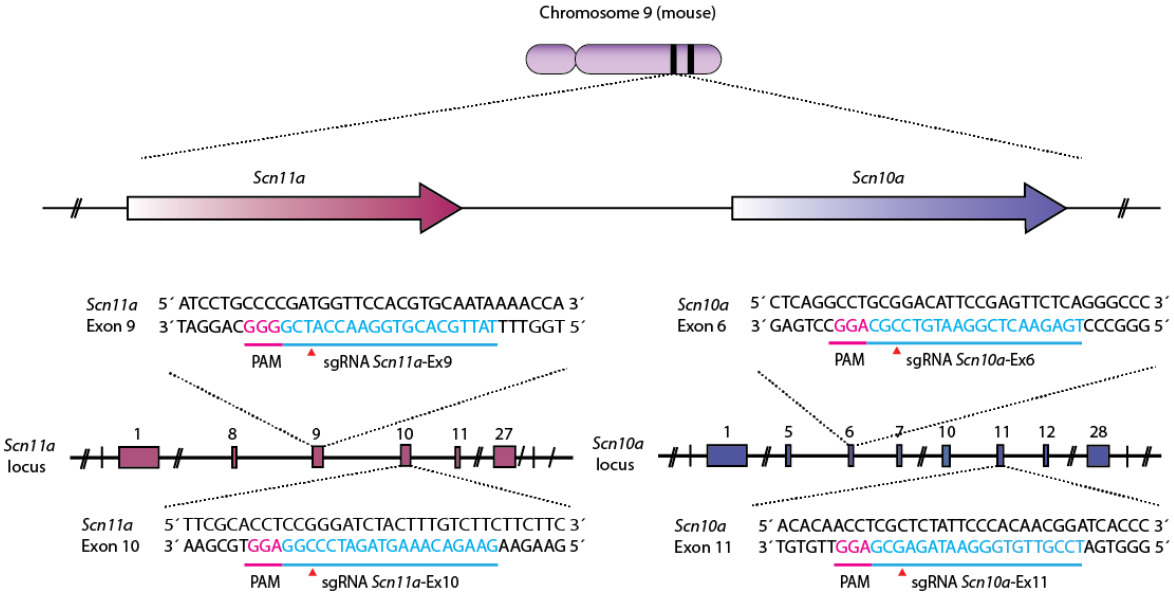

Figure 17. Targeting strategy of the *Scn10a* and *Scn11a* genes.
Schematic representation of *Scn10a* and *Scn11a* genomic locus in the mouse and the selected target sites. Both *Scn10a* and *Scn11a* are located in close proximity on chromosome 9. The single guide RNA (sgRNA) target sites are located in exon 6 and 11 for *Scn10a* and in exon 9 and 10 for *Scn11a*. The 20-nt guide sequence (in blue) comprising the 5'-end of the sgRNA is shown. The protospacer adjacent motif (PAM; 5'-NGG-3'; pink) of the *Streptococcus pyogenes* Cas9 is located 3' of the target sequence. The SpCas9 enzyme introduces a double-strand-break three nucleotides upstream of the PAM (red triangles), triggering imperfect non-homologous end-joining repair pathways. Ex, Exon.

5.2.2 Construction of CRISPR-Cas9 plasmids.

The four 20-nt sgRNA sequences with or without an extra 5'-G were directionally cloned into the pX330 vector, which co-expresses hSpCas9 and an sgRNA cloning site under the chicken beta-actin hybrid (CBh) and human U6 promoters, respectively (*147*) (Figure 18A).

5.2.3 Generation of *Scn10a/Scn11a* double-knockout mice by pronuclear injection of CRISPR-Cas9 plasmids.

Next, the feasibility of using CRISPR-Cas9 plasmids to generate DKO mice was addressed. The four pX330 plasmids were simultaneously microinjected into pronuclei of fertilised eggs at a final concentration of 5 ng/µl or 10 ng/µl prior to transplantation into the oviducts of pseudopregnant female mice. A total of approximately 100 zygotes collected from C57/BL6 mice were used for each injection. To reduce the risk of DNA integration into the host genome, plasmid DNA was injected in its circular form as illustrated in Figure 18A. One foster mother per injection gave rise to six pups for the first injection (5 ng/µl) and five for the second one (10 ng/µl). Tail biopsies were taken at postnatal day 10 for genomic DNA extraction. As an initial genotyping screening, PCRs for each exon were performed (PCR A, B, C, D; Figure 18B) to detect mutations induced by NHEJ using primer pairs listed in Table 10, subjected to 2% agarose gel electrophoresis (Figure 18C, 14D), and further sequenced. Surprisingly, none of the pups had modified alleles in any of the four exons targeted (Figure 18D). Hence, this approach was discontinued, and alternative strategies were considered (see below).

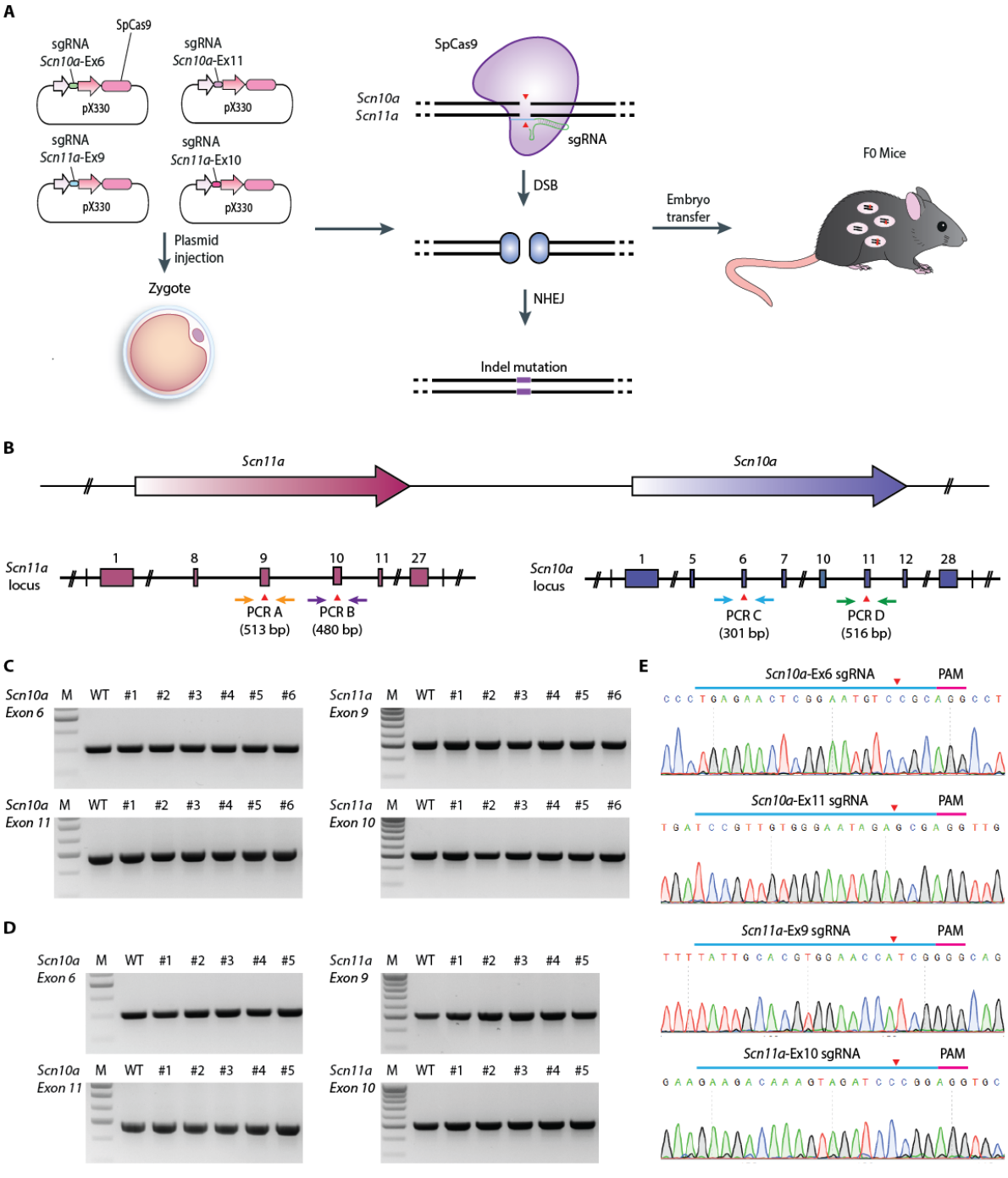

Figure 18. Generation of *Scn10a/Scn11a* double-knockout mice by pronuclear DNA injection.
(A) Scheme of the targeting strategy. Zygotes were microinjected in the pronuclei with four pX330 plasmids, each expressing *Streptococcus pyogenes* Cas9 (SpCas9) and an sgRNA targeting the respective exons of *Scn10a* and *Scn11a*. SpCas9 causes a double-strand break (DSB) that triggers the non-homologous end joining (NHEJ) repair pathways leading to indel mutations (violet box). (B) Genotyping strategy to detect genome-engineered alleles. PCR primers were designed to amplify the targeted sites on each gene (small coloured arrows in orange, violet, blue and green). The predicted sizes of each PCR product are given. The red triangles indicate the predicted SpCas9 cleavage site. (C,D) Analysis of PCR products from F_0 generation mice by 2% agarose gel electrophoresis. To detect NHEJ-induced mutations in *Scn10a* and *Scn11a*, PCRs A, B, C, and D were performed as an initial step. (E) Direct sequencing of the PCR products was performed confirming that all mice were wild-type (WT). The 20-nt guide sequence (blue bar on top) comprising the 5'-end of the crRNA is shown followed by the protospacer adjacent motif (PAM; 5'-NGG-3'; pink). bp, base pairs; Ex, exon; M, Molecular weight marker.

5.2.4 Generation of knockout mice by cytoplasmic injection of SpCas9 mRNA and sgRNA.

As the use of plasmid DNA for the generation of the DKO mice was unsuccessful, a second round of injections was performed using mRNA. For this purpose, the pX330 plasmids were used as template for the generation of four sgRNAs targeting *Scn10a* and *Scn11a* by the T7 RNA polymerase/promoter in vitro transcription system. To test whether *Scn10a*/*Scn11a*$^{-/-}$ DKO mice could be produced, these validated sgRNAs (Figure S6) were microinjected together with SpCas9 mRNA into the cytoplasm of ~100 one-cell mouse embryos at 6.25 ng/µl for each sgRNA and 25 ng/µl for SpCas9 mRNA as illustrated in Figure 19A. Pseudopregnant female mice were implanted with the resulting viable embryos, and two of them gave birth to a total of 16 pups. Genomic DNA was prepared from mouse tails, and genotyping PCRs were performed for each exon as described in the previous section followed by 2 % agarose gel electrophoresis. As can be seen in Figure 19A, using this approach several mice were genetically modified as assessed by the presence of bands of different size. Interestingly, a single band of the same size was detected for *Scn10a*-Ex6 in all pups except for #11 and #14 (12.5%), which seemed to miss the entire exon as judged by the lack of PCR amplification. A missing amplicon was also observed for *Scn11a*-Ex9 in pups #8 (6.25%), whereas in pups #13 and #14 *Scn11a*-Ex10 was missing (12.5%). Also, more than two bands were observed in animal #4 (*Scn11a*-Ex10), indicating that this mouse was heterozygous. Moreover, pups number #7, #8 presented a faster-migrating PCR-product for *Scn11a*-Ex10, suggesting a homozygous deletion. Furthermore, PCR amplification with primers spanning a larger region around the cleavage site confirmed a larger deletion in pups #7 (*Scn10a*-Ex6) and #4 (*Scn11a*-Ex10) (Figure S7).

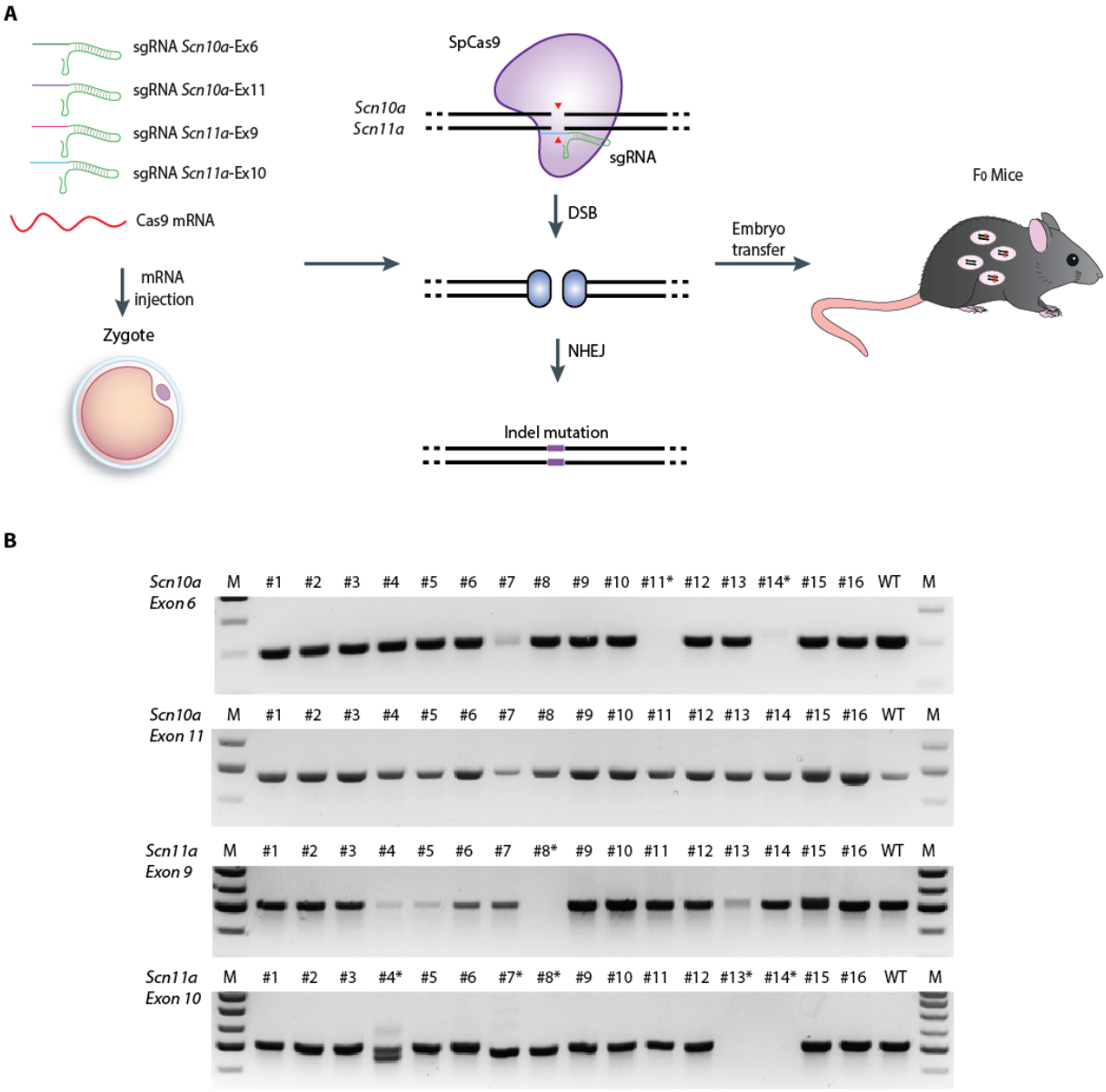

Figure 19. Successful generation of *Scn10a/Scn11a* double-knockout mice by cytoplasmic injection of Cas9 mRNA and sgRNA.

(A) Schematic representation of the targeting strategy: zygotes were microinjected with four sgRNAs targeting the respective exons of *Scn10a* and *Scn11a* and *Streptococcus pyogenes* Cas9 (SpCas9) mRNA, aiming to cause a double-strand break (DSB) that would trigger the non-homologous end joining (NHEJ). (B) Identification of founder mice from F_0 generation by 2% agarose gel electrophoresis. To detect NHEJ-induced mutations in *Scn10a* and *Scn11a*, PCRs A, B, C, and D (shown in figure 18B) were performed. Mice presenting an altered band pattern are marked by asterisks (*). Ex, exon; M, Molecular weight marker.

To analyse the F_0 mice in more detail, polyacrylamide gel electrophoresis (PAGE)-based genotyping was performed, as it enables the identification of heterozygous and homozygous mutations with higher sensitivity than separation in agarose gels (*137*). Thus, the genomic regions spanning the targeted sites were PCR amplified and subjected to 5% PAGE. In case of heterozygous indel mutations, DNA heteroduplexes with a characteristic mobility pattern will form enabling the assessment of number and type of mutation. In wild-type control mice, PCR amplification yielded one single band of the respective size for each exon (Figure 20A). However, multiple heteroduplexes were detected in 9 of 16 mutant mice (56.25%), which was significantly higher than aberrant bands identified by 2% agarose gel electrophoresis (18.75%). Several animals displayed a single pair of heteroduplex bands, indicating one dominant type of indel mutation. For instance, animals #4, #13 and #15 revealed heterozygosity for *Scn10a*-Ex11 (18.75%). In addition, animals #4, #7, #9, #11, #12, #13, #14 and #15 were heterozygous for *Scn11a*-Ex9 (50%), while animals #4, #6 and #15 bear heterozygous mutations in *Scn11a*-Ex10 (18.75%). Remarkably, pups #4 and #15 were heterozygous for the three exons (12.5%) and exhibited multiple pairs of heteroduplex bands, suggesting mosaicism.

Using this method one can also identify homozygously targeted mice with small indels. For this purpose, PCR products from F_0 mutant mice were mixed with products from wild-type mice followed by brief denaturation and annealing, and once more subjected to 5% PAGE. As can be observed in Figure 20B, mouse #6 (*Scn11a*-Ex9), as well as mice #7 and #12 (Scn11a-Ex10), exhibited migration patterns indicative for homozygous indels.

It is important to notice that an absence of a heteroduplex does not exclude that gene editing has occurred. Thus, sequencing was done to confirm results as well as to identify mice with nonsense or frameshift mutations. Additionally, PCR products were subcloned into TOPO vector to allow allele-specific analysis. Several targeted mutations were found in the F_0 mice, including small deletions, small insertions, and nucleotide substitutions.

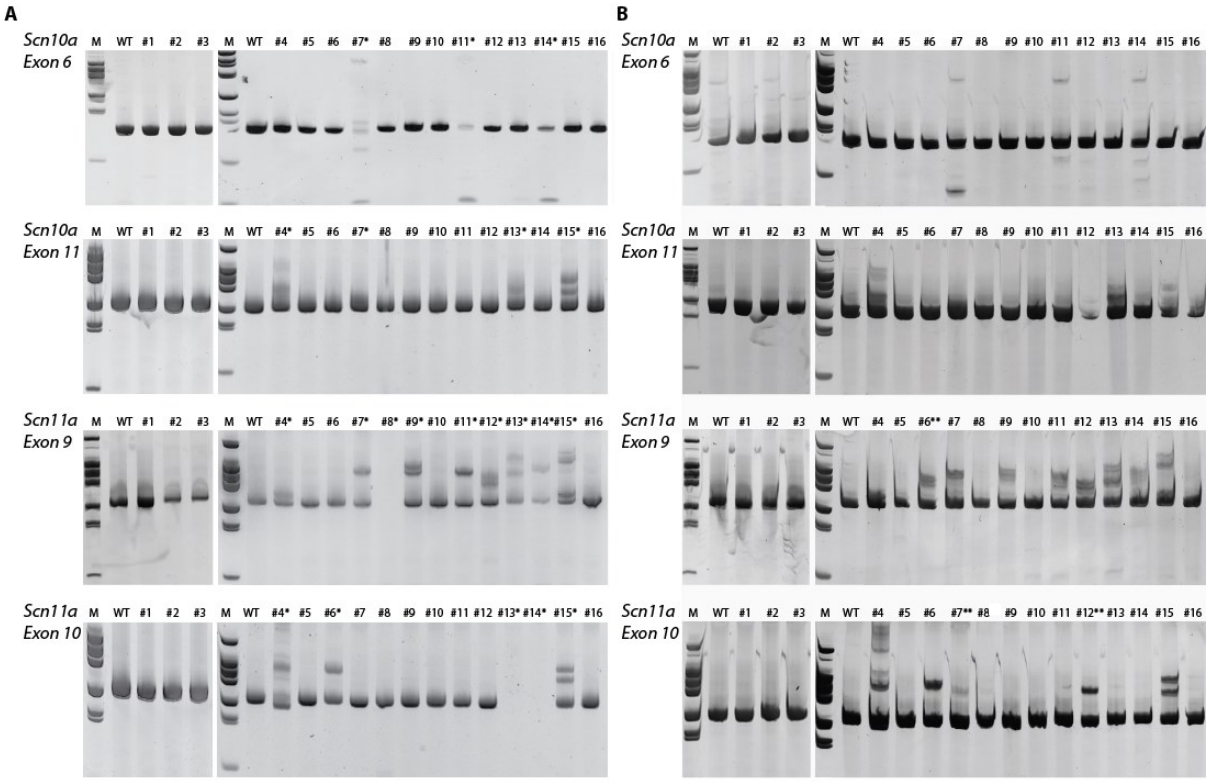

Figure 20. Detection of CRISPR/Cas9-mediated genome-modified *Scn10a* and *Scn11a* mice by PAGE.

Pups from F_0 generation were screened for targeted modifications in *Scn10a* and *Scn11a* loci using the PAGE-based genotyping method. (A) 5% PAGE analysis detected heteroduplex DNA in mice # 4, #6, #7, #9, #11, #12, #13, #14 and #15, indicating the presence of heterozygous mutations (indicated by asterisks, *). Homoduplex DNA only was detected in DNA from mice # 1, #2, #3, #5, #8, #10, and #16, similarly to wild-type DNA. (B) When mixing PCR products from F0 mice with PCR products from wild-type mice, mouse #6 (exon 9) as well as mice # 7 and #12 (exon 10) exhibited migration patterns from heteroduplex DNA (marked by two asterisks, **), indicating homozygous indel-mutations. M, Molecular weight marker.

5.2.4.1 Precise large deletions can be induced by the CRISPR/Cas9 system

The use of more than one sgRNA might lead to larger deletions between both sgRNA target sites. To test this possibility, a combination of primers from PCRs A, B, C and D was used to amplify deleted regions between cleavage sites as shown in Figure 21A. In *Scn11a*, the CRISPR targeting sites are separated by only 1.2 kb. The forward primer of PCR A and the reverse primer of PCR B were combined (PCR E, Figure 21A) to amplify the anticipated deleted region of ~0.5 kb. As shown in Figure 21B, several mice presented a band of smaller size, suggesting that different rearrangements occurred in these animals. Sequencing confirmed that four mice (#5, #6 and #14, #15) contained an allele with a precise exon junction leading to a premature stop codon (25%), as illustrated in Figure 21C. On the contrary, pups #4 and #9 contained a large deletion following the cleavage site of exon 9, but exon 10 was indeed present. More precisely, animal #4 was missing a region of 1050 bp together with a Δ1 bp in exon 10, while pup #9 had a Δ1078 bp (see Figure 22). Pup #13

presented an allele with an extra nucleotide in the junction. While the possible outcome of the rearrangements in the first two pups (#4, #9) is hard to predict as half of exon 9 is missing, the modification in the latter (#13) is detrimental as it leads to a premature stop codon. Furthermore, several mice that were not further analysed presented a faint band at the expected size, suggesting they might carry a similar deletion.

The two targeting sites located in *Scn10a* are separated by 6.65 kb. Deletion of this region would lead to a substantially smaller PCR product of approximately 0.5 kb when combining the forward primer of PCR C and the reverse primer of PCR D (PCR F, Figure 21A). Interestingly, 2% agarose gel electrophoresis of the resulting PCR products revealed that 2 out of 16 mice (12.5%) carried the desired deletion as can be seen in Figure 21B. Sequencing of the PCR products confirmed that both mice exhibited a precise joining of predicted cleavage sites (Figure 21D), leading to a premature stop codon in *Scn10a*.

To test whether an even larger deletion was induced, a PCR using the forward primer of PCR A and the reverse primer of PCR D was performed. Deletion of the 141 kb region between the most distant cleavage sites would produce a band of ~470 bp (PCR G, Figure 21A). Strikingly, pups #7 and #14 presented this astonishingly large deletion as can be seen in Figure 21B. Sequencing confirmed that both mice contained an allele with a precise exon junction leading to a premature stop codon (12.5 %), as shown in Figure 21E.

5.2.4.2 Establishing a detailed genotype for F_0 mice.

Based on the previous findings, a genotype for each of the 16 mice was determined. A comprehensive description of the mutations found in the F_0 mice is depicted in Figure 22, and the results are summarised in Table 13.

Interestingly, some mice carried homozygous mutations in both alleles. For instance, mouse # 11 had a homozygous Δ1 bp in both genes. Although mosaicism cannot be excluded, this mouse seems to be a homozygous DKO. This observation strongly suggests that a combined *Scn10a* and *Scn11a*-deficiency is not lethal.

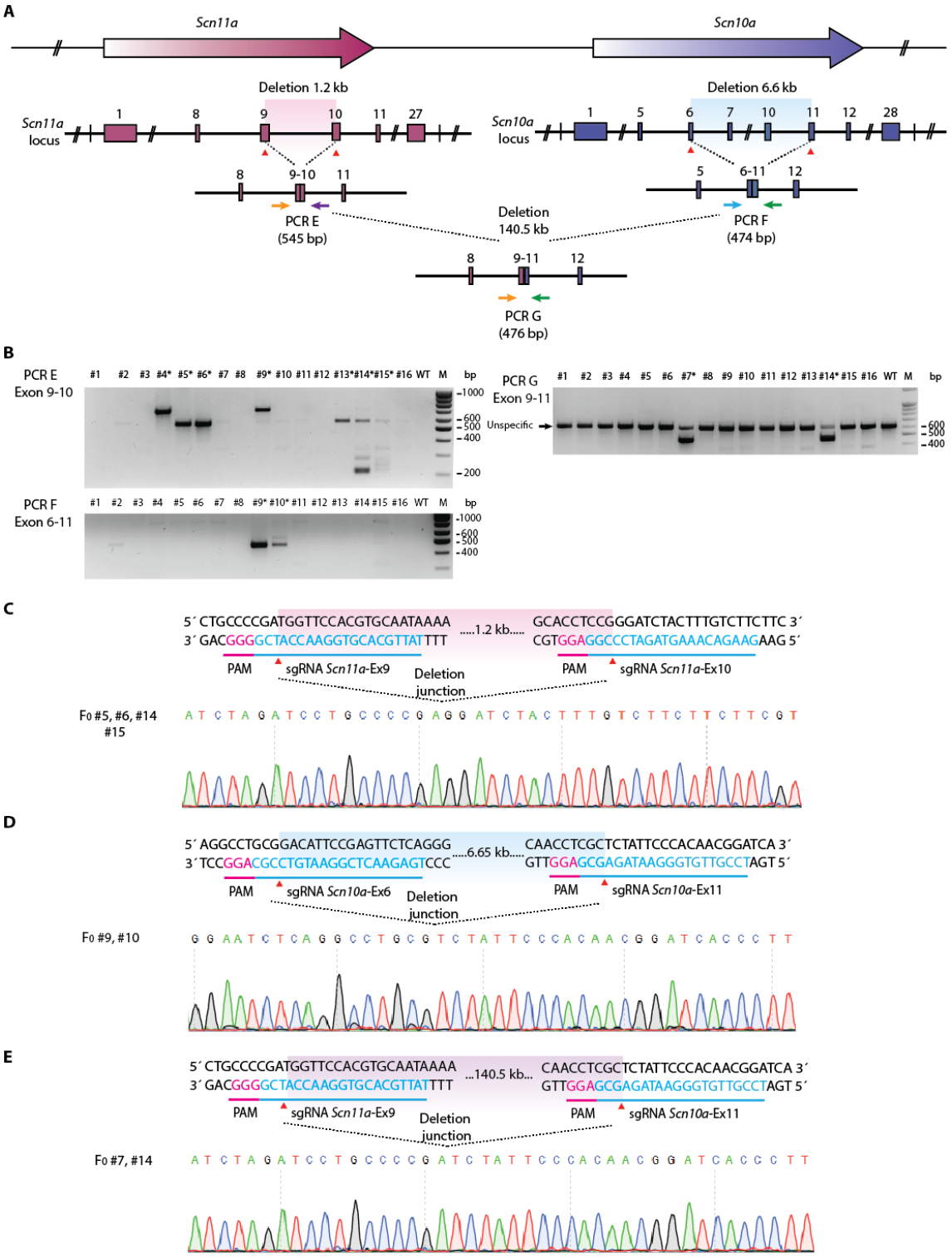

Figure 21. Detection of CRISPR/Cas9-mediated large deletions between *Scn10a* and *Scn11a* target sites

(A) Genotyping strategy to detect genome-engineered alleles with large deletions. PCR primers (small coloured arrows: in orange, green, violet and blue) were designed to amplify the targeted sites in each gene (see Figure 18B) and combined to amplify the desired product. The predicted sizes of each PCR product are depicted. Red triangles indicate the SpCas9 cleavage site. (B) Identification of founder mice from F_0 generation by 2% agarose gel electrophoresis having large deletions. To detect large deletions within each gene and between both genes, PCRs E, F and G were performed. Mice presenting an altered pattern are marked by asterisks (*). (C) Representative sequence trace of mice bearing deletions between *Scn11a*-Ex10 and *Scn10a*-Ex9, (D) between *Scn10a*-Ex6 and *Scn10a*-Ex11, and (E) between both *Scn10a* and *Scn11a*. bp, base pairs; Ex, exon; kb, kilobases; M, Molecular weight marker.

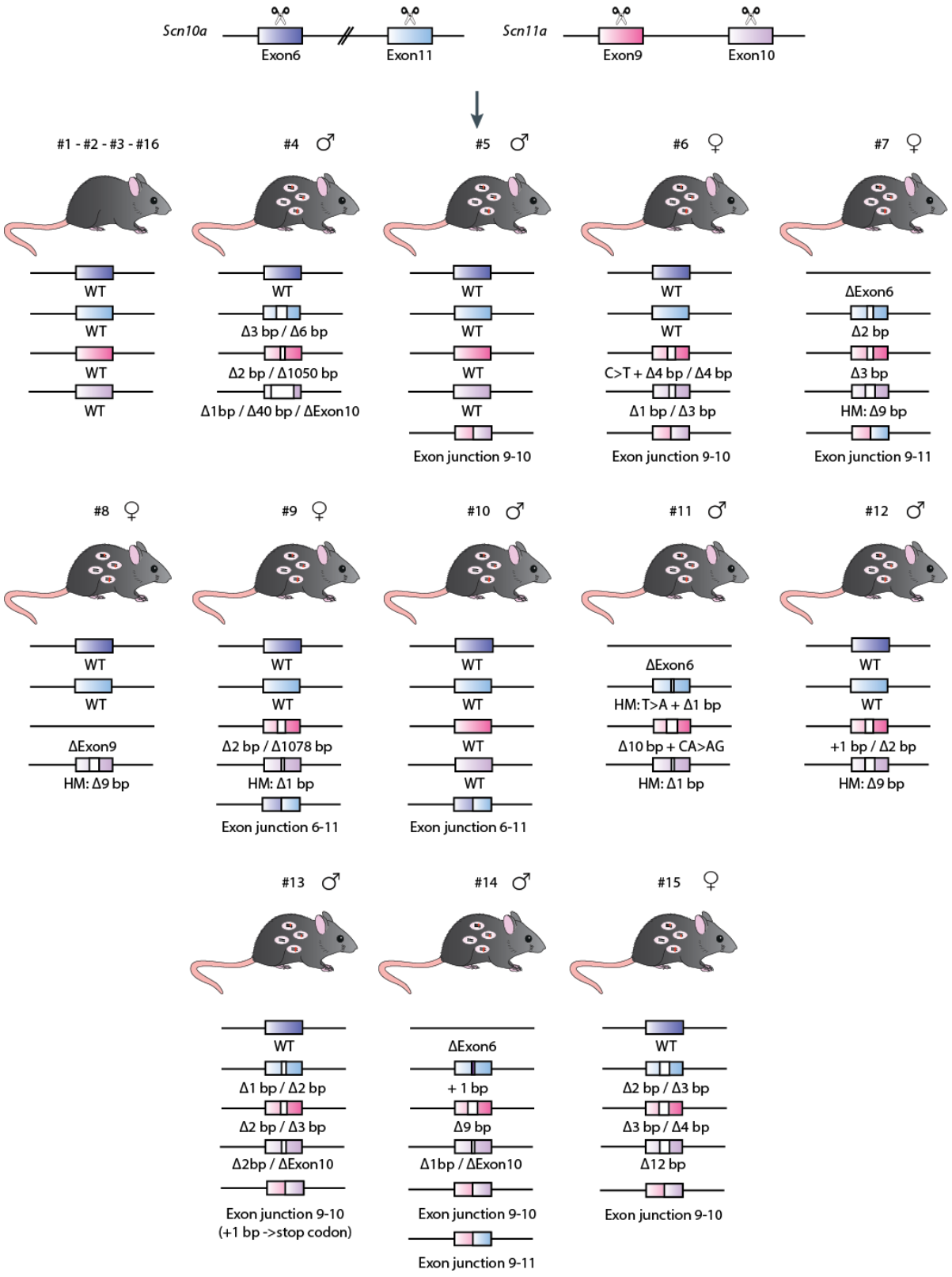

Figure 22. Schematic summary of all rearrangements found in the F_0 mice for *Scn10a* and *Scn11a*.

Several mutations were found in the F_0 mice, including small deletions (Δ, white box inside each exon) ranging from 1 to 40 base pairs (bp), small insertions (number of inserted base pairs (bp) indicated by "+", violet box inside each exon), nucleotide substitutions (>) as well as large deletions, exon deletions (ΔExon), and exon junctions. Several mice were mosaics, bearing different allele combinations. Alleles were found in heterozygosity unless stated as homozygous (HM). ->, leading to; /, or; ♂, male; ♀, female, WT, wild type.

Table 13. Statistics of the generation of *Scn10a* and *Scn11a* double-knockout mice by cytoplasmic injection of Cas9 mRNA and sgRNAs.

	Total
Injected embryos	105 (100%)
Implanted viable embryos	45 (42.8%)
Newborns	16 (15.2%)
≥ 1 modified allele	12 (75%)
Mutant for Exon 6	3 (18.75%)
Mutant for Exon 11	6 (37.5%)
Mutant for Exon 9	10 (62.5%)
Mutant for Exon 10	10 (62.5%)
Mutant for *Scn10a* only	1 (6.25%)
Mutant for *Scn11a* only	4 (25%)
Mutant for both *Scn10a* and *Scn11a*	7 (43.75%)
Containing deletions between *Scn10a* Exon 6 and 11	2 (12.5%)
Containing deletions between *Scn11a* Exon 9 and 10	5 (31.25%)
Containing deletions between *Scn11a* Exon 9 and 11	2 (12.5%)

Percentages of genetically modified mice were calculated over the total number of newborn F_0 mice (16) obtained by mRNA injection.

5.2.4.3 Founder selection and analysis of germline transmission from F_0 mice to their progeny

Given the high number of detected mosaic mice, it was important to identify germline alleles that could be transmitted to the offspring leading to a DKO line. Therefore, two mice were chosen for further breedings, F_0#11 and F_0#14, as they contained the most promising alleles for gene disruption. The first animal contained a heterozygous deletion of the entire *Scn10a*-Ex6, a homozygous T>A c.1392 mutation along with a Δ1 bp in *Scn10a*-Ex11, a heterozygous Δ10 bp together with a substitution (CA>AG) in *Scn11a*-Ex9, and a homozygous Δ1 bp in *Scn11a*-Ex10. The second animal was mosaic and contained several null mutations including exon junctions between *Scn11a*-Ex9 and Ex10 as well as *Scn11a*-Ex9 joined with *Scn10a*-Ex11.

Both animals were mated with two C57BL/6J female mice, and the progeny was analysed. As depicted in Figure 23, F_0#14 transmitted several mutations, including 2, 3, or 9 bp deletions, and a 14 bp insertion plus a G>T substitution (Figure S8). However, none of the allele combinations was suitable for the generation of a DKO line.

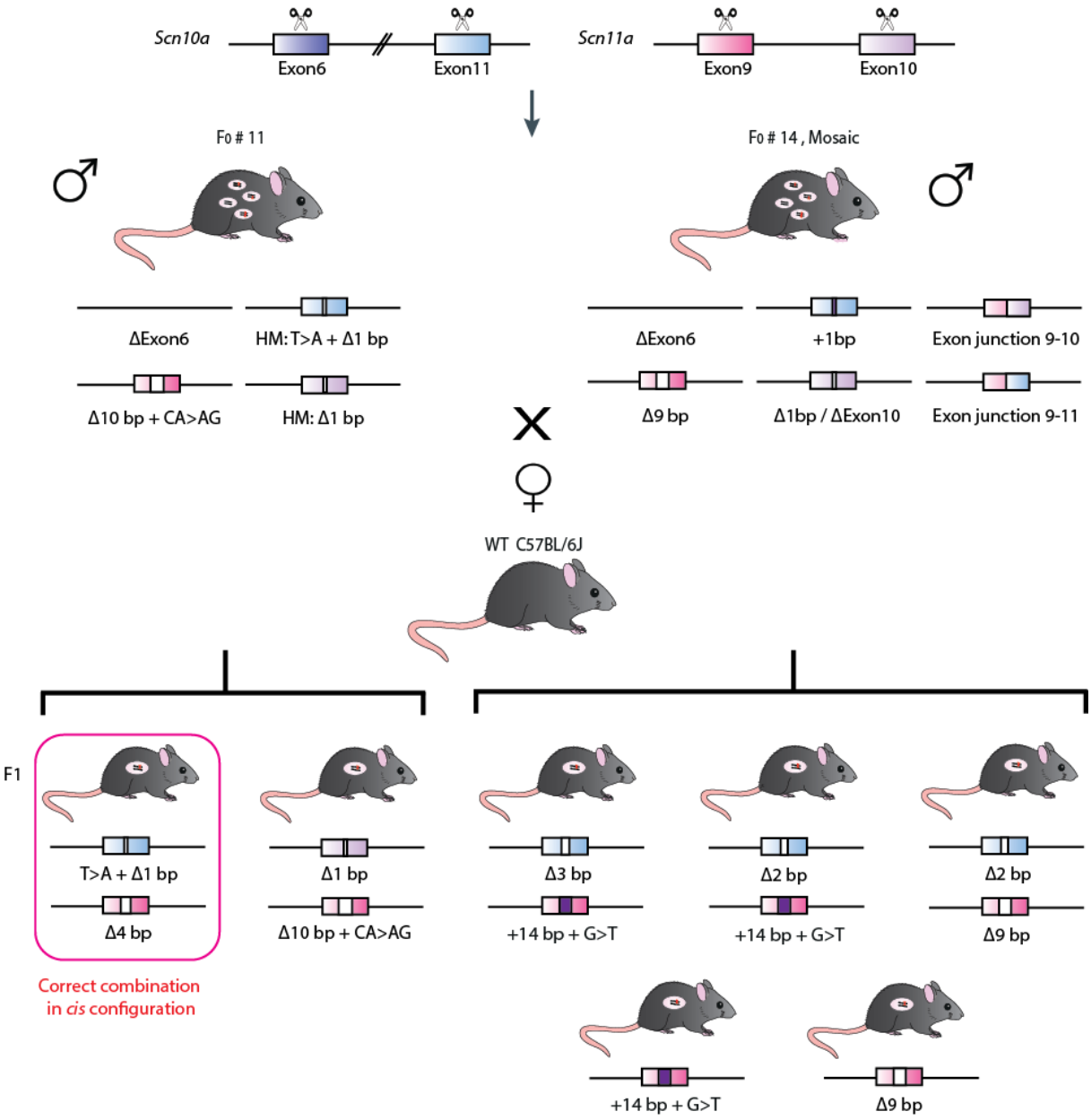

Figure 23. Analysis of germline transmission from F_0 mice to their progeny.

F_0 mice #11 and #14 were mated with wild-type C57BL/6 mice, and their progeny (F_1) were genotyped to identified transmitted alleles. Deletions (Δ) are represented by a white box inside each exon while insertions (+) are depicted by a violet box. Mice from F_0#11 had two different allele combinations: some animals had a Δ1 bp in *Scn11a*-Ex10 and a Δ10 bp plus a CA>AG substitution in *Scn11a*-Ex9, while others had a Δ1 bp in *Scn10a*-Ex11 and a Δ4 bp in *Scn11a*-Ex9. Only the latter represented a useful rearrangement, targeting both genes. Mosaic mouse #14 transmitted five different allele combinations, including Δ3 bp or Δ2 bp in *Scn10a*-Exon11 and a 14 bp insertion plus a G>T substitution or a Δ9 bp in *Scn11a*-Ex9.; Alleles were found in heterozygosity unless stated as homozygous (HM). Abbreviations: bp, base pairs.

On the other hand, F_0#11 transmitted two different allele combinations. As shown in Figure 23, half of the offspring from this mouse contained the expected Δ1 bp in *Scn11a*-Ex10 along with the Δ10 bp plus substitution (CA>AG) in *Scn11a*-Ex9 that together caused a premature stop codon in *Scn11a*. However, these animals had no mutations in *Scn10a*. The other half of the littermates contained a T>A substitution along with a Δ1 bp in *Scn10a*-Ex11 plus a novel

Δ4 bp in *Scn11a*-Ex9 (see Figure S8). Interestingly, in this case, mutations causing a premature stop codon in both genes occurred in *cis*. Taken together, these results suggest that a detailed analysis of the F_1 generation is essential to identify which mice carry the desired genome-engineered alleles.

5.2.4.4 Off-target analysis in CRISPR/Cas-mediated mutants.

The CRISPR-Cas9 system can lead to undesired off-target (OT) cleavage and subsequent unwanted mutations as the SpCas9 enzyme can tolerate certain mismatches between the sgRNA and the target DNA as well as use an alternative PAM sequence, 5'-NAG (*138*). In the present study, OT sequences were computationally identified and ranked using the online design tool from Benchling (www.benchling.com) (Table S3, S4, S5, S6), tolerating up to four mismatches in the target gRNA sequence (*138*). For each sgRNA, primers for the top five OT sequences and OT coding regions were designed (Table 11). The regions containing the potential OT sites were amplified and further sequenced to determine if any mutations or changes occurred. Only the founder chimaera (F_0#11) and two F_1 founder animals (F_1#5, F_1#6) were analysed. A total of 23 OT sites were examined (five OT sites for *Scn10a*-Ex6 and six for each *Scn10a*-Ex11, *Scn11a*-Ex9/10). Although other potential OT effects cannot be excluded, no indel mutation was observed in the analysed OT regions in any of the mutant mice (Figure S9), suggesting a high specificity of the CRISPR-Cas9 system.

5.3 Knockout validation and phenotype assessment.

Two F1 mice containing the correct allele combination were further mated to generate a *Scn10a/ Scn11a* $^{-/-}$ mouse line. *Scn10a/Scn11a* DKO mice were born at the expected Mendelian ratio from heterozygous breedings, indistinguishable from *Scn10a/Scn11a* wild-type mice. In addition, they did not show an increased mortality compared to their wild-type littermates. Sequencing of *Scn10a/Scn11a* $^{-/-}$ mice confirmed the correct transmission of the desired alleles (Figure 24A). Moreover, homozygous *Scn10a/Scn11a* DKO mice were fertile and did not show apparent abnormalities or deficits until 24 months of age.

Importantly, *Scn10a* and *Scn11a* mRNA expression was not detected by qPCR in the dorsal root ganglia of these mice (using primers targeting intact exons - 4/5 for *Scn10a*, 12/13 for *Scn11a*- listed in Table 12) as shown in Figure 24C. *Gapdh* expression served as housekeeping gene for all cDNA samples.

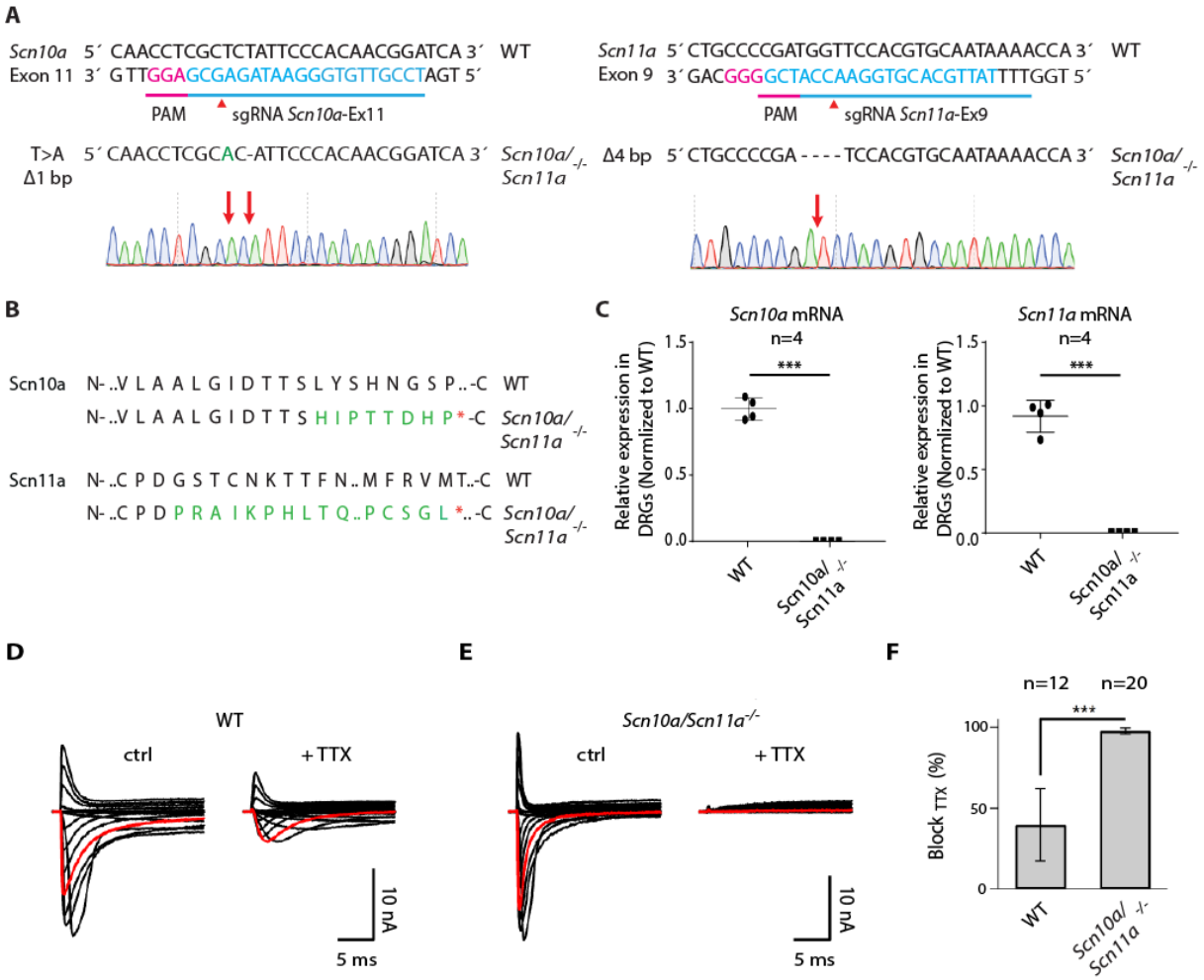

Figure 24. Validation of the *Scn10a/Scn11a* double-knockout mouse model.

(A) DNA sequencing of *Scn10a/Scn11a* $^{-/-}$ mice confirmed a T>A substitution along with a Δ1 bp in *Scn10a*-Ex11 plus a Δ4 bp in *Scn11a*-Ex9. Red arrows indicate the respective mutations in the chromatogram. (B) Both mutations lead to premature stop codons. (C) qPCR analysis of wild-type (WT, *Scn10a/Scn11a*$^{+/+}$) and *Scn10a/Scn11a*$^{-/-}$ dorsal root ganglia (DRGs) revealed that mRNA levels for both genes were not detectable in double-knockout mice. *Gapdh* expression served as housekeeping gene control for all cDNA samples. (D) Whole-cell current recordings from WT-DRG neurones before (ctrl) and after the addition of tetrodotoxin (TTX). (E) Whole-cell current recordings from *Scn10a/Scn11a* $^{-/-}$ DRG neurones before (ctrl) and after the addition of TTX. (F) Inhibition of sodium currents obtained from WT and *Scn10a/Scn11a*$^{-/-}$ DRG neurones in response to application of TTX at a concentration of 1µM. Error bars indicate SEM. The number of individual experiments n is indicated. Statistical significance was tested with a two-sided unpaired Student's t-test. Δ, deletion.

Additionally, the double-knockout was verified by electrophysiological studies conducted by Dr. Enrico Leipold (Department of Biophysics, Jena). Nociceptive sensory neurones express a variety of sodium channel isoforms, including the tetrodotoxin resistant (TTX-R) $Na_V1.8$ and $Na_V1.9$ (*33*, *34*) and TTX-sensitive sodium channels (*162–165*), as well as voltage-dependent calcium channels (*166*). Figure 24D illustrates the effect of TTX on total voltage-gated sodium current elicited by step depolarizations in small diameter dorsal root ganglion (DRG) neurones isolated from wild-type mice. As expected, upon application of 1 µM tetrodotoxin (TTX) the only sodium currents recorded are carried by the TTX-R sodium channels $Na_V1.8$

and $Na_V1.9$. On the contrary, *Scn10a/Scn11a*$^{-/-}$ small diameter DRG neurones show complete inhibition of sodium currents upon TTX application, demonstrating the absence of endogenous $Na_V1.8$ and $Na_V1.9$, thus verifying the successful knockout of *Scn10a* and *Scn11a*. Together, these results show that *Scn10a/Scn11a*$^{-/-}$ mice were successfully generated with the CRISPR-Cas9 system by cytoplasmic injection of Cas9 mRNA and sgRNAs.

5.4 *Scn10a/Scn11a*$^{-/-}$ DRGs enable functional analysis of human $Na_V1.8$ and $Na_V1.9$.

To investigate whether the activity of the TTX-R channels can be rescued in the DKO-DRG neurones, whole-cell current recordings were performed from isolated DRG neurones transiently transfected with wild-type (wt) cDNA constructs encoding human $Na_V1.8$ and $Na_V1.9$. As shown in Figure 25B and Figure S10, successful transfection gave rise to functional expression of human $Na_V1.8$ and $Na_V1.9$.

ND7/23 cells (hybrids of neuroblastoma and dorsal root ganglia cells) were also transfected with wt$Na_V1.9$ as a positive control, as they were previously shown to enable the expression of functional human $Na_V1.9$ channels (*57*, *167*). As in these cells all endogenous sodium channels can be effectively inhibited with TTX, they represent a useful tool for the functional analysis of $Na_V1.9$. As shown in Figure 25A, the characteristic slowly activating and inactivating $Na_V1.9$-specific currents are evoked by step depolarizations in transfected cells. However, the achievable $Na_V1.9$-specific current amplitudes obtained were significantly low, ultimately making the analysis time-consuming. On the contrary, in DKO-DRG neurones transfected with wt$Na_V1.9$ considerably larger current amplitudes were observed, allowing a more precise analysis of the channel kinetics. Moreover, thanks to the absence of TTX-R $Na_V1.8$ channels in the DKO-DRGs, which would interfere with recordings of $Na_V1.9$-specific currents (*57*), the new DKO-model provides a powerful, straightforward expression system for the analysis of $Na_V1.9$ channels at high resolution.

Therefore, to prove that this mouse model can be used as an expression system to study mutations in TTX-R channels, in particular in $Na_V1.9$, isolated DRG neurones from DKO mice were transiently transfected with $Na_V1.9$-L811P variant (c.2432T>C, p.Leu811Pro), which leads to pain insensitivity in humans. Transfection of ND7/23 with this variant showed a left-shift in the resting membrane potential, indicating that mutant channels are active under resting conditions, as well as a slower inactivation kinetics (*57*). We were able to reproduce these results using the DKO-DRG neurones (Figure 25B, C), suggesting these cells are a

valuable tool for the characterization of TTX-R channel variants involved in human disease as well as for pharmacological studies.

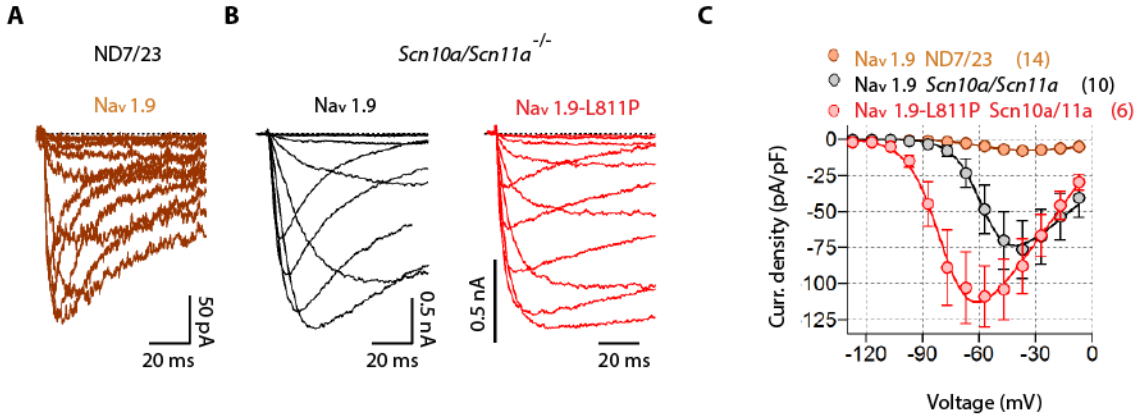

Figure 25. Dorsal root ganglion neurones from *Scn10a/Scn11a* $^{-/-}$ mice as a tool for studying the impact of $Na_V1.9$ mutations.

(A) Representative current responses of whole-cell patch-clamp measurements from ND7/23 cells transfected with wild-type $Na_V1.9$. From a holding potential of −137 mV, currents were evoked by depolarizations ranging from -127mV up to -7mV in 10-mV steps. (B) An identical set of experiments to the ones shown in (A) was performed with DRG neurones obtained from *Scn10a/Scn11a* $^{-/-}$ mice transfected with either wild-type $Na_V1.9$ or mutant p.L811P. (C) $Na_V1.9$-specific mean maximal current densities obtained from experiments shown in A and B. Error bars indicate SEM, the number of experimental replicas n is indicated. Continues lines are data fits according to a Hodkin-Huxley formalism assuming one activation gate(*57*, *65*).

6. Discussion

One of the breakthroughs in the past decades of molecular biology has been the sequencing of the Human Genome, an international research effort that has provided us with the complete map of all genes in our species. Thanks to this innovation, nowadays we can comprehensively diagnose human diseases at gene level. However, only a few of the estimated 20.000 protein-coding genes in the human genome have a well-defined function (*168*). Hence, understanding gene function and the consequences of genetic variations remain an important goal and a major challenge.

Comparative genomics has revealed high sequence homology between large parts of mouse and human genomes (*169*). Therefore, mice have proven a well-suited model for *in vivo* functional genomics in human research. A straightforward method to elucidate the function of a gene is to generate a complete knockout and characterise the phenotype. Up to now, gene knockouts have proven suitable for elucidating the role of genes involved in a wide variety of biological pathways, including human behaviour, physiology, metabolism, development and cancer (*170*). In addition, gene knockout organisms are excellent models for studying the underlying mechanisms of human genetic diseases and provide an invaluable tool for the development of new therapeutic approaches (*171*).

Over the past two decades, this method has been used to unveil the role of more than 5,000 mammalian genes (*172*). However, when using classical homologous recombination approaches (see Figure 26A), targeting efficiency is usually low and requires screening of several hundreds of embryonic stem (ES) cell clones. Besides, gene targeting is dependent on both the length and the extent of homology between the donor vector and the target locus (*173*, *174*), thus requiring the generation of huge vectors to achieve a higher recombination efficiency. Hence, this approach remains arduous, expensive, time-consuming, and is not well suited for targeting different loci at the same time.

An alternative method to perform targeted genome-editing is the use of zinc-finger nucleases (ZFNs) and transcription activator-like effector nucleases (TALENs). These enzymes are artificially produced by the fusion of several DNA-binding modules that recognise 3 (ZFNs) or 1 nt (TALENs) in the target DNA sequence fused with a FokI endonuclease. The resulting enzymes recognise specific genomic locations via protein-DNA interactions (*68*). The FokI

domain is responsible for the generation of a double strand break (DSB) in the target site, which is subsequently repaired via the error-prone non-homologous end joining (NHEJ) pathway, often leading to small indels. Specific mutations can also be achieved by co-introduction of a homologous single or double-stranded DNA via homology-dependent repair (HDR) or high-fidelity homologous recombination (HFHR) (*175*). Following these principles, numerous research groups have recently efficiently generated gene-targeted mice and rats by injecting mRNA coding ZFNs or TALENs directly into the zygote (*176*, *177*). Nevertheless, the design and preparation of these enzymes have proven labour intensive and complex, ultimately halting the spread and use of this technique.

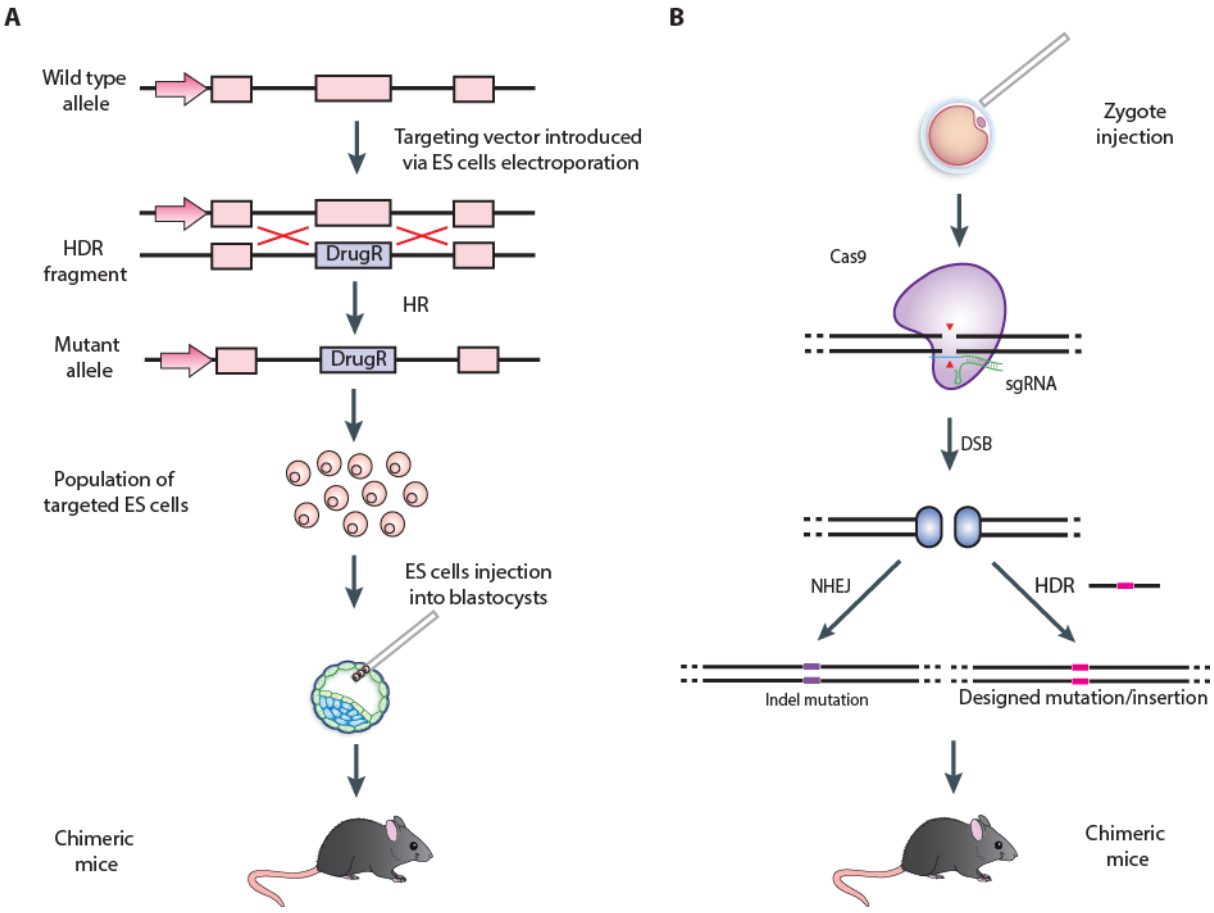

Figure 26. Conventional gene targeting vs. CRISPR-Cas9 genome editing.

(A) Conventional gene targeting usually involves homologous recombination (HR) for the introduction of modified alleles in combination with a drug resistance gene in embryonic stem (ES) cells. It requires at least 8 months to obtain homozygous mutants: 2 to 3 weeks for preparing the HR fragment and ES cell electroporation, 1 month for screening of HR-positive cells, 1 month for chimaera production, 3 more months to obtain heterozygous mice plus 3 extra months to get the first homozygous mice. (B) CRISPR-Cas-mediated-genome editing exploits the generation of sequence specific double strand breaks (DSBs). The single guide RNA (sgRNA) and Cas9 can be introduced in mouse zygotes to generate a DSB and can be repaired by two distinct mechanisms. The non-homologous end joining (NHEJ) is highly error-prone and often leads to small indels (violet box). Homologous directed repair (HDR) enables the introduction of designed mutations or insertions (pink box) via a reference single or double stranded DNA. Using the CRISPR-Cas system, chimeric mice can be generated as fast as in one month, making the process simple and straightforward.

The recently developed CRISPR-Cas9 genome editing technology has certainly revolutionised the field of genetics, not only in organisms in which gene manipulation was not previously possible but also in the laboratory mouse. Similarly to ZFNs/TALENs, the Cas9 enzymes are endonucleases that can be programmed to cause a site-specific DSB and exploit the cellular repair machinery to produce mutations (Figure 26B). However, in contrast to ES gene-targeting and ZFNs/TALENs nucleases, the CRISPR-Cas9 system is highly efficient, less time consuming, straightforward, and exhibits a remarkable versatility for complex editing and simultaneous targeting of loci, as proven by the results presented in this thesis. In addition, the CRISPR-Cas9 system provides a simple method to disrupt genes in all types of cell lines.

6.1 Generation of *Ntrk1*-KO PC12 cells

In this study, genome-edited rat PC12 cells were successfully generated using the NmeCas9 by targeting the enzyme to exon 5 of the *Ntrk1* gene. However, the targeting efficiency obtained (20%) was significantly lower than previously reported (*131*, *132*). This might be due to the nature of PC12 cells. These cells are not easy to handle and have low division rates. From the 200 starting single cell clones, only 30 proliferated into colonies. From the latter, two clones were homozygously targeted, and the indels introduced by NHEJ caused a frameshift mutation. Neither clone expressed *Ntrk1*, as assessed by qPCR. As expected, these clones were not able to differentiate into a neuron-like phenotype or trigger the PI3K or MAPK pathways upon NGF treatment. Moreover, the selected gRNA only had two predicted off-target sites, as examined by Benchling and COSMID, making off-target analysis straightforward. None of these locations contained undesired indel mutations. Compared to other reports (*73, 132)*, the results suggest that NmeCas9 has a similar or lower on-target cleavage activity than SpCas9 but a reduced off-target effect on a genomic level (*132*). Thus, although only very limited studies have been made for the use of NmeCas9 to target endogenous loci in mammalian cells (*131,132*), this enzyme may represent an excellent choice for genome engineering applications.

6.2 Functional analysis of novel NTRK1 missense mutations

In this thesis, three novel missense mutations in the NTRK1 gene found in patients diagnosed with HSAN-IV are reported. The generated *Ntrk1*-KO PC12 cells proved to be a valuable tool for studying the underlying disease mechanisms of these NTRK1 mutations in a physiologically relevant cellular context. Mutation p.N365K is located in the extracellular

portion of the receptor. Specifically, in the second immunoglobulin-like domain of the protein, which is partially responsible for NGF binding (20). Based on the location of the mutation, one could anticipate that it could prevent NGF binding. However, western blot analysis and immunofluorescence revealed that this variant is not properly transported to the plasma membrane and is retained in the endoplasmic reticulum (ER), most probably due to protein misfolding (see Figure 27). Moreover, this mutation highly reduced the differentiation capacity of transfected *Ntrk1*-KO PC12 cells and did not activate the MAPK or Akt signalling pathways. Interestingly, two recently reported mutations responsible for an HSAN-IV phenotype, p.L93P and p.L213P, located in the leucine-rich and first immunoglobulin domain respectively, likewise produce the 110 kDa NTRK1 isoform only and are retained in the ER compartment, suggesting a common pathogenic mechanism responsible for the disease (178–180). Protein misfolding not only affects protein function but also leads to aggregation and toxicity. Accumulation of misfolded proteins in the ER, which contributes directly to ER-stress-induced neuronal apoptosis, is a common cause of developmental and progressive neurodegenerative disorders (181). Misfolded proteins that are induced by gene mutations have been identified in other neurodegenerative diseases, such as Parkinson's and Alzheimer's disease, in which accumulation of misfolded proteins induces neuronal loss and cognitive deficits (181), which is consistent with the mental retardation often seen in HSAN-IV patients (180).

Neurotrophin signalling is a complex, highly regulated process. A series of studies provided evidence that supports a model in which neurotrophin-NTRK receptor complexes are internalised in distal axons into an endocytic signalling platform termed the 'signalling endosome' (*182*). Sustained MAPK signalling needed for neuronal differentiation seems to be maintained exclusively from endosomal locations through activation of Rap1, a member of the GTPase family, while transient activation of Ras-dependent signalling along with Akt phosphorylation occurs at the cell surface to promote neuronal survival (*159*, *160*). Mutation p.I505N localises to the very end of the juxtamembrane region of the NTRK1 receptor, while p.Q633R localises to the middle of the tyrosine kinase domain. None of these mutations affect residues that may interfere with receptor autophosphorylation or protein function. However, these mutants were unable to induce differentiation of *Ntrk1*-KO PC12 cells into a neuronal-like phenotype after three days of NGF treatment, suggesting that they are not rare polymorphisms, but disease-causing missense mutations. When the cellular localisation was addressed, both mutants partly localised to the plasma membrane, suggesting there is no

defective glycosylation and consequent membrane trafficking defect. Moreover, Western blot analysis confirmed the presence of the fully glycosylated mature isoform of ~140 kDa in both mutants. Additionally, Akt phosphorylation kinetics induced by NGF were not altered in transfected cells. However, when the Erk pathway was addressed, a significant difference between these mutant receptors was observed after 30 min of NGF stimulation. In cells transfected with wtNTRK1, Erk activation has its peak at 5 min post-NGF stimulation and remains almost constant for 30 min. However, in cells transfected with mutants p.I505N and p.Q633R, Erk activation can be observed after 5 and 10 min of NGF treatment suggesting proper Ras activation, but it is not detected after 30 min, probably due to defective Rap1 activation. Thus, based on these results, it can be speculated that these mutants have deficient internalisation into early endosomes or fail to interact with adaptor proteins needed for Rap1 activation (See Figure 27).

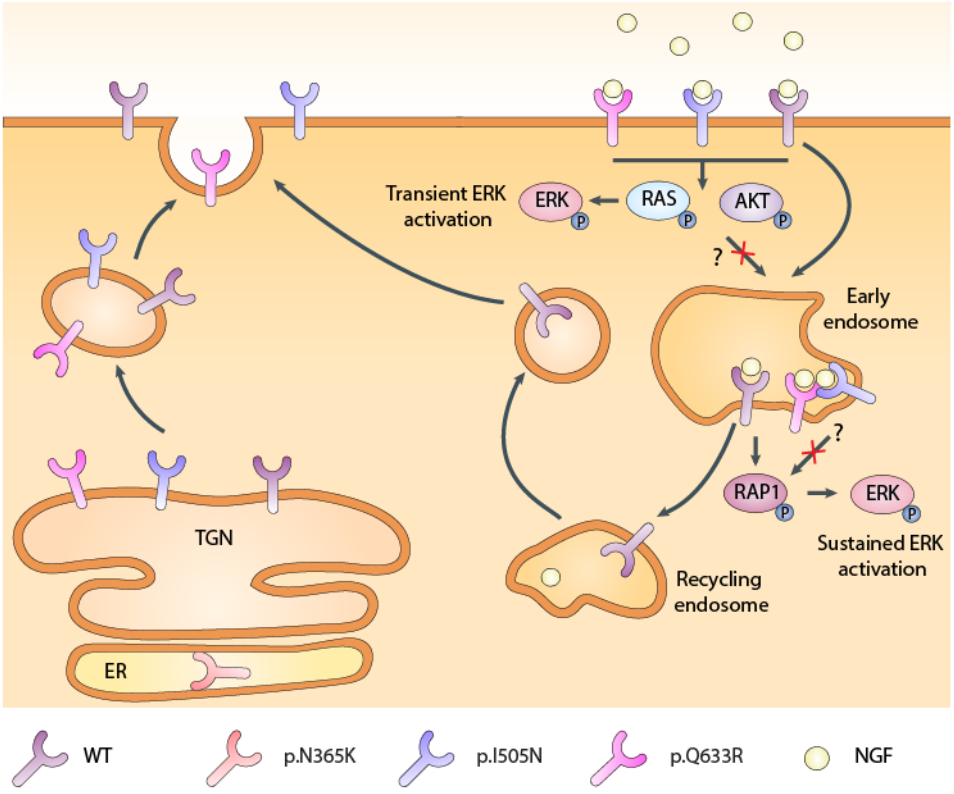

Figure 27. Proposed differential trafficking of NTRK1 mutants.

All NTRK1 receptors are translocated from the trans-Golgi network (TGN) to the plasma membrane except for mutant p.N365K, which remains in the endoplasmic reticulum (ER). Upon nerve growth factor (NGF) binding, wtNTRK1, mutants p.Q633R and p.I505N can activate the PI3K signalling pathway, which results in AKT activation, as well as a transient activation of ERK through Ras, promoting cell survival. Activated wtNTRK1 is internalised by endocytosis and promotes sustained activation of ERK through a pathway that involves Rap1 (a Ras-like small GTPase) in early endosomes (*160*). Sustained activation of ERK/MAPK elicits cell differentiation. However, in mutants p.Q633R and p.I505N either internalisation or interaction of the receptor with adaptor proteins needed for Rap1 activation seems to be impaired.

6.3 Generation of *Scn10a* and *Scn11a* double-knockout mice

6.3.1 Pronuclear injection of SpCas9/sgRNA expressing vectors vs. mRNA injection of SpCas9 and sgRNA.

One method that can be used to generate genetically modified mice by the CRISPR-Cas9 system is the pronuclear injection of the pX330 vector containing the single guide RNA (sgRNA) and the *Streptococcus pyogenes* humanised Cas9 (hSpCas9) endonuclease (*73*). Upon injection of the plasmid into one of the pronuclei of fertilised oocytes, SpCas9 is guided to the target site and generates a DSB, subsequently producing indels that will most likely cause a frameshift in the reading frame. Despite several groups successfully generated KO mice by this approach (*183–185*), including us (data not shown), upon injection of four pX330 vectors targeting the different exons of *Scn10a* and *Scn11a* into C57BL/6N zygotes, unfortunately, no mutations were detected in the desired loci. Another possible method is the cytoplasmic injection of SpCas9 mRNA and in vitro transcribed sgRNAs. When these components were injected into zygotes, we observed mutation rates up to 75%, including several mice containing mutations in all the alleles targeted (18.7%).

Although DNA injection is less expensive, time-efficient, and evades the preparation of RNA, which requires careful handling and storage, as reported by other groups (*183–185*) and based on my own experience, the targeting efficiency is significantly lower. This can be attributed to the toxicity of DNA and expression efficiency of the CRISPR/Cas9 components upon injection. In fact, as plasmids require transcription, pronuclear injection is needed, but identifying the tolerable plasmid-DNA-concentration for injection into embryos was a complicated task. Injection into pronuclei was more damaging to zygotes than injection of the same volume or concentration of editing reagents into the cytoplasm. Also, injections with higher DNA concentrations than reported in the results section resulted in several failed attempts to obtain viable embryos and pups (data not shown). Despite numerous attempts over an extended period of time, only eleven pups were born from DNA injections compared to the amount of injected embryos (~5%), and none was genetically modified. Thus, these results suggest that injection of pX330 plasmids into the pronucleus of zygotes may not be the preferred method for the generation of genetically modified mouse models.

In contrast, the generation of mice carrying germline mutated alleles of interest was remarkably successful via mRNA injection. Cytoplasmic injection of a mixture containing

sgRNAs and SpCas9 mRNA might facilitate protein translation. Moreover, it proved to be less toxic for the embryos, yielded three-fold more live born pups compared to the number of injected embryos (~15%) than DNA injection, and the overall editing efficiency was significantly higher. Based on these results (and data not shown) injecting SpCas9 mRNA at 25 ng/µl and sgRNA at a concentration between 25 to 6.25 ng/µl into the cytoplasm yields good survival of embryos and efficient editing by NHEJ. Another advantage of cytoplasmic injection is that visible pronuclei are not necessary for fertilised eggs to be injected, thus enabling injection in a broader range of oocytes, ultimately reducing total superovulated mice numbers. The results suggest that ten donor mice (~10 embryos/mice) might be sufficient for the generation of genetically modified mice by cytoplasmic injection of editing reagents.

All methods needed to be established, including plasmid cloning, PCR amplification of DNA templates, in vitro transcription (IVT), guide validation, and, in particular, microinjection. Once this was achieved, the whole process became straightforward and highly efficient, taking approximately three weeks. Indeed, in less than seven months the *Scn10a*/*Scn11a*$^{-/-}$ (F_1) line was established (see Figure 28). Moreover, backcrossing was not necessary as C57BL/6N zygotes were used, thus generating mice with a pure genetic background. Overall, the results support the fact that mRNA injection of SpCas9 and sgRNA is a rapid, simple and reproducible method for the one-step generation of double-knockout mice.

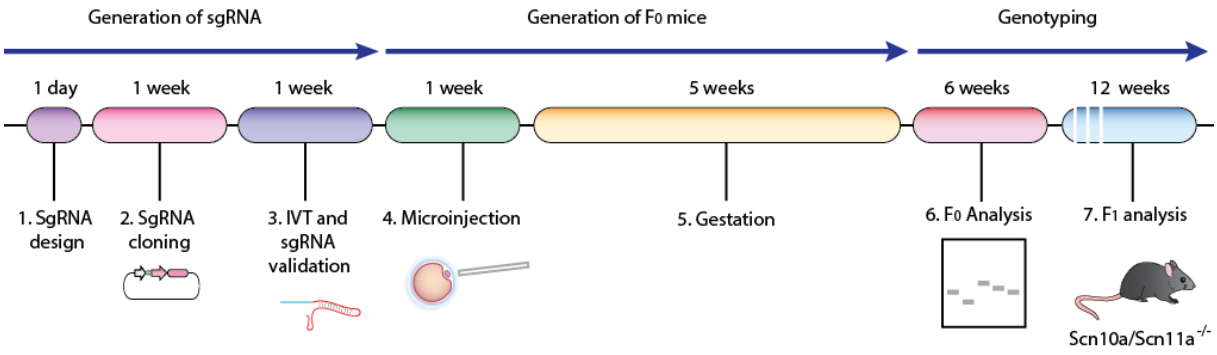

Figure 28. Optimal timeline and key steps from design to genotyping for the generation of *Scn10a/Scn11a* double-knockout mice using the CRISPR-Cas9 system.
The process can be divided into three main phases: generation of gene-specific sgRNAs (1-4), microinjection of mouse zygotes followed by implantation into pseudopregnant females to obtain F_0 mice (4 -5), and genotyping of F_0 and F_1 mice carrying mutated alleles of interest (6-7).

6.3.2 The CRISPR-cas system can be used to target neighbouring genes

Usually, the generation of mice carrying mutations in several genes requires time-consuming intercrossing of single-mutant mice. However, as the *Scn10a* and *Scn11a* genes are in close physical chromosomal distance (genetically) linked, i.e. they are inherited together, this

procedure is not applicable to generate DKO mice. On the other hand, the distance between *Scn10a* and *Scn11a* excludes one-step homologous recombination strategies. Instead, a sequential approach may be considered, targeting one gene first, and subsequently, use this line as donor for the disruption of the second gene. Still, this process is extremely labour intensive, necessitating multiple consecutive cloning steps and subsequent breeding steps (*147*). Hence, the CRISPR-Cas9 system proves to be highly advantageous as it provides a methodology for efficient simultaneous one-step targeted mutagenesis of genomic loci in mice.

6.3.3 Analysing the outcome of CRISPR genome editing in mice.

Though several reports describe the generation of mouse models via CRISPR-aided mutagenesis, only a few mention the diverse modifications that may occur and their complexity in detail (*161*, *186*). Cas9-generated DSBs directed at multiple loci and within various parts of the same gene led to complex allelic outcomes, and each founder mouse carried a different combination of mutated alleles, overlaid with the issue of mosaicism at each locus.

One unexpected result was the robustness and the high number of mosaic animals (43.75 %) carrying three or more modified alleles obtained by microinjection of RNA-CRISPR-reagents into zygotes, which became an outstanding challenge. Cas9 mRNA translation is most likely delayed until after the first cell division as transcription and translation are suppressed in mouse zygotes (*187*). Moreover, editing may happen after several cell divisions, due to the persistence of Cas9/sgRNA complexes, further contributing to genetic mosaicism.

Therefore, the complexity of allelic variations generated by the microinjection of CRISPR/Cas9 reagents into embryos requires detailed genotyping analysis. Several techniques can be employed to characterise the mutants, including agarose electrophoresis, Surveyor® (*73*) or T7EI assays, PAGE (*137*), Sanger or next generation sequencing (*188*), and Droplet Digital PCR (*189*). For the production of *Scn10a*/*Scn11a*$^{-/-}$ mice, 2% agarose electrophoresis and 5 % PAGE were chosen as initial screening steps. PAGE proved to be an excellent, simple, and efficient screening methodology, enabling the identification of homozygously and heterozygously targeted mice. The results suggest that for future applications, PAGE can be sufficient as an initial screening. However, as described by Zhu et al., a higher gel percentage is recommended to increase the sensitivity of the results (*137*).

Moreover, PAGE gels are cost-saving and were easier to perform than the Surveyor® or T7EI assays (data not shown).

However, none of these assays can reveal the exact nature of the mutations. Sanger sequencing was essential to confirm the actual mutation, and this information was used to assess the potential impact on encoded protein and identify the best founder animal to generate the double-knockout line. Still, one drawback of this method is that direct sequencing of amplicons from founder mice in almost all cases resulted in overlapping and asynchronous chromatograms due to the presence of two or more different alleles. To overcome this problem, the PCR products were cloned into plasmids, followed by Sanger sequencing of a sufficient number of independent clones (usually 10) to identify all alleles in the sixteen CRISPR-derived founder animals. This entire process was time-consuming, as not all allelic variants were revealed by a single PCR, especially in mosaics. Indeed, as for some animals no amplicon was detected for a certain PCR, suggesting exon deletion, a second PCR spanning a larger region from the cut site was needed to reveal the exact mutation. Moreover, several mice contained exon junctions between the target sites, which also required subcloning and further sequencing. One alternative to overcome this problem, but costly, is to use next-generation-sequencing of PCR-amplified target loci from founder mice, which also enables simultaneous analysis of potential off-target sites. Thus, Sanger sequencing remains the best alternative for small labs to analyse CRISPR-edited mice.

Regarding targeting efficiency, as previously mentioned, 75% of mice contained mutated alleles. Alleles bearing small indels, exon deletions, and fusions between exons were found in the F_0 mice. In particular, 18.75 % for *Scn10*-Ex6, 37.5% for *Scn10*-Ex11, 62.5% for *Scn11*-Ex9 and *Scn11a*-Ex10. Moreover, 43.75% were mutant for both genes, 43.75% contained larger deletions within the same gene, and 12.5% contained a 140 kb deletion between both genes. Although all sgRNAs had a similar on-target activity (see below), consistent with other reports, allele frequency appears to depend on the genomic loci. Moreover, additionally to the alleles characterised in the F_0, several new alleles appeared in the F_1 generation, as they might have been underrepresented in the analysed tissue. Thus, even if a correct allele combination is found in the F_0 generation, the real analysis should be done in the F_1 to ensure the allele of interest was transmitted. The F_1 stage enables the final characterization of each mutant, as the results obtained in the F_0 generation rely heavily on the tissue from where the DNA sample was extracted (see Figure 28).

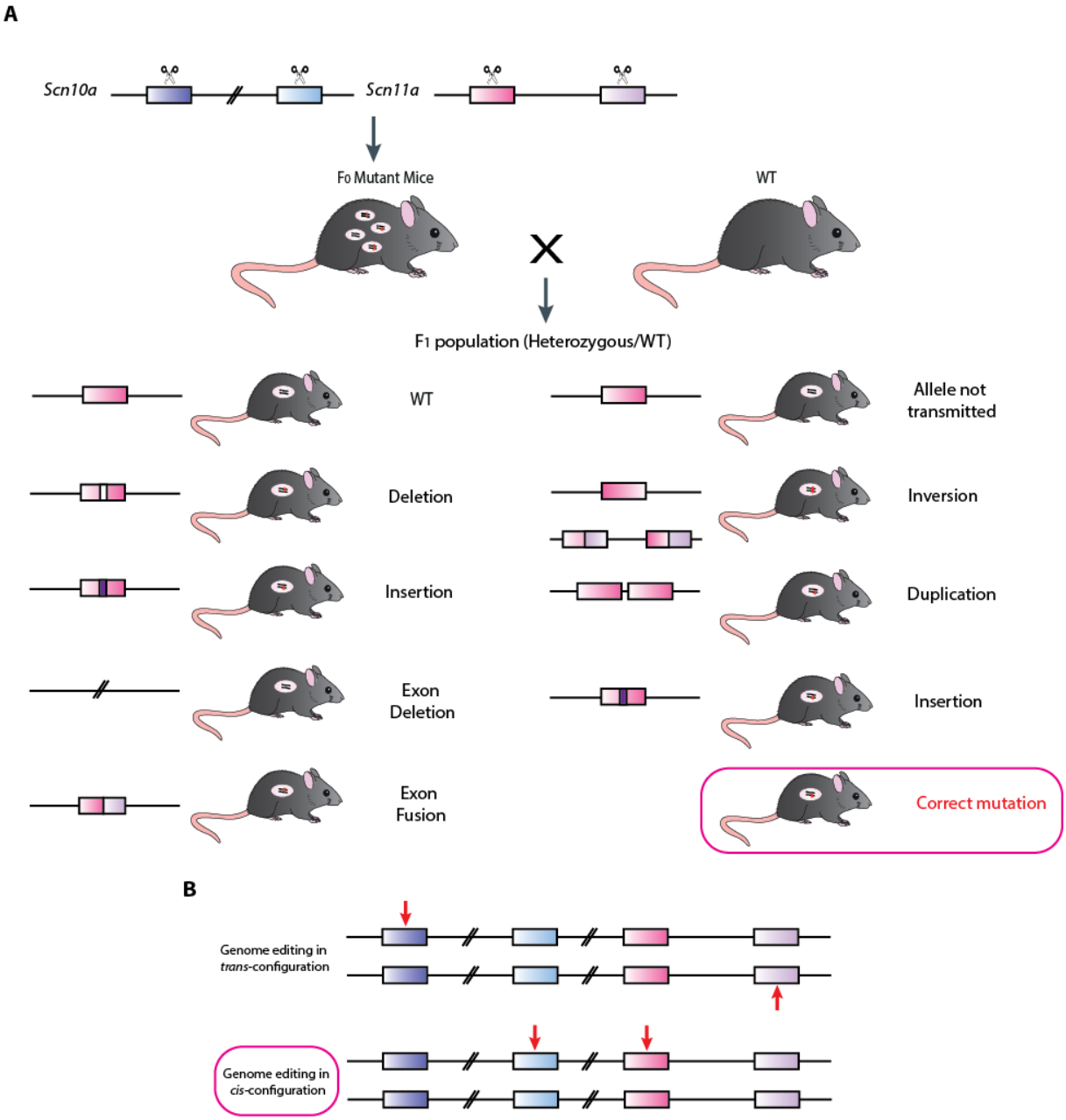

Figure 29. Complexity of the germline transmission: potential alleles and chromosome rearrangements resulting from several genome-editing events.

(A) Founder F_0 mice should always be considered as mosaic animals. Mating a founder F_0 with a WT counterpart allows the generation of a heterozygous F_1 animal population. Edited alleles can bear small indels, exon deletions, inversions, and duplications. The use of multiple sgRNAs significantly increases the complexity of the alleles that can be generated, as in addition to the single indels in each exon, inversions, deletions and fusions between exons can be produced. Allele frequency depends on the loci, relative sgRNA efficiency, presence of microhomology, and size of the interval to be deleted. Moreover, additionally to the alleles characterised in the F_0, new alleles can appear in the F_1 population, as they might have been underrepresented in the analysed tissue. (B) Targeting consecutive genes leads to two types of chromosome rearrangements. Editing can occur in *trans* or *cis* configuration. Solely the latter is useful to generate a *Scn10a/Scn11a* double-knockout line. Therefore, due to the complexity of the possible outcomes, PCR amplification and Sanger sequencing of all F_0 and F_1 animals generated should be performed to establish the exact genetic context of the mutant strain.

6.3.4. SpCas9 targeting activity and specificity.

One of the main concerns of CRISPR-genome editing is targeting specificity. Several factors determine the cleavage specificity of the Cas9 endonucleases. Firstly, the presence of the PAM sequence at the 3' end of the gRNA binding site is a requisite for Cas9 cleavage (*125*). Although a Cas9 of a given bacterial species has a preference for a certain PAM sequence, it has been demonstrated that other PAMs can also be tolerated. For instance, the SpCas9 has a preference for a 5′-NGG PAM sequence (*125*), but it has been shown it can also use an alternative 5′-NAG PAM (*138*).

Secondly, the guide sequence. The gRNA pairs with the complementary DNA sequence in the genome (on target) but also binds to other sequences with imperfect matches (off-targets) (*138*, *190*, *191*). Hsu et al. demonstrated that SpCas9 cleavage activity relies on the correct matching of the 8–12 nucleotides proximal to the PAM, termed seed sequence. However, one base pair mismatches, DNA bulges or RNA bulges, as well as few mismatches distal to the PAM can be tolerated (*138*). Additionally, they generated an online tool that predicts potential off-target (OT) binding sites in the genome and calculates quality scores for each gRNA (high scores reflect higher specificity). In addition, it calculates an OT hit score based on the number, position, and distribution of mismatches to predicted OT sequences (scores reflect the probability of gRNA binding) (*138*). Moreover, base composition of the gRNA and the surrounding DNA genomic region plays a major role in sgRNA efficiency (*138*, *139*). Doench et al. proved that Spcas9 prefers certain nucleotides at a certain position of the gRNA. Based on this observation, they elaborated a scoring algorithm to predict which guides have higher activity (on target score, higher scores reflect higher activity) (*139*).

Therefore, when designing a guide sequence for genome targeting, the specificity regarding off-target potential as well as the on-target score is crucial. For the generation of the DKO mouse, the online design tool from Benchling was used for gRNA selection, as it integrates both on-target and off-target scores algorithms. The complete sequence of *Scn10a* and *Scn11a* was screened for a guide sequence with the least number of off-target sites and the highest on-target activity (sg*Scn10a*-Ex6: OT-score 91.9,on-target 54.5; sg*Scn10a*-Ex11: OT-score 88.5, on-target 77.5; sg*Scn11a*-Ex9: OT-score 90.6, on-target 54.6; sg*Scn11a*-Ex10: OT-score 80.2, on-target 64.5). Potential OT cleavage was examined for each gRNA in the F_0 and F_1 founder animals. Consistent with online predictions, Sanger sequencing analysis of 5-6 of the highest-scoring OT sites revealed no undesired mutations in these animals. The on-target score can be

reflected in the higher mutation rates obtained. Thus, based on these results, it is highly important to select gRNAs with high off-target and on-target scores to avoid unwanted mutations and to maximise enzyme activity, respectively. Moreover, consistent with recent reports (*147*), these results suggest that potential off-target effects may not be a major concern for the implementation of the CRISPR-Cas9 system in genome modification in mouse zygotes. Nevertheless, whole genome sequencing would be necessary to fully evaluate OT effects.

6.3.5 *Scn10a/Scn11a* -/- DRG neurones as an expression system

The phenotypic characterization of the double–knockout mice is currently ongoing, and the animals will be assessed for alterations in the pain-sensing pathways. Moreover, the generated DKO mice are an excellent model to study $Na_V1.9$ function. The voltage-gated sodium channel $Na_V1.9$ has recently been implicated in distinct human pain syndromes, including patients with congenital analgesia (*57–59*) and painful neuropathies (*60–65*). Both conditions are characterised by dominant gain-of-function mutations in $Na_V1.9$. However, the functional characterization of the different mutations will enhance our knowledge on these pain syndromes and will clarify the diverse phenotypic outcomes, which depend on the type of missense mutation.

Studying human $Na_V1.9$ is a challenging task due to poor heterologous expression in mammalian cells, especially in non-neuronal cells (*192*). One option to investigate mutations in $Na_V1.9$ is the generation of knock-in mouse models. However, in DRG neurones, the assessment of the mechanism by which the mutated ion channel is interfering with normal cell function is highly compromised by the overlapping expression of $Na_V1.8$ channels (*57*). Now, these limitations can be overcome by using cells from our genetic mouse model. Indeed, $Na_V1.8$ and $Na_V1.9$ currents were absent in DRG neurones derived from DKO mice, and transfection of human pain-related $Na_V1.9$ mutations was successful.

Interestingly, $Na_V1.9$-specific drugs might be an alternative treatment for pain syndromes. However, this will require exact knowledge on the channel properties and electrophysiological characteristics of pain-related mutations and our double-knockout mouse model has outstanding potential as a tool for this analysis.

7. Conclusion and outlook

Chronic pain affects millions of people worldwide. Inadequate or insufficient treatment of these disorders is partially due to a lack of knowledge regarding the underlying molecular mechanisms of pain. Therefore, to gain a deep insight into such mechanisms additional cellular and animal models are needed.

In the present work, two independent models for *in vitro* and *in vivo* study of pain-related genes were successfully generated using the CRISPR-Cas system that will enable the exploration of pain mechanisms. Compared with traditional genome editing technologies, this short RNA-directed Cas9 endonuclease system proved to be simple, easily programmable and allowed me to generate genetically-engineered cells and to target multiple sites in the mouse genome in one step. In fact, this system has proven to be suitable to generate both germline and somatic indels. Thus, the CRISPR-Cas9 system may act as a novel tool in pain research for establishing disease models and studying gene function. Furthermore, taking advantage of the homology-directed repair pathways, specific guide RNAs targeting mutations in pain-associated genes may in the future provide an *in vivo* gene correction therapy and may be a new approach for transcriptional activation or repression of pain-related genes in patients with chronic pain.

Using the *Ntrk1*-KO model, we hope to shed light on the mechanism of action of neurotrophin signalling. Here, potentially pathogenic mutations in patients with loss of pain perception were functionally assessed and further rated as pathogenic. However, until now, the precise mechanisms of NTRK1 internalisation and recycling and its role in disease remain unclear. Further questions that should be addressed by future work include: what is the role of the mutated amino acids (505 and 633) of the NTRK1 protein in internalisation and recycling? Which interaction partners might fail to interact with the mutant proteins? Investigation of Rap1 activation by these mutants and internalisation assays might be helpful to dissect the mechanism, and experiments are currently ongoing.

DRGs from double KO-mice with simultaneous disruption of Nav1.8 and Nav1.9 will be an ideal model to study disease-associated mutants in these sodium channels. Behavioural and electrophysiological analysis of this mouse model might be useful to clarify the role of these sodium channels in pain perception. Moreover, both models might reveal new therapeutic targets for pain management and serve as a tool for drug development.

Supplementary Material

I. Supplementary Figures

Figure S1. Alignment and conservation analysis of mutated residues in NTRK1.

A

	Gene	aa	Alignment									
p.N365K		365	T	L	L	A	A	**K**	P	F	G	Q	A
H. sapiens	ENST00000524377	365	T	L	L	A	A	**N**	P	F	G	Q	A
M. musculus	ENSMUSG00000028072	368	T	L	L	A	A	**N**	P	Y	G	Q	A
G. gallus	ENSGALG00000019019	355	T	L	V	V	Q	**N**	P	L	G	R	A
D. rerio	ENSDARG00000004586	359	T	I	I	V	K	**N**	K	L	G	R	D
X. tropicalis	ENSXETG00000018040	299	T	I	L	V	W	**N**	M	L	G	S	A

	Gene	aa	Alignment									
p.I505N		505	A	C	V	H	H	**N**	K	R	R	D	I
H. sapiens	ENST00000524377	505	A	C	V	H	H	**I**	K	R	R	D	I
M. musculus	ENSMUSG00000028072	508	T	C	V	H	H	**I**	K	R	Q	D	I
G. gallus	ENSGALG00000019019	496	A	C	V	H	H	**V**	Q	R	R	D	I
D. rerio	ENSDARG00000004586	500	-	C	V	Q	H	**I**	K	R	K	D	I
X. tropicalis	ENSXETG00000018040	440	A	C	V	Q	H	**I**	K	R	R	D	I

	Gene	aa	Alignment									
p.Q633R		633	L	A	V	A	S	**R**	V	A	A	G	M
H. sapiens	ENST00000524377	633	L	A	V	A	S	**Q**	V	A	A	G	M
M. musculus	ENSMUSG00000028072	636	L	A	V	A	S	**Q**	V	A	A	G	M
G. gallus	ENSGALG00000019019	624	L	Q	I	A	T	**Q**	I	A	S	G	M
D. rerio	ENSDARG00000004586	625	L	H	I	A	A	**Q**	I	A	S	G	M
X. tropicalis	ENSXETG00000018040	568	L	Q	I	A	S	**Q**	I	A	S	G	M

B

Mutation	*Mutation Taster prediction score*	*SIFT prediction score*	*Polyphen prediction score*
p.N365K	0.999	0	1.000
p.I505N	0.999	0	1.000
p.Q633R	0.999	0.01	0.970

(A) All putative NTRK1 missense and nonsense mutations resulted in the change of an evolutionarily conserved amino acid. Protein sequence data are for human (NTRK1, NP_00252) and mouse (NP_001028296.1) as representatives for mammals, *Xenopus tropicalis* for amphibians (NP_001079579.1), *Danio rerio* for fish (NP_001288285), *Gallus Gallus* for birds (NP_990709.1). Multiple sequence alignment was performed using *blastp* (*142*). The candidate mutations are shown in red, and the amino acid at that position in the different species is shown in blue. (B) All mutations were predicted to be disease causing by Mutation Taster, where a value close to 1 indicates a high 'security' of the prediction. In addition, the missense mutations were also predicted to be probably damaging by Polyphen, were the most severe mutations are given a score of 1 as well as by SIFT, where they were predicted to be damaging by the lowest score of 0.

Figure S2. Genotyping of CRISPR-genome-edited PC12 cells by non-denaturating polyacrylamide gel electrophoresis (PAGE).

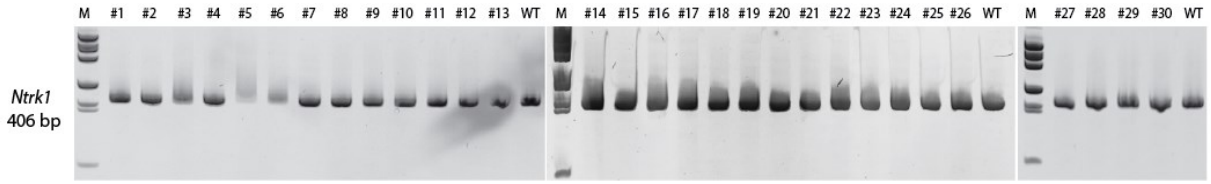

Thirty PC12 cell clones were screened for targeted modifications in *Ntrk1* using 5% PAGE-based genotyping. Only homoduplex DNA was detected. M; molecular weight marker; bp: base pairs.

Figure S3. CRISPR/Cas9 mediated *Ntrk1* mutations in PC12 cells.

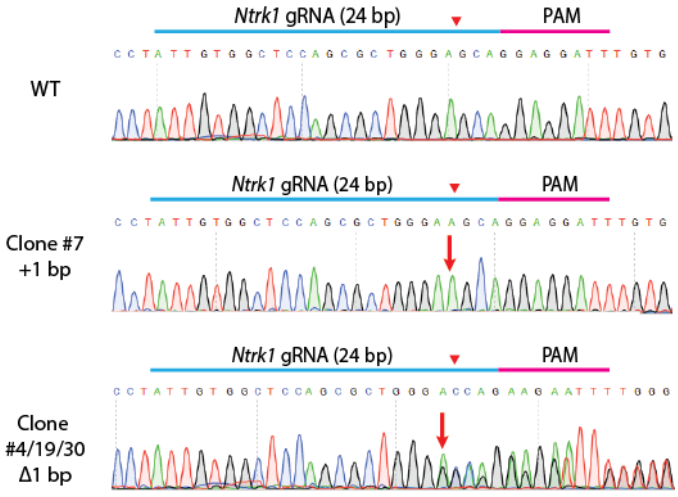

Representative *Ntrk1* sequences from the different clones obtained by Sanger sequencing. Small indels were identified at the sgRNA targeted site (red arrows), including a 1 bp insertion (+1 bp) as well as a 1 bp deletion (Δ1 bp) in heterozygosity and homozygosity. The 24-nt guide sequence (blue bars on top) followed by the protospacer adjacent motif (PAM; 5′-NNNNGATT-3′; pink line) of the *Neisseria meningitides* Cas9 are shown as well as the cleavage site (red triangle).

Figure S4. Off-target analysis of CRISPR-genome edited *Ntrk1*-KO PC12 cells.

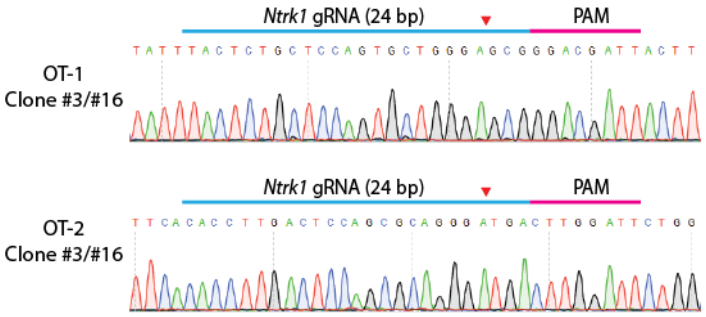

Results of the sequencing analysis of *Ntrk1*-Ex5 sgRNA potential off-target (OT) sites. Direct sequencing of the PCR-amplified OT sites from clone #3 and clone #16, both bearing a homozygous 1 bp deletion in *Ntrk1*. Neither clone presented undesired genome-editing events in the predicted OT regions. The 24-nt guide sequence (blue bars on top) followed by the protospacer adjacent motif (PAM; 5′-NNNNGATT-3′; pink line) of the *Neisseria meningitides* Cas9 are shown as well as the cleavage site (red triangle).

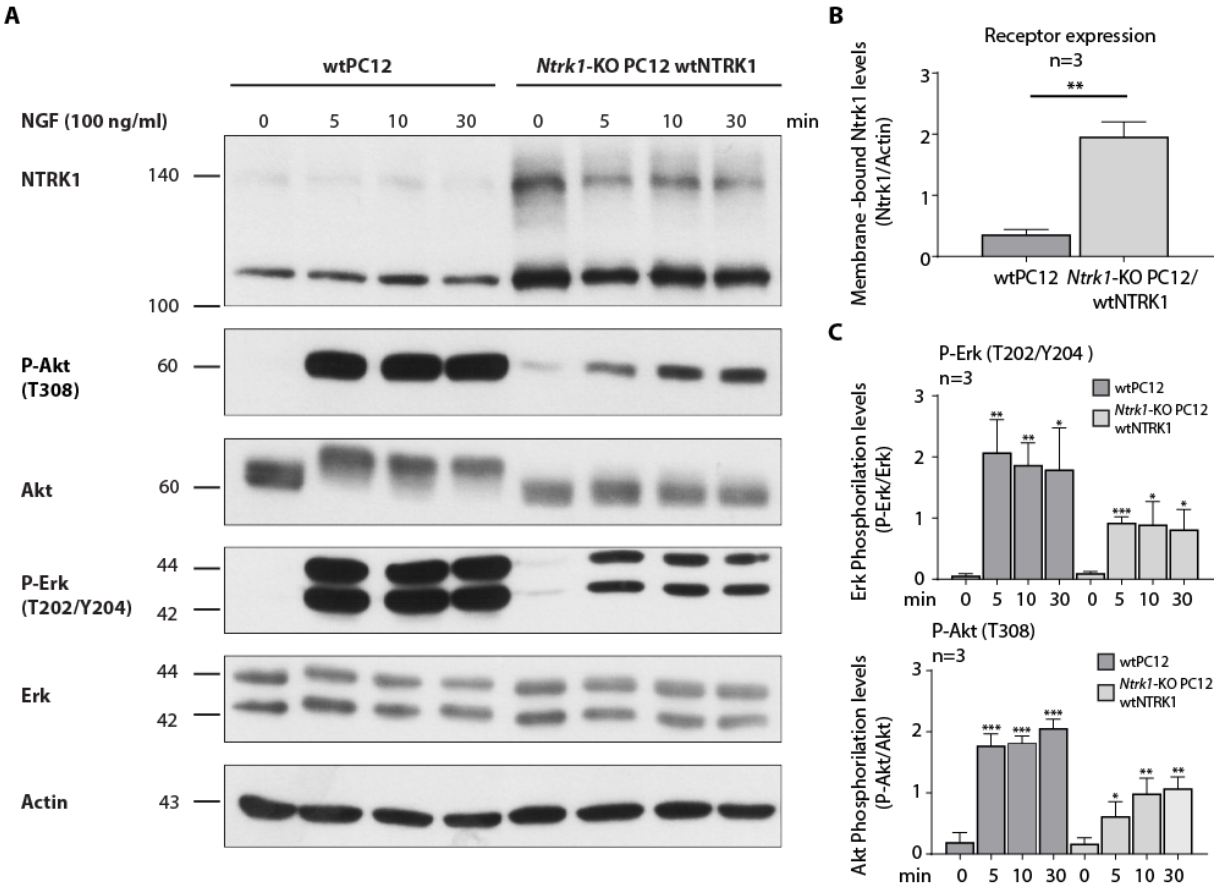

Figure S5. The wtNTRK1-myc construct can recapitulate Erk and Akt signalling in *Ntrk1*-KO PC12 cells

(A) To test whether the wtNTRK1-myc cDNA construct can rescue the wild-type phenotype, *Ntrk1*-KO PC12 cells transfected with the construct and compared to wtPC12 cells by Western blot analysis. Y-axis: molecular weight in kilodaltons (kDa). (B) Membrane-bound receptor levels (upper band ~140 kDa). The increase in the second band given by the anti-NTRK1 antibody in transfected samples suggests that the unspecific band detected previously (see figure 13) overlaps with the band corresponding to the immature form of the receptor (~110 kDa) as suggested in the literature (*153, 154*). (C) Time course of Erk and Akt phosphorylation. The time course data of panel A is shown in quantitative terms. The number of gels analysed quantitatively is given by "n". Phosphorylation levels are compared to time point 0 in each cell population. Data calculated by a two-tailed unpaired t-test, are given as mean ± SEM; *P<0.05: **P<0.01; ***P<0.001.

Figure S6. Validation of sgRNA produced by in vitro transcription.

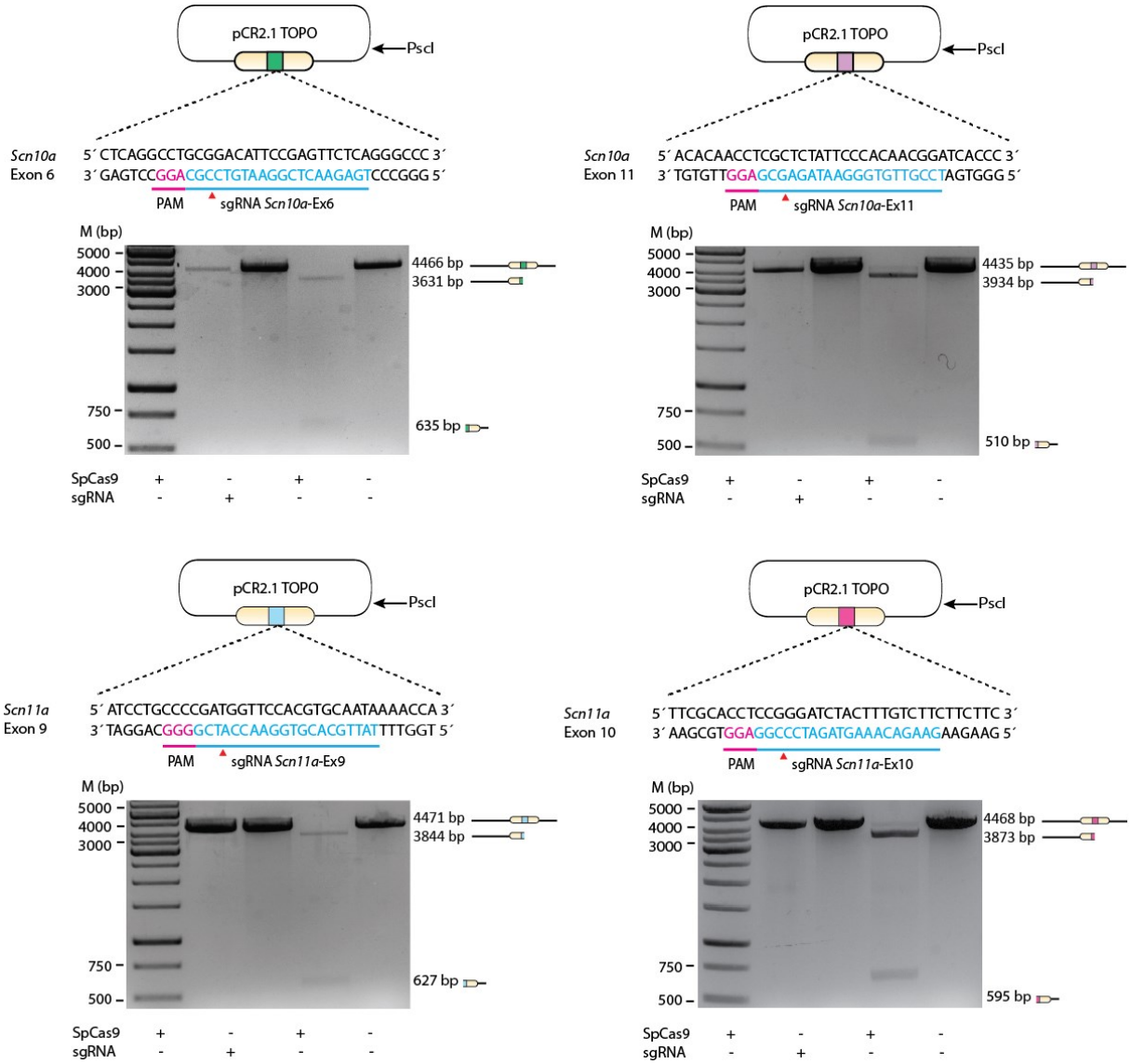

PCR products from PCR A, B, C and D (see Figure 18B) from wild-type mice were cloned into TOPO vectors and further linearized with *PscI*. These vectors were then mixed with different combinations of sgRNA and cell lysate prepared from HEK293T previously transfected with pX330 plasmids expressing SpCas9. After 4 hr incubation at 37°C, DNA was purified and analysed by 1 % agarose gel electrophoresis. On the right of each gel the expected cleavage products and their predicted sizes are depicted. Only in reaction number three, where all the components needed by SpCas9 to produce a blunt-end double-strand break in the DNA are present, two bands were obtained as result of efficient cleavage. M; molecular weight in base pairs; bp: base pairs.

Figure S7. Detection of CRISPR/Cas9-mediated large deletions in *Scn10a* and *Scn11a*

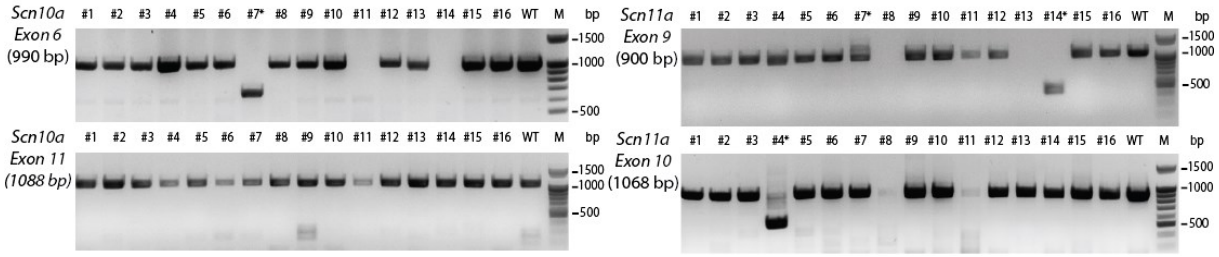

To detect large NHEJ-induced mutations in *Scn10a* and *Scn11a*, PCR primers (listed in Table 10) were designed to amplify a region of ~ 1 kb spanning the targeted sites on each exon. The predicted sizes of each PCR are depicted. DNA was amplified and analysed by 2% agarose gel electrophoresis. Mice presenting an altered band pattern are marked by asterisks (*). M, molecular marker; bp, base pairs.

Figure S8. Sequencing analysis of transmitted alleles from F_0 mice #11 and #14 to their offspring.

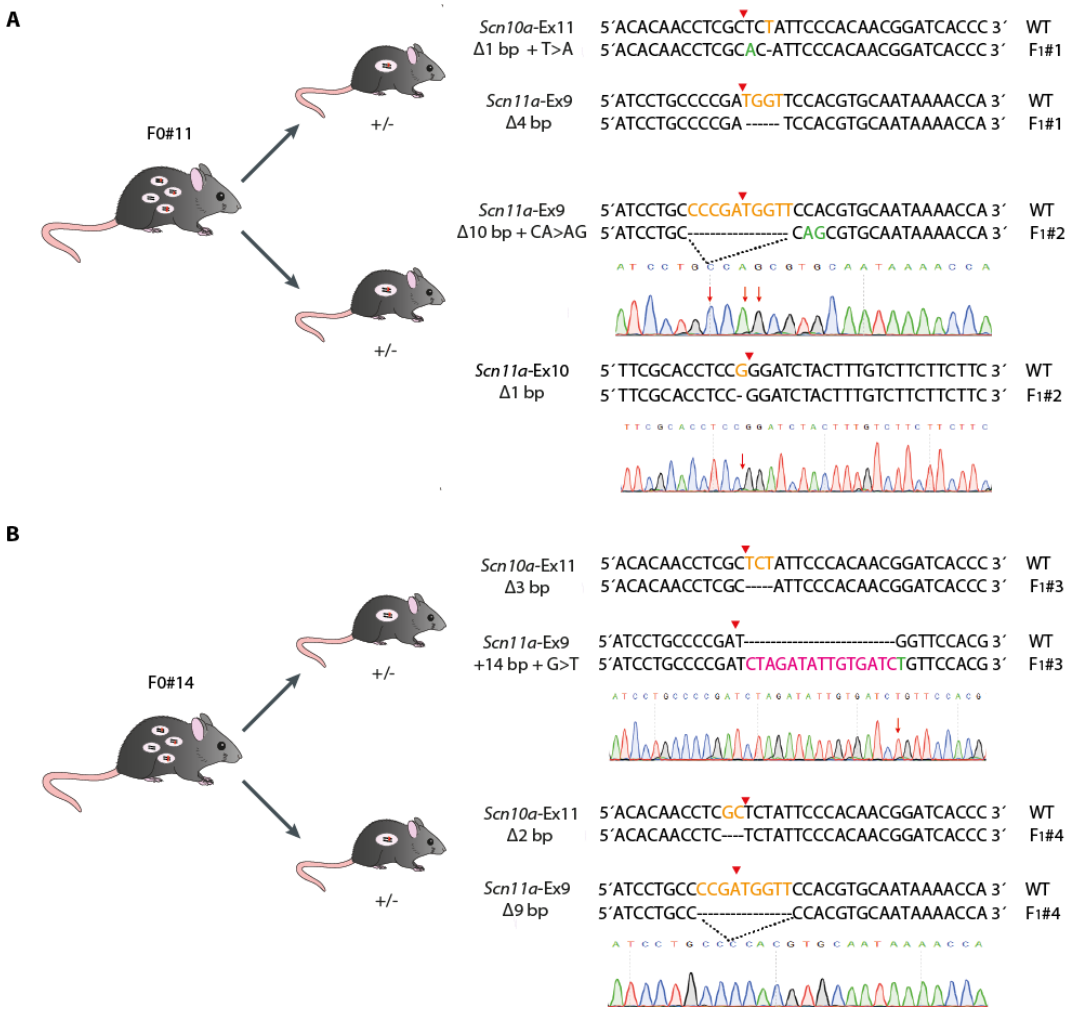

F_0 mice #11 and #14 were mated with wild-type (WT) C57BL/6J mice, and their offspring (F_1 mice) was genotyped with PCRs A, B, C and D (see figure 18B) to identify the inherited alleles. (A) Sequencing analysis revealed that F_0 #11 transmitted two combinations of alleles. Half of the offspring displayed a Δ1 bp along with a T>A substitution in *Scn10a*-Ex11 and a Δ4 bp in *Scn11a*-Ex9 while the rest exhibited mutations only in *Scn11a*. (B) Mouse F_0#14 showed a more complex inheritance pattern, bearing mutated exons in both genes in several combinations. Two examples are shown. +n, insertion; bp, base pairs; Δ, deletion.

Figure S9. Off-target analysis of selected F_0 and F_1 mice.

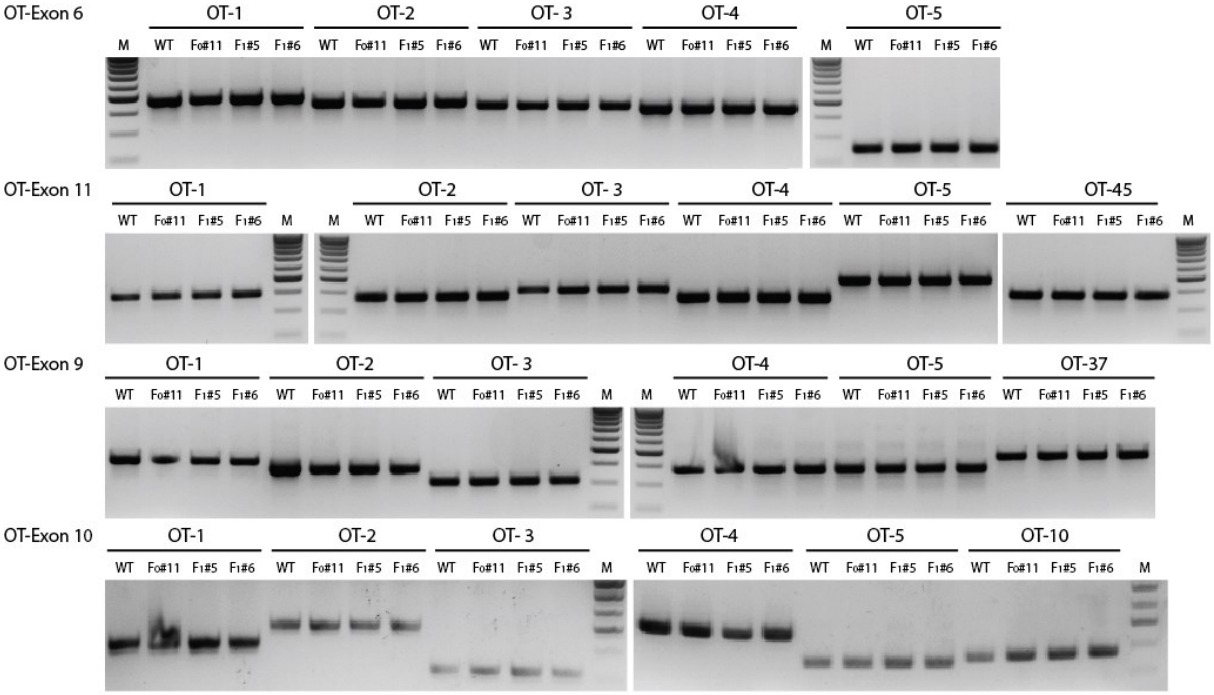

PCRs were performed for each selected animal using specific primers for each off-target (OT). Mouse F_0#11 was the chimeric mouse used as founder for the generation of the *Scn10a/Scn11a* double-knockout mouse line, parent of F_1 animals (#5 and #6) used for further breedings. All PCR products were sequenced. No additional detectable mutations were noticed. M, Molecular weight marker.

Figure S10. Dorsal root ganglion neurones from *Scn10a/ Scn11a* $^{-/-}$ mice as a tool for studying the impact of $Na_V1.8$ mutations.

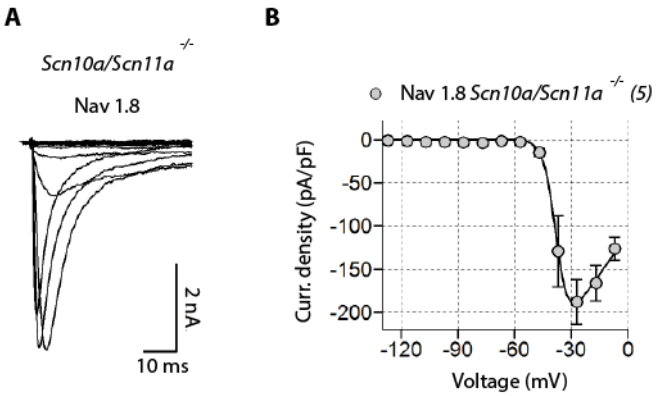

(A) Representative current responses of whole-cell patch-clamp measurements from DRG neurones isolated from *Scn10a/Scn11a*$^{-/-}$ mice upon transfection with wild-type $Na_V1.8$. From a holding potential of −137 mV, currents were evoked by step depolarizations ranging from -127mV up to -7mV in 10-mV steps. (B) $Na_V1.8$-specific mean maximal current densities obtained from experiments shown in A. Error bars indicate SEM, the number of experimental replicas n is indicated. Continues lines are data fits according to a Hodkin-Huxley formalism assuming one activation gate (*57*, *65*).

Table S1. Total number of potential off-target sites identified by COSMID for g*Ntrk1*-Ex5

OT	*Result*	*Query type*	*Mismatch*	*Chromosome Position*	*Cut site*	*Score*
NTRK1	TTGTGGCTCCAGCGCTGGGAGCAGGAGGATT	No indel	0	Chr2:187154076-187154106	187154087	0
OT-1	TGTGGCTCCAGCGCTGGGAGCAGGAGGATT	Del 22, or Del 23	0	Chr2:187154076-187154105	187154087	0.61
OT-2	TGTGGCTCCAGCGCTGGGAGCAGGAGGATT	Del 21	1	Chr2:187154076-187154105	187154087	0.71
OT-3	TTGTGGCTCCAGCGCTGGGAGCAGGAGGAT	Del PAM 3	1	Chr2:187154077-187154106	187154088	40.51
OT-4	TTGTGGCTCCAGCGCTGGGAGCAGGAGGAT	Del PAM 1, or Del PAM 2	0	Chr2:187154077-187154106	187154088	20.51
OT-5	ATTGTGGCTCCAGCGCTGGGAGCAGGAGGATT	Ins 22	1	Chr2:187154076-187154107	187154087	0.9
OT-6	ATTGTGGCTCCAGCGCTGGGAGCAGGAGGATT	Ins 21	1	Chr2:187154076-187154107	187154087	0.9
OT-7	TTGTGGCTCCAGCGCTGGGAGCAGGAGGATTT	Ins PAM 3	1	Chr2:187154075-187154106	187154086	40.7
OT-8	TTGTGGCTCCAGCGCTGGGAGCAGGAGGATTT	Ins PAM 2	0	Chr2:187154075-187154106	187154086	20.7
OT-9	TTGTGGCTCCAGCGCTGGGAGCAGGAGGATTT	Ins PAM 1	0	Chr2:187154075-187154106	187154086	20.7

Total number of off-target (OT) sites predicted by COSMID (*140*) including sites with three or fewer mismatches, 1 bp deletions and up to two mismatches, and 1 bp insertions and up to two mismatches, and in the 19 bases of the guide sequence next to the protospacer adjacent motif (PAM)(*132*). All OTs detected correspond to Exon 5 of the *NTRK1* gene. Abbreviations: chr, chromosome number.

Table S2. Total number of potential off-target sites identified by the design tool from Benchling for g*Ntrk1*-Ex5.

OT	*Sequence*	*PAM*	*Score*	*Gene*	*Chromosome Position*	*Mismatches*
NTRK1	ATTGTGGCTCCAGCGCTGGGAGCA	GGAGGATT	100	ENSRNOG00000013953	chr2: 187154087	0
OT-1	TACTCTGCTCCAGTGCTGGGAGCG	GGACGATT	0.882		chr20: 31417639	8
OT-2	ACCTTGACTCCAGCGCAGGGATGA	CTTGGATT	0.046		chr2: 257540060	7
OT-3	CCGCTGGCTCCAGCCTGGCGAGCA	GGTTGATT	0.038		chr11: 90022669	8

Total number of off-target (OT) sites predicted by the CRISPR Design Tool from Benchling (www.benchling.com) including sites with four or fewer mismatches in the first 20 protospacer adjacent motif (PAM) proximal bases. All potential OTs correspond to non-coding or intronic regions. Mismatches in the target sequence are indicated in red letters. Abbreviations: chr, chromosome number.

Table S3. Total number of potential off-target sites identified by the design tool from Benchling for the sgRNA *Scn10a*-Exon 6.

OT	*Sequence*	*PAM*	*Score*	*Gene*	*Chromosome Position*	*Mismatches*
Scn10a	TGAGAACTCGGAATGTCCGC	AGG	100.000	ENSMUSG00000034533	chr9: 119671568	0
OT-1	AGGGAACTCAGAATGTCCAC	TGG	0.625		chr14: 110170208	4
OT-2	GGGGACCTGGGAATGTCCGC	GGG	0.562		chr1: 131211261	4
OT-3	TGAGGACAAGCAATGTCCGC	AAG	0.489		chr8:122977885	4
OT-4	TGAGAGCTGGGAATGTCCTC	AAG	0.407		chr16: 35367290	3
OT-5	AAAGAACTCTGAATGTCAGC	GGG	0.385		chr6: 38519594	4
OT-6	CAAGAACTCTGAATGTCTGC	TGG	0.385		chr2: 20597435	4
OT-7	TGTGAACCAGGAATGTCCCC	AAG	0.362		chr11: 11653594	4
OT-8	GGAGAACTCCCAATGTCCTC	CAG	0.328		chr5: 125663257	4
OT-9	TGACAACCCAGAATGTCAGC	AAG	0.326		chr18: 55230433	4
OT-10	TAAGAACTCCAAGTGTCCGC	CAG	0.325		chr15: 12615438	4
OT-11	TGAGAAATCGGAATGTCCCT	AGG	0.314		chr8: 114032119	3
OT-12	TGTGAAGTTGGAATGTCCCC	CAG	0.250		chr13: 95079451	4
OT-13	TGAGATCTGGGAATGTCTGC	TGG	0.243		chr2: 181690506	3
OT-14	TGATAACTAGAAATGTCCCC	TGG	0.199		chr9: 117804299	4
OT-15	TGAGAAATCTGTATGTACGC	TGG	0.192		chr3: 41488127	4
OT-16	TTAGAACTCAAAATGTCTGC	AAG	0.191		chr3: 60059456	4
OT-17	AGAGAATTCGGAATGTTCCC	AGG	0.188		chr19: 58913590	4
OT-18	TCAGTACTCGGAATTTCCAC	AAG	0.185		chr1: 187848814	4
OT-19	TGAGGATTTGGAATCTCCGC	CAG	0.180		chr9: 42351819	4
OT-20	AGAGAACTTTGAATGCCCGC	GGG	0.179		chr6: 34495150	4
OT-21	TGAGTACTGGGAATGTCCTT	AGG	0.163		chr2: 150567912	4
OT-22	TGAGTTCTCAGAATGGCCGC	CAG	0.162		chr7: 24725533	4
OT-23	TGAGTTCTCAGAATGGCCGC	CAG	0.162		chr7: 24689610	4
OT-24	TGAGTTCTCAGAATGGCCGC	CAG	0.162		chr7: 24676536	4
OT-25	TCAGAACTCAGAATGTATGC	CAG	0.141		chr1: 81120688	4
OT-26	TGGGAACTGGGTATTTCCGC	AGG	0.137		chr14: 48941288	4
OT-27	TAAGGACTCGGGAAGTCCGC	AGG	0.131		chr14: 120343747	4
OT-28	TGAGAACTCCTAATGTCCTA	CAG	0.114		chr11: 33225940	4
OT-29	TAAGAACTTGGAATGTCAGG	TGG	0.112		chrX: 134949187	4
OT-30	TGAAAACTCGGAATGTACAG	GGG	0.097		chr3: 92265952	4
OT-31	TGAAAACTCGGAATGTACAG	GGG	0.097		chr3: 92231160	4
OT-32	TGAGAACTGGGCATGTGCGA	GGG	0.082		chr6: 50358283	4
OT-33	TGAGAACTAGAAGTGTCCTC	TAG	0.067		chr2: 154945305	4
OT-34	GGAGAACTCGGAATGTGTGT	TAG	0.066		chr13: 28954992	4
OT-35	TGAGAACTTGGAACTTCCGC	AAG	0.065		chr7: 115886045	3
OT-36	TGAGAAATCTGAATTTCAGC	TGG	0.056		chr10: 116217195	4
OT-37	TGTGAACTTGGAAAGTCCCC	CAG	0.056		chr1: 85890163	4
OT-38	AGAGAACTCGGAATGGCCCG	CAG	0.049		chr11: 68188153	4
OT-39	TGAGAACTTGCAATGTCAGT	AAG	0.048		chr14: 86599851	4
OT-40	TGAGAACTGGGTGTCTCCGC	AAG	0.045		chr17: 19192603	4
OT-41	TGAGAACTGGGGATGTCAGG	GAG	0.042		chr4: 43420073	4
OT-42	TGAGAACTCTGATTGTCAAC	TAG	0.035		chr1: 94355003	4
OT-43	TGAGAACTTGCAATGTCATC	CAG	0.035		chr8: 51342565	4
OT-44	TGAGAACGGGGAATGACAGC	TGG	0.035		chr8: 94915747	4
OT-45	TGAGAACCAGGAATGCCTGC	AAG	0.035		chr6: 145666834	4
OT-46	TGAGAACTCTGAATGACCCA	TGG	0.034		chrX: 157402930	4
OT-47	TGAGAACTCGGAAGGACCGA	GAG	0.029		chr9: 118962579	3
OT-48	TGAGAACTCGGAAGGTGAGC	AAG	0.028		chr11: 90578690	3
OT-49	TAAGAACTCGGAAGATCCCC	CAG	0.025		chr14: 24836534	4

Total number of off-target (OT) sites predicted by the CRISPR Design Tool from Benchling (www.benchling.com) including sites with four or fewer mismatches in the first 20 protospacer adjacent motif (PAM) proximal bases. All potential OTs correspond to non-coding or intronic regions. Mismatches in the target sequence are indicated in red letters. Abbreviations: chr, chromosome number.

Table S4. Total number of potential off-target sites identified by the design tool from Benchling for the sgRNA *Scn10a*-Exon 11.

OT	*Sequence*	*PAM*	*Score*	*Gene*	*Chromosome Position*	*Mismatches*
Scn10a	TCCGTTGTGGGAATAGAGCG	AGG	100.000	ENSMUSG00000034533	chr9: 119664918	0
OT-1	GCCTCTGTGGGAATAGAGCC	TGG	0.879		chr19: 6042293	4
OT-2	TGCTGTGTGGGAATAGAGCC	CAG	0.849		chr5: 62382474	4
OT-3	GGCGTTGGGGGAATAGAGAG	GAG	0.680		chr9: 45112530	4
OT-4	GCTGTTGTGTGAATAGAGGG	TGG	0.625		chr13: 90740432	4
OT-5	TGCAGTGTGGGAATAGAGTG	CAG	0.620		chr4: 48195265	4
OT-6	TCTGTTAAGGGAATAGAGCA	GAG	0.553		chr5: 29776395	4
OT-7	TTCCTTGTGGAAATAGAGCA	CAG	0.506		chr3: 158156305	4
OT-8	TTCTTTATGGGAGTAGAGCG	GGG	0.442		chr11: 59289013	4
OT-9	TCCGCTGTGGGAATGGAGCC	CAG	0.429		chr17: 87503561	3
OT-10	TCAGCTCTGGGAATAGAGAG	TAG	0.408		chr7: 130598493	4
OT-11	TGCCTGGTGGGACTAGAGCG	AAG	0.388		chr13: 55963264	4
OT-12	ACCGAGGTGGGAATAGAGAG	AGG	0.388		chr12: 68982805	4
OT-13	TCAGTTGTGAGGATAGAGCC	AAG	0.371		chr2: 121926992	4
OT-14	AACGTTGTGGGCATAGAGAG	GGG	0.352		chr9: 94709662	4
OT-15	TCCATGGTGAGAGTAGAGCG	GAG	0.344		chr15: 93719436	4
OT-16	GCAGTTGTGGGAATAGAGTC	TGG	0.332		chr4: 11876396	4
OT-17	TCCATTGTAAGAATAGAGTG	CAG	0.327		chr2: 70387671	4
OT-18	TCTGTTTTGGAAATAGAGCT	AAG	0.317		chr10: 31207351	4
OT-19	TCTGCTGTGGGGGTAGAGCG	GGG	0.317		chr5: 24505153	4
OT-20	ACAGTTGTGGGAATAGTGTG	TGG	0.286		chr15: 88646989	4
OT-21	TCCTTGGTGGAAATAGAGCT	TGG	0.279		chr13: 60292087	4
OT-22	TTTGTTGTGGGAATGGAGCC	CAG	0.257		chr2: 119486623	4
OT-23	TCTTTTGTGGGGATAGAACG	CAG	0.189		chrX: 100656733	4
OT-24	TGAGTTGTGGGAATGGAGTG	GGG	0.187		chr5: 23619100	4
OT-25	TACCTTGTGGGAATACAGCA	AGG	0.167		chr12: 3518625	4
OT-26	CCTGTTGTGGGAACAGAGCC	CAG	0.146		chr12: 99720030	4
OT-27	GCCGCTGTGGGAAGAGAGCT	GAG	0.145		chr7: 122482891	4
OT-28	TTCGCTGTGGGAAGAGAGCC	GAG	0.139		chr6: 93838755	4
OT-29	TCTGGTGTGGGAATAGAAGG	CAG	0.133		chr1: 131554460	4
OT-30	TCCAGTGTGGGAAGAGAGCA	AAG	0.129		chr4: 153900254	4
OT-31	ACCGTTGTGAGGAAAGAGCG	GAG	0.118		chr12: 39858458	4
OT-32	TCTGTTGTGAGAACAGAGCT	CAG	0.115		chr1: 173353530	4
OT-33	ACCGTCGTGGGAATGGAGGG	TGG	0.114		chr6: 21852533	4
OT-34	TCCGTTTTGCGAATGGTGCG	GAG	0.108		chr12: 117159895	4
OT-35	TCCTTAGTGGGAATAGACCC	TAG	0.107		chr12: 68620762	4
OT-36	TGCCTTGTGGGAAAAGAGGG	GAG	0.103		chr11: 94562020	4
OT-37	ACCGTTCTGGGAATAGATAG	GAG	0.097		chr13: 107703179	4
OT-38	TCCTCTGTGGGAAAAGAGGG	TAG	0.094		chr15: 73798946	4
OT-39	TCTGTTCTGGGAAGAGAGCC	AGG	0.088		chr19: 57923168	4
OT-40	TCCTTTGTGGGAGTGGAGCT	TAG	0.083		chr4: 94389482	4
OT-41	TCAGTTGTGGTAATAGCACG	TGG	0.080		chr7: 88978651	4
OT-42	TCTGTTGTGGGGATGGAGGG	AAG	0.080		chr7: 73290835	4
OT-43	TCCTTTGTGGGTATGGAGTG	CAG	0.078		chr4: 46692927	4
OT-44	GCCATTGTGGGAAGAGAACG	TAG	0.064		chr14: 26446951	4
OT-45	TCCGCTGTGTGAAACGAGCG	CGG	0.060	ENSMUSG00000048109	chr3: 107333005	4
OT-46	TCCCTTGTGGGAATAGGACC	TAG	0.060		chr1: 175875509	4
OT-47	TCCGTGCTTGGAACAGAGCG	GGG	0.058		chr5: 120495192	4
OT-48	TCCATTGTGGGTAGAGAGTG	AGG	0.043		chr8: 91652321	4
OT-49	TCCTTTGTGGGAATGGAACA	AAG	0.043		chr4: 103544966	4

Total number of off-target (OT) sites predicted by the CRISPR Design Tool from Benchling (www.benchling.com) including sites with four or fewer mismatches in the first 20 protospacer adjacent motif (PAM) proximal bases. All potential OTs correspond to non- coding or intronic regions, with the exception of OT-45. Mismatches in the target sequence are indicated in red letters. Abbreviations: chr, chromosome number.

Table S5. Total number of potential off-target sites identified by the design tool from Benchling for the sgRNA *Scn11a*-Exon 9.

OT	*Sequence*	*PAM*	*Score*	*Gene*	*Chromosome Position*	*Mismatches*
Scn11a	TATTGCACGTGGAACCATCG	GGG	100.000	ENSMUSG00000034115	chr9: 119805789	0
OT-1	TCTTCCAAGTGGAACCATCT	TGG	0.869		chr10: 51549703	4
OT-2	TCTCTCACGTGGAACCATCT	TGG	0.849		chr11: 28366048	4
OT-3	GATGGCAAGTGGAACCTTCG	TAG	0.758		chr18: 33773846	4
OT-4	TCTTACAGGTGGAACCTTCG	GAG	0.726		chr3: 126690764	4
OT-5	TATGGCACGTAGAACCATGG	AGG	0.671		chr16: 91789464	3
OT-6	TTTTGAAGGTGGAACCATCA	GAG	0.520		chr4: 92313958	4
OT-7	TATAGAAAGTGGAACCATCT	CAG	0.486		chrX: 16710367	4
OT-8	TATGGCACGGTGAACCATCT	TAG	0.406		chr11: 34460728	4
OT-9	TCTTCCACGTGGAACCGTCT	TGG	0.374		chr10: 76095514	4
OT-10	AAGTGCACATGGAACCAACG	GGG	0.246		chr17: 76095514	4
OT-11	AATTGCACCTGCAACCTTCG	GAG	0.225		chr17: 4494324	4
OT-12	TATGGGACATGGAACCATAG	CAG	0.219		chrX: 113526302	4
OT-13	TAGTGGAGGTGGAACCAGCG	TAG	0.218		chr9: 105132758	4
OT-14	TCTTTCACGTGGAACCACCT	TGG	0.193		chr8: 50731570	4
OT-15	GATTGCAAGTGGAAACATAG	GGG	0.185		chr4: 55408805	4
OT-16	GATTGCAAGTGGAAACATAG	GGG	0.185		chrX: 66973307	4
OT-17	GATTGCAAGTGGAAACATAG	GGG	0.185		chrX: 60482203	4
OT-18	TCTTGCTCGTGGAACCTTTG	GGG	0.181		chr6: 128120470	4
OT-19	TATCCCACGTGGAACCACCT	TGG	0.179		chrX: 35472632	4
OT-20	TATCCCACGTGGAACCACCT	TGG	0.179		chrX: 35141230	4
OT-21	TATCCCACGTGGAACCACCT	TGG	0.179		chrX: 30050074	4
OT-22	TATCCCACGTGGAACCACCT	TGG	0.179		chrX: 28880882	4
OT-23	TATCCCACGTGGAACCACCT	TGG	0.179		chrX: 28534090	4
OT-24	TATCCCACGTGGAACCACCT	TGG	0.179		chrX: 27873121	4
OT-25	TATCCCACGTGGAACCACCT	TGG	0.179		chrX:27421341	4
OT-26	TATCCCACGTGGAACCACCT	TGG	0.179		chrX:25046915	4
OT-27	TCTTTCACGTGGAACTATCA	GAG	0.165		chr11: 89478822	4
OT-28	TTTTTCACGTGGAACTATCT	TGG	0.165		chr12: 13777520	4
OT-29	TATTGCACATGGAACCACCC	TAG	0.161		chr3: 81035831	3
OT-30	GATTGCAAGTGGAACAATAG	GGG	0.120		chr5: 140546979	4
OT-31	TTTTGCATGTGGAGCCTTCG	GGG	0.112		chr12:108214161	4
OT-32	AATTGCACATGGAAGCATGG	AAG	0.111		chr3: 14063929	4
OT-33	TATTTCACTTGGAATCATTG	AGG	0.097		chr18: 48608593	4
OT-34	TATTGAACGTGCAACCCTCC	TGG	0.089		chr2: 162247255	4
OT-35	TATTGAACTAGGAGCCATCG	GAG	0.077		chr4: 132309367	4
OT-36	TATTGCAGGTTGAACCTGCG	CAG	0.070		chr14: 18180814	4
OT-37	TCTTGCACGTGGGACCAACA	CAG	0.067	ENSMUSG00000042063	chr12: 16061941	4
OT-38	TATTGCACATGAAAACATCA	GGG	0.056		chr6: 116061941	4
OT-39	TATTGCACAAGGAGCCATAG	TAG	0.043		chr6: 37039752	4
OT-40	TAGTGCACGTGGTAGCACCG	TGG	0.037		chr7: 68482657	4
OT-41	TATTGCAAGTGGAACTTTAG	GAG	0.034		chr4: 44715021	4
OT-42	TATTGCACTTGGCAGCATGG	GGG	0.032		chr9: 29284954	4
OT-43	TATTGCACTTGGAACCTGAG	GGG	0.023		chr1: 178188677	4
OT-44	TATTGCTCGTGTAACAACCG	AAG	0.019		chr13: 25059304	4

Total number of off-target (OT) sites predicted by the CRISPR Design Tool from Benchling (www.benchling.com) including sites with four or fewer mismatches in the first 20 protospacer adjacent motif (PAM) proximal bases. All potential OTs correspond to non-coding or intronic regions, except OT-37. Mismatches in the target sequence are indicated in red letter. Abbreviations: chr, chromosome number.

Table S6. Total number of potential off-target sites identified by the design tool from Benchling for the sgRNA *Scn11a*-Exon 10.

OT	*Sequence*	*PAM*	*Score*	*Gene*	*Chromosome Position*	*Mismatches*
Scn11a	GAAGACAAAGTAGATCCCGG	AGG	100.000	ENSMUSG00000034115	chr9:119804555	0
OT-1	AGGGACAAAGTAGATCCCGA	AGG	0.867		chr11:78371724	4
OT-2	GAAAACAAGGTAGATCCCAG	TGG	0.739		chr18:82284987	3
OT-3	AAAGGCAAACTAGATCTCGG	GGG	0.706		chrX:134088247	4
OT-4	GAAGAGAGAGTAGATCCCAG	CAG	0.667		chr15:94075525	3
OT-5	GCACAGAAGGTAGATCCCGG	AGG	0.551		chr6:17840372	4
OT-6	GGAGATAAAGTAGATCCTGG	AAG	0.478		chrX:36902393	3
OT-7	AAAGTCTAAGTAGATCCCAG	AAG	0.443		chr14:16576089	4
OT-8	CAAGACCCAGTAGATCCCTG	AAG	0.438		chr12:54023022	4
OT-9	TAATACAACGTAGATCCCTG	TGG	0.411		chr12:77888009	4
OT-10	TAAAACAAAGTTGATCTCGG	TGG	0.390	ENSMUSG00000035601	chr4:45308473	4
OT-11	GAAGGCAAAGGAGATCCAGG	GGG	0.381		chr6:122409883	3
OT-12	GTTGACAAAGTGGATCACGG	GAG	0.376		chr14:66984627	4
OT-13	GAAGAGAAAGCAGATCCCTG	GGG	0.370		chr11:94676523	3
OT-14	GAGAAGAAAGTAGATCCCAG	AGG	0.362		chr15:79490098	4
OT-15	GAAAACATTGTAGATCCCAG	GGG	0.355		chr13:22240429	4
OT-16	AAAGTCAAAGTGGATCCCAG	GAG	0.339		chr9:77809123	4
OT-17	GAAGACAGAGAAGATCCTGG	AAG	0.336		chr13:95410046	3
OT-18	CAAGACAAAGTGGATTCCGG	TGG	0.325		chr13:111837591	3
OT-19	GACAACAAAGTGGATCCCAG	CAG	0.315		chr13:72173477	4
OT-20	CAAGCCAAAGTAAATCACGG	TGG	0.307		chr2:65158901	4
OT-21	GATGACACAGTTGATCCCTG	CAG	0.301		chr2:35301981	4
OT-22	AAAAAGAAAGTAGAGCCCGG	GAG	0.293		chr9:85518417	4
OT-23	GGAGACAAAATGGATCCCAG	AAG	0.284		chr7:88362578	4
OT-24	GAACACAAAGTAAATCCTGG	AAG	0.278		chr1:67029199	3
OT-25	GCAGACAGAGTAGATCTCAG	CAG	0.262		chr14:67450100	4
OT-26	TAAGAAAAAGGAGATCACGG	AGG	0.257		chr17:52275721	4
OT-27	AAAGACAAATTAGATCTCAG	GGG	0.244		chr15:99294059	4
OT-28	GGAGACAATGGAGATCTCGG	AAG	0.244	ENSMUSG00000033653	chr16:21470214	4
OT-29	GTAGACTAAGGAGATCCCTG	TGG	0.243		chr15:72688736	4
OT-30	GAAGACAGAATTGATCCCTG	GGG	0.237		chr14:74471147	4
OT-31	GAATACAAAGTAGATTTCGG	GGG	0.232		chr12:119239205	3
OT-32	GAAGACAGCGGGGATCCCGG	GAG	0.231	ENSMUSG00000053199	chr9:51765721	4
OT-33	CAAAACAAAGAAGATCCGGG	GAG	0.229		chr1:20905953	4
OT-34	GGAGAGATAGTAGATCCAGG	AAG	0.228		chr3:67992708	4
OT-35	GAAAACTAAGGAGATCCCAG	TGG	0.227		chr15:43528199	4
OT-36	GACAACAATGTAGATCCTGG	CAG	0.227		chr2:132778487	4
OT-37	GAAGGGAAAGGAGATCTCGG	AAG	0.227		chr5:101980052	4
OT-38	GCAGAGAAAGAACATCCCGG	TAG	0.221		chr11:46382271	4
OT-39	GAAGAGAAACGGGATCCCGG	TGG	0.219		chr12:102399813	4
OT-40	GGAGACCAAGTGGATCCCTG	AGG	0.218		chr13:23039538	4
OT-41	GAGAACAAAGAAGATCCTGG	TAG	0.211		chr13:70531874	4
OT-42	GAAGTTAAAGCAGATCCCTG	GAG	0.197		chr8:66364173	4
OT-43	GGAGAAAAAGTTGATCCCTG	GAG	0.195		chr12:49449931	4
OT-44	GAATAAAAAGTGCATCCCGG	CAG	0.187		chr14:93121091	4
OT-45	GAACAGAAAGTTGATCCCCG	AAG	0.183	ENSMUSG00000005506	chr2:91013801	4
OT-46	GAAGACATCATAGATCCTGG	TAG	0.176		chr16:70537075	4
OT-47	GGAGACACAGCAGATGCCGG	GAG	0.174		chr1:90184337	4
OT-48	GAGGACCAAGGAGAACCCGG	AAG	0.174		chr14:40918070	4
OT-49	GAAGACAAAGTGGAACCCGA	GAG	0.158		chr16:33147788	3

Total number of off-target (OT) sites predicted by the CRISPR Design Tool from Benchling (www.benchling.com) including sites with four or fewer mismatches in the first 20 protospacer adjacent motif (PAM) proximal bases. All potential OTs correspond to non-coding or intronic regions, except OT-10, 28, 32, and 45. Mismatches in the target sequence are indicated in red letter. Abbreviations: chr, chromosome number.

II. Plasmid Maps

1. pSimpleII-U6-tracrRNA-U6-BsmBI-NLSNmCas9-HA-NLS(s), Addgene #47868

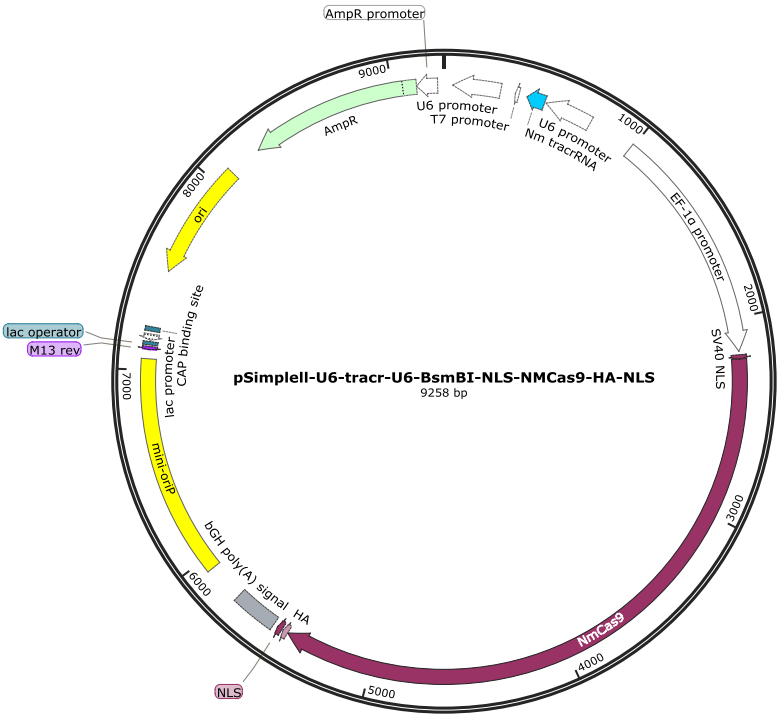

2. pSimpleII-U6-tracrRNA-U6-BsmBI-NLSNmCas9-HA-NLS-CMV-GFP

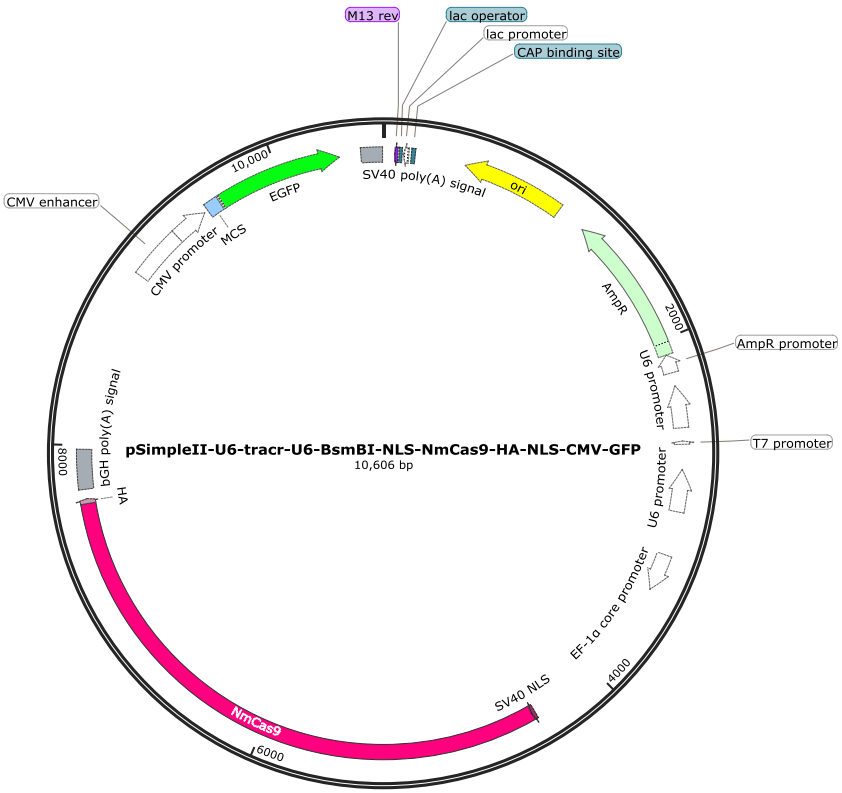

3. pCI-neo-NTRK1

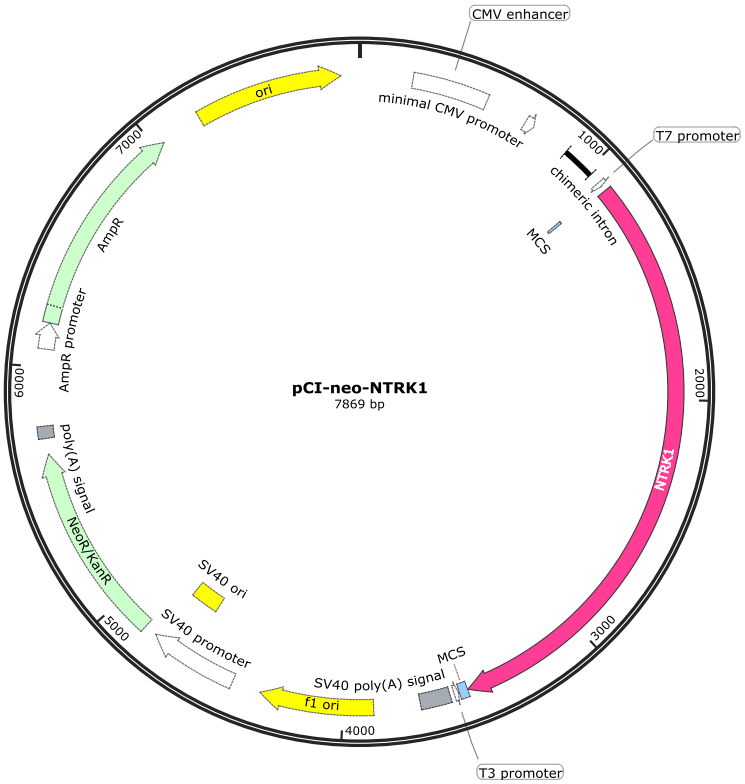

4. pCI-neo-NTRK1-myc

5. pX330-U6-chimeric_BB-CBh-hSpCas9 (Addgene plasmid #42230)

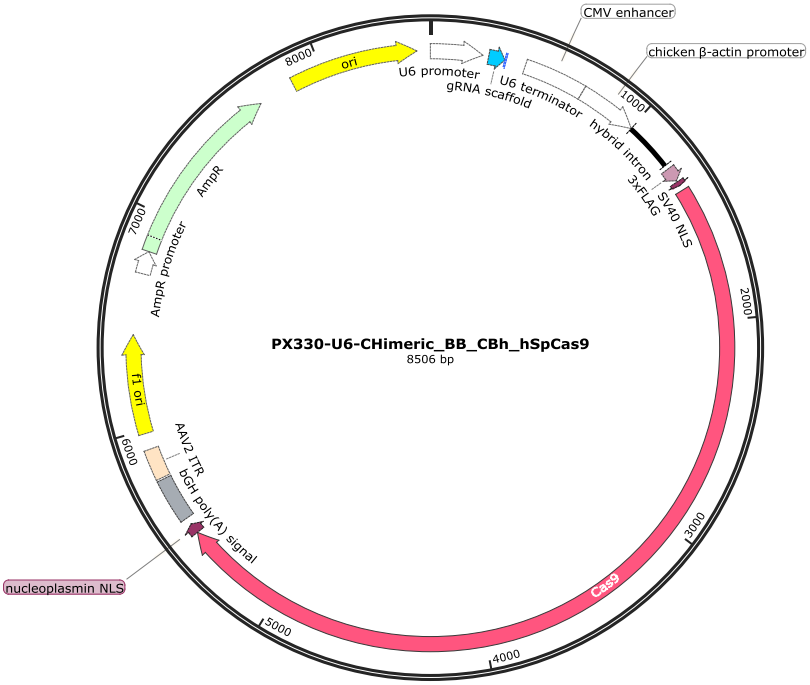

References

1. H. Merskey, N. Bogduk, IASP taxonomy. *Updat. from Pain Terms, A Curr. List with Defin. Notes Usage" (pp 209-214) Classif. Chronic Pain, Second Ed. IASP Task Force Taxon.* (2012), pp. 209–214.
2. A. I. Basbaum, T. M. Jessell, *Principles of Neural Science* (2000).
3. A. I. Basbaum, D. M. Bautista, G. Scherrer, D. Julius, Cellular and Molecular Mechanisms of Pain. *Cell*. **139** (2009), pp. 267–284.
4. E. W. Gregg *et al.*, Prevalence of lower-extremity disease in the U.S. adult population ≥40 years of age with and without diabetes: 1999-2000 National Health and Nutrition Examination Survey. *Diabetes Care*. **27**, 1591–1597 (2004).
5. A. Höke, Animal models of peripheral neuropathies. *Neurotherapeutics*. **9**, 262–9 (2012).
6. A. Rotthier, J. Baets, V. Timmerman, K. Janssens, Mechanisms of disease in hereditary sensory and autonomic neuropathies. *Nat Rev Neurol*. **8**, 73–85 (2012).
7. P. J. Dyck *et al.*, The prevalence by staged severity of various types of diabetic neuropathy, retinopathy, and nephropathy in a population based cohort The Rochester Diabetic Neuropathy Study. *Neurology*. **43**, 817–817 (1993).
8. J. Langer, H. H. Goebel, S. Veit, Eccrine sweat glands are not innervated in hereditary sensory neuropathy type IV. An electron-microscopic study. *Acta Neuropathol.* **54**, 199–202 (1981).
9. M. Nolano *et al.*, Absent innervation of skin and sweat glands in congenital insensitivity to pain with anhidrosis. *Clin. Neurophysiol.* **111**, 1596–1601 (2000).
10. Y. Indo, Genetics of congenital insensitivity to pain with anhidrosis (CIPA) or hereditary sensory and autonomic neuropathy type IV. *Clin. Auton. Res.* **12** (2002).
11. K. Huehne *et al.*, Novel missense, insertion and deletion mutations in the neurotrophic tyrosine kinase receptor type 1 gene (NTRK1) associated with congenital insensitivity to pain with anhidrosis. *Neuromuscul. Disord.* **18**, 159–166 (2008).
12. I. Kurth *et al.*, Whole exome sequencing in congenital pain insensitivity identifies a novel causative intronic NTRK1-mutation due to uniparental disomy. *Am. J. Med. Genet. Part B Neuropsychiatr. Genet.* **171**, 875–878 (2016).
13. E. Sarasola, J. A. Rodriguez, E. Garrote, J. Aristegui, M. J. Garcia-Barcina, A short in-frame deletion in NTRK1 tyrosine kinase domain caused by a novel splice site mutation in a patient with congenital insensitivity to pain with anhidrosis. *BMC Med. Genet.* **12**, 86 (2011).
14. T.-S. Nam *et al.*, Novel NTRK1 mutations associated with congenital insensitivity to pain with anhidrosis verified by functional studies. *J. Peripher. Nerv. Syst.* **22**: 92–99 (2017).
15. R. Altassan *et al.*, Exome sequencing identifies novel *NTRK1* mutations in patients with HSAN-IV phenotype. *Am. J. Med. Genet. Part A*. **173**, 1009–1016 (2017).

16. A. Greco, R. Villa, M. A. Pierotti, Genomic organization of the human NTRK1 gene. *Oncogene*. **13**, 2463–2466 (1996).

17. H. U. G. Weier, A. P. Rhein, F. Shadravan, C. Collins, D. Polikoff, Rapid physical mapping of the human trk protooncogene (NTRK1) to human chromosome 1q21-q22 by P1 clone selection, fluorescence in situ hybridization (FISH), and computer-assisted microscopy. *Genomics*. **26**, 390–393 (1995).

18. P. W. Mantyh, M. Koltzenburg, L. M. Mendell, L. Tive, D. L. Shelton, Antagonism of nerve growth factor-TrkA signaling and the relief of pain. *Anesthesiology*. **115**, 189–204 (2011).

19. M. Barbacid, The Trk family of neurotrophin receptors. *J. Neurobiol.* **25** (1994), pp. 1386–1403.

20. R. T. Uren, A. M. Turnley, Regulation of neurotrophin receptor (Trk) signaling: suppressor of cytokine signaling 2 (SOCS2) is a new player. *Front. Mol. Neurosci.* **7** (2014), doi:10.3389/fnmol.2014.00039.

21. S. R. Datta, A. Brunet, M. E. Greenberg, Cellular survival: A play in three akts. *Genes Dev.* **13** (1999), pp. 2905–2927.

22. J. Yuan, B. A. Yankner, Apoptosis in the nervous system. *Nature*. **407**, 802–809 (2000).

23. I. Dikic *et al.*, Shc binding to nerve growth factor receptor is mediated by the phosphotyrosine interaction domain. *J. Biol. Chem.* **270**, 15125–15129 (1995).

24. J. I. S. MacDonald, E. A. Gryz, C. J. Kubu, J. M. Verdi, S. O. Meakin, Direct binding of the signaling adapter protein Grb2 to the activation loop tyrosines on the nerve growth factor receptor tyrosine kinase, TrkA. *J. Biol. Chem.* **275**, 18225–18233 (2000).

25. M. E. Cunningham, R. M. Stephens, D. R. Kaplan, L. A. Greene, Autophosphorylation of activation loop tyrosines regulates signaling by the TRK nerve growth factor receptor. *J. Biol. Chem.* **272**, 10957–10967 (1997).

26. a Obermeier *et al.*, Tyrosine 785 is a major determinant of Trk--substrate interaction. *EMBO J.* **12**, 933–941 (1993).

27. M. V. Chao, Neurotrophins and their receptors: A convergence point for many signalling pathways. *Nat. Rev. Neurosci.* **4**, 299–309 (2003).

28. L. Gao *et al.*, Oral and Craniofacial Manifestations and Two Novel Missense Mutations of the NTRK1 Gene Identified in the Patient with Congenital Insensitivity to Pain with Anhidrosis. *PLoS One*. **8** (2013), doi:10.1371/journal.pone.0066863.

29. T. E. Willnow, C. M. Petersen, A. Nykjaer, VPS10P-domain receptors - regulators of neuronal viability and function. *Nat. Rev. Neurosci.* **9**, 899–909 (2008).

30. D. L. H. Bennett, C. G. Woods, Painful and painless channelopathies. *Lancet Neurol.* **13** (2014), pp. 587–599.

31. W. a Catterall, Voltage-gated sodium channels at 60: structure, function and pathophysiology. *J. Physiol.* **590**, 2577–89 (2012).

32. J. J. Toledo-Aral *et al.*, Identification of PN1, a predominant voltage-dependent sodium channel expressed principally in peripheral neurons. *Proc. Natl. Acad. Sci.* **94**, 1527–1532 (1997).

33. A. N. Akopian, L. Sivilotti, J. N. Wood, A tetrodotoxin-resistant voltage-gated sodium channel expressed by sensory neurons. *Nature*. **379** (1996), pp. 257–262.

34. S. D. Dib-Hajj, L. Tyrrell, J. A. Black, S. G. Waxman, NaN, a novel voltage-gated Na channel, is expressed preferentially in peripheral sensory neurons and down-regulated after axotomy. *Proc. Natl. Acad. Sci. U. S. A.* **95**, 8963–8968 (1998).

35. M. Minett *et al.*, Distinct Nav1.7-dependent pain sensations require different sets of sensory and sympathetic neurons. *Nat. Commun.* **3**, 791–799 (2012).

36. N. T. Blair, B. P. Bean, Roles of tetrodotoxin (TTX)-sensitive Na+ current, TTX-resistant Na+ current, and Ca2+ current in the action potentials of nociceptive sensory neurons. *J. Neurosci.* **22**, 10277–10290 (2002).

37. M. Renganathan, T. R. Cummins, S. G. Waxman, Contribution of Na(v)1.8 sodium channels to action potential electrogenesis in DRG neurons. *J. Neurophysiol.* **86**, 629–640 (2001).

38. R. I. Herzog, T. R. Cummins, S. G. Waxman, Persistent TTX-resistant Na+ current affects resting potential and response to depolarization in simulated spinal sensory neurons. *J. Neurophysiol.* **86**, 1351–64 (2001).

39. J. A. R. Ostman, M. A. Nassar, J. N. Wood, M. D. Baker, GTP up-regulated persistent Na+ current and enhanced nociceptor excitability require NaV1.9. *J. Physiol.* **586**, 1077–87 (2008).

40. B. T. Priest *et al.*, Contribution of the tetrodotoxin-resistant voltage-gated sodium channel NaV1.9 to sensory transmission and nociceptive behavior. *Proc. Natl. Acad. Sci. U. S. A.* **102**, 9382–7 (2005).

41. S. D. Dib-Hajj *et al.*, Two tetrodotoxin-resistant sodium channels in human dorsal root ganglion neurons. *FEBS Lett.* **462**, 117–120 (1999).

42. L. Djouhri *et al.*, Sensory and electrophysiological properties of guinea-pig sensory neurones expressing Nav 1.7 (PN1) Na+ channel alpha subunit protein. *J. Physiol.* **546**, 565–576 (2003).

43. Y. Yang *et al.*, Mutations in SCN9A, encoding a sodium channel alpha subunit, in patients with primary erythermalgia. *J. Med. Genet.* **41**, 171–174 (2004).

44. C.-W. Huang, H.-J. Lai, P.-Y. Huang, M.-J. Lee, C.-C. Kuo, The Biophysical Basis Underlying Gating Changes in the p.V1316A Mutant Nav1.7 Channel and the Molecular Pathogenesis of Inherited Erythromelalgia. *PLOS Biol.* **14**, e1002561 (2016).

45. T. Stadler, A. O. O'Reilly, A. Lampert, Erythromelalgia Mutation Q875E Stabilizes the Activated State of Sodium Channel Nav1.7. *J. Biol. Chem.* **290**, 6316–6325 (2015).

46. Y. Yang *et al.*, Nav1.7-A1632G Mutation from a Family with Inherited Erythromelalgia: Enhanced Firing of Dorsal Root Ganglia Neurons Evoked by Thermal Stimuli. *J. Neurosci.* **36**, 7511–7522 (2016).

47. C. R. Fertleman *et al.*, SCN9A Mutations in Paroxysmal Extreme Pain Disorder: Allelic Variants Underlie Distinct Channel Defects and Phenotypes. *Neuron*. **52**, 767–774 (2006).

48. M. R. Suter *et al.*, p.L1612P, a Novel Voltage-gated Sodium Channel Nav1.7 Mutation Inducing a Cold Sensitive Paroxysmal Extreme Pain Disorder. *Anesthesiology*. **122**, 414–423 (2015).

49. D. T. Kim, E. Rossignol, K. Najem, L. H. Ospina, Bilateral congenital corneal anesthesia in a patient with SCN9A mutation, confirmed primary erythromelalgia, and paroxysmal extreme pain disorder. *J. Am. Assoc. Pediatr. Ophthalmol. Strabismus*. **19**, 478–479 (2015).

50. C. G. Faber *et al.*, Gain of function Nav1.7 mutations in idiopathic small fiber neuropathy. *Ann. Neurol.* **71**, 26–39 (2012).

51. J. J. Cox *et al.*, An SCN9A channelopathy causes congenital inability to experience pain. *Nature*. **444**, 894–898 (2006).

52. K. B. Nilsen *et al.*, Two novel SCN9A mutations causing insensitivity to pain. *Pain*. **143**, 155–158 (2009).

53. F. Amaya *et al.*, Diversity of expression of the sensory neuron-specific TTX-resistant voltage-gated sodium ion channels SNS and SNS2. *Mol. Cell. Neurosci.* **15**, 331–42 (2000).

54. C. G. Faber *et al.*, Gain-of-function Nav1.8 mutations in painful neuropathy. *Proc. Natl. Acad. Sci. U. S. A.* **109**, 19444–9 (2012).

55. D. Cazzato, G. Lauria, Small fibre neuropathy. *Curr. Opin. Neurol.*, 1 (2017).

56. R. Dabby *et al.*, Painful small fiber neuropathy with gastroparesis: A new phenotype with a novel mutation in the SCN10A gene. *J. Clin. Neurosci.* **26**, 84–88 (2016).

57. E. Leipold *et al.*, A de novo gain-of-function mutation in SCN11A causes loss of pain perception. *Nat. Genet.* **45**, 1399–404 (2013).

58. V. Phatarakijnirund *et al.*, Congenital insensitivity to pain: Fracturing without apparent skeletal pathobiology caused by an autosomal dominant, second mutation in SCN11A encoding voltage-gated sodium channel 1.9. *Bone*. **84**, 289–298 (2016).

59. M. K. King, E. Leipold, J. M. Goehringer, I. Kurth, T. D. Challman, Pain insensitivity: distal S6-segment mutations in NaV1.9 emerge as critical hotspot. *Neurogenetics* (2017), doi:10.1007/s10048-017-0513-9.

60. X. Y. Zhang *et al.*, Gain-of-Function mutations in SCN11A cause familial episodic pain. *Am. J. Hum. Genet.* **93**, 957–966 (2013).

61. X.-R. Leng, X.-H. Qi, Y.-T. Zhou, Y.-P. Wang, Gain-of-function mutation p.Arg225Cys in SCN11A causes familial episodic pain and contributes to essential tremor. *J. Hum. Genet.* (2017), doi:10.1038/jhg.2017.21.

62. H. Okuda *et al.*, Infantile Pain Episodes Associated with Novel Nav1.9 Mutations in Familial Episodic Pain Syndrome in Japanese Families. *PLoS One*. **11**, e0154827 (2016).

63. C. Han *et al.*, The Domain II S4-S5 Linker in Nav1.9: A Missense Mutation Enhances Activation, Impairs Fast Inactivation, and Produces Human Painful Neuropathy. *NeuroMolecular Med.* **17**, 158–169 (2015).

64. Han C, Yang Y,te MorscheRH*, et al.* Familial gain-of-function $Na_v1.9$ mutation in a painful channelopathy *J Neurol Neurosurg Psychiatry* (2017);**88:**233-240.

65. E. Leipold *et al.*, Cold-aggravated pain in humans caused by a hyperactive NaV1.9 channel mutant. *Nat. Commun.* **6**, 10049 (2015).

66. E. Marban, T. Yamagishi, G. F. Tomaselli, Structure and function of voltage-gated sodium channels. *J. Physiol.*, 647–57 (1998).

67. B. A. Brouwer *et al.*, in *Journal of the Peripheral Nervous System* (2014), vol. 19, pp. 53–65.

68. P. D. Hsu, E. S. Lander, F. Zhang, Development and applications of CRISPR-Cas9 for genome engineering. *Cell*. **157**, 1262–1278 (2014).

69. R. Mario *et al.*, Altering the Genome by Homologous Recombination. *Sci. Virol. Sci. Theor. Appl. Genet. Arch. Tierz. Kexue Tongbao K. Ozato al. Cell Differ. Aquac. Trans. Am. Fish. Soc*. **244**, 1288–1292 (1989).

70. M. Bibikova *et al.*, Stimulation of homologous recombination through targeted cleavage by chimeric nucleases. *Mol. Cell. Biol.* **21**, 289–97 (2001).

71. M. Bibikova, K. Beumer, J. K. Trautman, D. Carroll, Enhancing gene targeting with designed zinc finger nucleases. *Science*. **300**, 764 (2003).

72. M. Bibikova, M. Golic, K. G. Golic, D. Carroll, Targeted chromosomal cleavage and mutagenesis in Drosophila using zinc-finger nucleases. *Genetics*. **161**, 1169–1175 (2002).

73. L. Cong *et al.*, Multiplex Genome Engineering Using CRISPR/Cas System. *Science.* **339**, 819–824 (2013).

74. P. Mali *et al.*, RNA-guided human genome engineering via Cas9. *Science*. **339**, 823–6 (2013).

75. B. Alberts *et al.*, Molecular Cell Biology, 4. edition. *Biochem. Mol. Biol. Educ.* **Chapter 19** (2002), doi:10.1002/bmb.20373.

76. R. Barrangou, L. A. Marraffini, CRISPR-cas systems: Prokaryotes upgrade to adaptive immunity. *Mol. Cell*. **54** (2014), pp. 234–244.

77. R. Barrangou *et al.*, CRISPR provides acquired resistance against viruses in prokaryotes. *Science*. **315**, 1709–12 (2007).

78. C. R. Hale *et al.*, RNA-Guided RNA Cleavage by a CRISPR RNA-Cas Protein Complex. *Cell*. **139**, 945–956 (2009).

79. K. S. Makarova, N. V Grishin, S. A. Shabalina, Y. I. Wolf, E. V Koonin, A putative RNA-interference-based immune system in prokaryotes: computational analysis of the predicted enzymatic machinery, functional analogies with eukaryotic RNAi, and hypothetical mechanisms of action. *Biol. Direct*. **1**, 7 (2006).

80. L. A. Marraffini, E. J. Sontheimer, CRISPR interference limits horizontal gene transfer in staphylococci by targeting DNA. *Science.* **322**, 1843–1845 (2008).

81. Brouns SJ,Jore MM, Lundgren M, Westra ER, Slijkhuis RJ, Snijders AP, Dickman MJ, van der Oost J, Small CRISPR RNAs guide antiviral defense in prokaryotes. Science. (2008) Aug 15;321(5891):960-4. doi: 10.1126/science.1159689.

82. J. E. Garneau *et al.*, The CRISPR/Cas bacterial immune system cleaves bacteriophage and plasmid DNA. *Nature*. **468**, 67–71 (2010).

83. L. A. Marraffini, E. J. Sontheimer, CRISPR interference: RNA-directed adaptive immunity in bacteria and archaea. *Nat. Rev. Genet.* **11**, 181–90 (2010).

84. D. H. Haft, J. Selengut, E. F. Mongodin, K. E. Nelson, A guild of 45 CRISPR-associated (Cas) protein families and multiple CRISPR/cas subtypes exist in prokaryotic genomes. *PLoS Comput. Biol.* **1**, 0474–0483 (2005).

85. K. S. Makarova, Y. I. Wolf, E. V Koonin, The basic building blocks and evolution of CRISPR-CAS systems. *Biochem. Soc. Trans.* **41**, 1392–400 (2013).

86. K. S. Makarova, L. Aravind, N. V Grishin, I. B. Rogozin, E. V Koonin, A DNA repair system specific for thermophilic Archaea and bacteria predicted by genomic context analysis. *Nucleic Acids Res.* **30**, 482–496 (2002).

87. K. S. Makarova, L. Aravind, Y. I. Wolf, E. V Koonin, Unification of Cas protein families and a simple scenario for the origin and evolution of CRISPR-Cas systems. *Biol. Direct*. **6**, 38 (2011).

88. K. S. Makarova *et al.*, Evolution and classification of the CRISPR-Cas systems. *Nat. Rev. Microbiol.* **9**, 467–77 (2011).

89. J. van der Oost, E. R. Westra, R. N. Jackson, B. Wiedenheft, Unravelling the structural and mechanistic basis of CRISPR-Cas systems. *Nat. Rev. Microbiol.* **12**, 479–92 (2014).

90. J. Carte, R. Wang, H. Li, R. M. Terns, M. P. Terns, Cas6 is an endoribonuclease that generates guide RNAs for invader defense in prokaryotes. *Genes Dev.* **22**, 3489–3496 (2008).

91. E. Deltcheva *et al.*, CRISPR RNA maturation by *trans*-encoded small RNA and host factor RNase III. *Nature*. **471**, 602–607 (2011).

92. E. M. Gesner, M. J. Schellenberg, E. L. Garside, M. M. George, A. M. Macmillan, Recognition and maturation of effector RNAs in a CRISPR interference pathway. *Nat. Struct. Mol. Biol.* **18**, 688–692 (2011).

93. R. E. Haurwitz, M. Jinek, B. Wiedenheft, K. Zhou, J. A. Doudna, Sequence- and Structure-Specific RNA Processing by a CRISPR Endonuclease. *Science*. **329**, 1355–1358 (2010).

94. D. G. Sashital, M. Jinek, J. a Doudna, An RNA-induced conformational change required for CRISPR RNA cleavage by the endoribonuclease Cse3. *Nat. Struct. Mol. Biol.* **18**, 680–7 (2011).

95. R. Wang, G. Preamplume, M. P. Terns, R. M. Terns, H. Li, Interaction of the Cas6 riboendonuclease with CRISPR RNAs: Recognition and cleavage. *Structure*. **19**, 257–264 (2011).

96. C. Hale, K. Kleppe, R. M. Terns, M. P. Terns, Prokaryotic silencing (psi)RNAs in Pyrococcus furiosus. *RNA*. **14**, 2572–9 (2008).

97. N. G. Lintner *et al.*, Structural and functional characterization of an archaeal clustered regularly interspaced short palindromic repeat (CRISPR)-associated complex for antiviral defense (CASCADE). *J. Biol. Chem.* **286**, 21643–21656 (2011).

98. B. Wiedenheft *et al.*, Structures of the RNA-guided surveillance complex from a bacterial immune system. *Nature*. **477**, 486–489 (2011).

99. M. M. Jore *et al.*, Structural basis for CRISPR RNA-guided DNA recognition by Cascade. *Nat. Struct. & Mol. Biol.* **18**, 529–536 (2011).

100. K. S. Makarova *et al.*, An updated evolutionary classification of CRISPR-Cas systems. *Nat. Rev. Microbiol.* **13**, 722–736 (2015).

101. S. Shmakov *et al.*, Discovery and Functional Characterization of Diverse Class 2 CRISPR-Cas Systems. *Mol. Cell*. **60**, 385–397 (2015).

102. R. Louwen, R. H. J. Staals, H. P. Endtz, P. van Baarlen, J. van der Oost, The role of CRISPR-Cas systems in virulence of pathogenic bacteria. *Microbiol. Mol. Biol. Rev.* **78**, 74–88 (2014).

103. T. R. Sampson, D. S. Weiss, CRISPR-Cas systems: new players in gene regulation and bacterial physiology. *Front. Cell. Infect. Microbiol.* **4**, 37 (2014).

104. E. R. Westra, A. Buckling, P. C. Fineran, CRISPR-Cas systems: beyond adaptive immunity. *Nat. Rev. Microbiol.* **12**, 317–26 (2014).

105. J. K. Nuñez *et al.*, Cas1-Cas2 complex formation mediates spacer acquisition during CRISPR-Cas adaptive immunity. *Nat. Struct. Mol. Biol.* **21**, 528–34 (2014).

106. B. Wiedenheft, S. H. Sternberg, J. a. Doudna, RNA-guided genetic silencing systems in bacteria and archaea. *Nature*. **482**, 331–338 (2012).

107. N. Takeuchi, Y. I. Wolf, K. S. Makarova, E. V. Koonin, Nature and intensity of selection pressure on crispr-associated genes. *J. Bacteriol.* **194**, 1216–1225 (2012).

108. J. K. Nuñez, A. S. Y. Lee, A. Engelman, J. a. Doudna, Integrase-mediated spacer acquisition during CRISPR–Cas adaptive immunity. *Nature*. **519**, 193–198 (2015).

109. R. Heler *et al.*, Cas9 specifies functional viral targets during CRISPR-Cas adaptation. *Nature*. **519**, 199–202 (2015).

110. Y. Wei, R. M. Terns, M. P. Terns, Cas9 function and host genome sampling in type II-A CRISPR???cas adaptation. *Genes Dev.* **29**, 356–361 (2015).

111. S. A. Shah, S. Erdmann, F. J. M. Mojica, R. A. Garrett, Protospacer recognition motifs: mixed identities and functional diversity. *RNA Biol.* **10**, 891–9 (2013).

112. A. Bolotin, B. Quinquis, A. Sorokin, S. Dusko Ehrlich, Clustered regularly interspaced short palindrome repeats (CRISPRs) have spacers of extrachromosomal origin. *Microbiology*. **151**, 2551–2561 (2005).

113. F. J. M. Mojica, C. Díez-Villaseñor, J. García-Martínez, C. Almendros, Short motif sequences determine the targets of the prokaryotic CRISPR defence system. *Microbiology*. **155**, 733–740 (2009).

114. L. A. Marraffini, E. J. Sontheimer, Self versus non-self discrimination during CRISPR RNA-directed immunity. *Nature*. **463**, 568–71 (2010).

115. Y. Zhang *et al.*, Processing-Independent CRISPR RNAs Limit Natural Transformation in Neisseria meningitidis. *Mol. Cell*. **50**, 488–503 (2013).

116. B. Zetsche *et al.*, Cpf1 Is a Single RNA-Guided Endonuclease of a Class 2 CRISPR-Cas System. *Cell*. **163**, 759–771 (2015).

117. N. Beloglazova *et al.*, Structure and activity of the Cas3 HD nuclease MJ0384, an effector enzyme of the CRISPR interference. *EMBO J.* **30**, 4616–4627 (2011).

118. E. R. Westra *et al.*, CRISPR Immunity Relies on the Consecutive Binding and Degradation of Negatively Supercoiled Invader DNA by Cascade and Cas3. *Mol. Cell*. **46**, 595–605 (2012).

119. P. Samai *et al.*, Co-transcriptional DNA and RNA cleavage during type III CRISPR-cas immunity. *Cell*. **161**, 1164–1174 (2015).

120. O. O. Abudayyeh *et al.*, Abudayyeh, O. O. *et al*. C2c2 is a single-component programmable RNA-guided RNA-targeting CRISPR effector. *Science* **353** (2016).

121. G. P. C. Salmond, P. C. Fineran, A century of the phage: past, present and future. *Nat. Rev. Microbiol.* **13**, 777–86 (2015).

122. F. J. M. Mojica, C. Díez-Villaseñor, E. Soria, G. Juez, Biological significance of a family of regularly spaced repeats in the genomes of Archaea, Bacteria and mitochondria. *Mol. Microbiol.* **36** (2000), pp. 244–246.

123. R. Jansen, J. D. A. Van Embden, W. Gaastra, L. M. Schouls, Identification of genes that are associated with DNA repeats in prokaryotes. *Mol. Microbiol.* **43**, 1565–1575 (2002).

124. A. Quiberoni, S. Moineau, G. M. Rousseau, J. Reinheimer, H. W. Ackermann, Streptococcus thermophilus bacteriophages. *Int. Dairy J.* **20** (2010), pp. 657–664.

125. M. Jinek *et al.*, A Programmable Dual-RNA – Guided DNA Endonuclease in Adaptice Bacterial Immunity. *Science*. **337**, 816–822 (2012).

126. G. Gasiunas, R. Barrangou, P. Horvath, V. Siksnys, Cas9-crRNA ribonucleoprotein complex mediates specific DNA cleavage for adaptive immunity in bacteria. *Proc. Natl. Acad. Sci. U. S. A.* **109**, E2579-86 (2012).

127. J. D. Sander, J. K. Joung, CRISPR-Cas systems for editing, regulating and targeting genomes. *Nat. Biotechnol.* **32**, 347–355 (2014).

128. H. Nishimasu *et al.*, Crystal structure of Cas9 in complex with guide RNA and target DNA. *Cell*. **156**, 935–949 (2014).

129. C. Anders, O. Niewoehner, A. Duerst, M. Jinek, Structural basis of PAM-dependent target DNA recognition by the Cas9 endonuclease. *Nature*. **513**, 569–73 (2014).

130. M. Jinek *et al.*, Structures of Cas9 endonucleases reveal RNA-mediated conformational activation. *Science*. **343**, 1247997 (2014).

131. Z. Hou *et al.*, Efficient genome engineering in human pluripotent stem cells using Cas9 from Neisseria meningitidis. *Proc. Natl. Acad. Sci. USA*. **110**, 15644–15649 (2013).

132. C. M. Lee, T. J. Cradick, G. Bao, The Neisseria meningitidis CRISPR-Cas9 System Enables Specific Genome Editing in Mammalian Cells. *Mol. Ther.* **24**, 645–654 (2016).

133. L. A. Greene, A. S. Tischler, --start of pc12--Establishment of a noradrenergic clonal line of rat adrenal pheochromocytoma cells which respond to nerve growth factor. *Proc. Natl. Acad. Sci. U. S. A.* **73**, 2424–2428 (1976).

134. L. A. Greene, Nerve growth factor prevents the death and stimulates the neuronal differentiation of clonal PC12 pheochromocytoma cells in serum-free medium. *J. Cell Biol.* **78**, 747–755 (1978).

135. F. L. Graham, J. Smiley, W. C. Russell, R. Nairn, Characteristics of a human cell line transformed by DNA from human adenovirus type 5. *J. Gen. Virol.* **36**, 59–72 (1977).

136. W. F. SCHERER, J. T. SYVERTON, G. O. GEY, Studies on the propagation in vitro of poliomyelitis viruses. IV. Viral multiplication in a stable strain of human malignant epithelial cells (strain HeLa) derived from an epidermoid carcinoma of the cervix. *J. Exp. Med.* **97**, 695–710 (1953).

137. X. Zhu *et al.*, An efficient genotyping method for genome-modified animals and human cells generated with CRISPR/Cas9 system. *Sci Rep*. **4**, 6420 (2014).

138. P. D. Hsu *et al.*, DNA targeting specificity of RNA-guided Cas9 nucleases. *Nat. Biotechnol.* **31**, 827–32 (2013).

139. J. G. Doench *et al.*, Rational design of highly active sgRNAs for CRISPR-Cas9–mediated gene inactivation. *Nat. Biotechnol.* **32**, 1262–7 (2014).

140. T. J. Cradick, P. Qiu, C. M. Lee, E. J. Fine, G. Bao, COSMID: A Web-based Tool for Identifying and Validating CRISPR/Cas Off-target Sites. *Mol Ther Nucleic Acids*. **3**, e214 (2014).

141. P. A. Barker *et al.*, Tissue-specific alternative splicing generates two isoforms of the trkA receptor. *J. Biol. Chem.* **268**, 15150–15157 (1993).

142. S. F. Altschul, W. Gish, W. Miller, E. W. Myers, D. J. Lipman, Basic local alignment search tool. *J. Mol. Biol.* **215**, 403–10 (1990).

143. E. Lubeck, A. F. Coskun, T. Zhiyentayev, M. Ahmad, L. Cai, MutationTaster2: mutation prediction for the deep-sequencing age. *Nat. Methods Nat. Methods Nat. Methods*. **9**, 743–748 (2012).

144. I. A. Adzhubei *et al.*, A method and server for predicting damaging missense mutations. *Nat. Methods*. **7**, 248–249 (2010).

145. P. Kumar, S. Henikoff, P. C. Ng, Predicting the effects of coding non-synonymous variants on protein function using the SIFT algorithm. *Nat. Protoc.* **4**, 1073–1081 (2009).

146. M. S. Nahorski *et al.*, A novel disorder reveals clathrin heavy chain-22 is essential for human pain and touch development. *Brain*. **138**, 2147–2160 (2015).

147. H. Wang *et al.*, One-step generation of mice carrying mutations in multiple genes by CRISPR/cas-mediated genome engineering. *Cell*. **153**, 910–918 (2013).

148. F. A. Ran *et al.*, Genome engineering using the CRISPR-Cas9 system. *Nat. Protoc.* **8**, 2281–2308 (2013).

149. J. C. Daniel, G. B. Anderson, *Methods in mammalian reproduction*.Academic Press, (1978).

150. A. Nagy, M. Gertsenstein, K. Vintersten, R. Behringer, *Manipulating the Mouse Embryo* (2003).

151. G. E. Truett *et al.*, Preparation of PCR-quality mouse genomic dna with hot sodium hydroxide and tris (HotSHOT). *Biotechniques*. **29**, 52–54 (2000).

152. Y. Lin *et al.*, CRISPR/Cas9 systems have off-target activity with insertions or deletions between target DNA and guide RNA sequences. *Nucleic Acids Res.* **42**, 7473–7485 (2014).

153. L. C. Schecterson *et al.*, Trk activation in the secretory pathway promotes Golgi fragmentation. *Mol. Cell. Neurosci.* **43**, 403–413 (2010).

154. F. L. Watson, M. A. Porcionatto, A. Bhattacharyya, C. D. Stiles, R. A. Segal, TrkA glycosylation regulates receptor localization and activity. *J. Neurobiol.* **39**, 323–336 (1999).

155. T. Geetha, M. W. Wooten, TrkA receptor endolysosomal degradation is both ubiquitin and proteasome dependent. *Traffic*. **9**, 1146–1156 (2008).

156. Z.-Y. Chen, A Novel Endocytic Recycling Signal Distinguishes Biological Responses of Trk Neurotrophin Receptors. *Mol. Biol. Cell*. **16**, 5761–5772 (2005).

157. T. Yu *et al.*, Regulation of Trafficking of Activated TrkA Is Critical for NGF-Mediated Functions. *Traffic*. **12**, 521–534 (2011).

158. M. L. Grimes *et al.*, Endocytosis of activated TrkA: evidence that nerve growth factor induces formation of signaling endosomes. *J. Neurosci.* **16**, 7950–7964 (1996).

159. Y.-Z. Zhang, D. B. Moheban, B. R. Conway, A. Bhattacharyya, R. A. Segal, Cell surface Trk receptors mediate NGF-induced survival while internalized receptors regulate NGF-induced differentiation. *J. Neurosci.* **20**, 5671–5678 (2000).

160. C. Wu, C. F. Lai, W. C. Mobley, Nerve growth factor activates persistent Rap1 signaling in endosomes. *J. Neurosci.* **21**, 5406–16 (2001).

161. J. Widmark, G. Sundström, D. Ocampo Daza, D. Larhammar, Differential evolution of voltage-gated sodium channels in tetrapods and teleost fishes. *Mol. Biol. Evol.* **28**, 859–871 (2011).

162. P. G. Kostyuk, N. S. Veselovsky, A. Y. Tsyndrenko, Ionic currents in the somatic membrane of rat dorsal root ganglion neurons—I. Sodium currents. *Neuroscience*. **6**, 2423–2430 (1981).

163. J. M. Caffrey, D. L. Eng, J. A. Black, S. G. Waxman, J. D. Kocsis, Three types of sodium channels in adult rat dorsal root ganglion neurons. *Brain Res.* **592**, 283–297 (1992).

164. M. L. Roy, T. Narahashi, Differential Properties Ganglion Neurons of Tetrodotoxin-sensitive and Sodium Channels in Rat Dorsal Root. *J Neurosci*. **7212**, 2104–11 (1992).

165. A. A. Elliott, J. R. Elliott, Characterization of TTX-sensitive and TTX-resistant sodium currents in small cells from adult rat dorsal root ganglia. *J Physiol*. **463**, 39–56 (1993).

166. R. S. Scroggs, A. P. Fox, Calcium current variation between acutely isolated adult rat dorsal root ganglion neurons of different size. *J. Physiol.* **445**, 639–658 (1992).

167. C. G. Vanoye, J. D. Kunic, G. R. Ehring, A. L. George, Mechanism of sodium channel Na V 1.9 potentiation by G-protein signaling. *J. Gen. Physiol.* **141**, 193–202 (2013).

168. I. Ezkurdia *et al.*, Multiple evidence strands suggest that theremay be as few as 19 000 human protein-coding genes. *Hum. Mol. Genet.* **23**, 5866–5878 (2014).

169. S. G. Gregory *et al.*, A physical map of the mouse genome. *Nature*. **418**, 743–750 (2002).

170. C. Guan, C. Ye, X. Yang, J. Gao, A review of current large-scale mouse knockout efforts. *Genesis*. **48** (2010), pp. 73–85.

171. D. F. Hacking, "Knock, and it shall be opened": Knocking out and knocking in to reveal mechanisms of disease and novel therapies. *Early Hum. Dev.* **84** (2008), pp. 821–827.

172. W. C. Skarnes *et al.*, A conditional knockout resource for the genome-wide study of mouse gene function. *Nature*. **474**, 337–342 (2011).

173. C. Deng, M. R. Capecchi, Reexamination of gene targeting frequency as a function of the extent of homology between the targeting vector and the target locus. *Trends Cell Biol.* **2**, 325 (1992).

174. P. Hasty, J. Rivera-Pérez, A. Bradley, The length of homology required for gene targeting in embryonic stem cells. *Mol. Cell. Biol.* **11**, 5586–91 (1991).

175. D. B. Menke, Engineering subtle targeted mutations into the mouse genome. *Genesis*. **51**, 605–618 (2013).

176. T. Mashimo *et al.*, Efficient gene targeting by TAL effector nucleases coinjected with exonucleases in zygotes. *Sci. Rep.* **3** (2013), doi:10.1038/srep01253.

177. I. D. Carbery *et al.*, Targeted genome modification in mice using zinc-finger nucleases. *Genetics*. **186**, 451–459 (2010).

178. C. Miranda *et al.*, Novel pathogenic mechanisms of congenital insensitivity to pain with anhidrosis genetic disorder unveiled by functional analysis of neurotrophic tyrosine receptor kinase type 1/nerve growth factor receptor mutations. *J. Biol. Chem.* **277**, 6455–6462 (2002).

179. S. Mardy, Y. Miura, F. Endo, I. Matsuda, Y. Indo, Congenital insensitivity to pain with anhidrosis (CIPA): effect of TRKA (NTRK1) missense mutations on autophosphorylation of the receptor tyrosine kinase for nerve growth factor. *Hum. Mol. Genet.* **10**, 179–88 (2001).

180. M. L. Franco *et al.*, Mutations in TrkA causing congenital insensitivity to pain with anhidrosis (CIPA) induce misfolding, aggregation, and mutation-dependent neurodegeneration by dysfunction of the autophagic flux. *J. Biol. Chem.* **291**, 21363–21374 (2016).

181. M. Wang, R. J. Kaufman, Protein misfolding in the endoplasmic reticulum as a conduit to human disease. *Nature*. **529**, 326–335 (2016).

182. C. L. Howe, W. C. Mobley, Long-distance retrograde neurotrophic signaling. *Curr. Opin. Neurobiol.* **15**, 40–48 (2005).

183. D. Mashiko *et al.*, Feasibility for a large scale mouse mutagenesis by injecting CRISPR/Cas plasmid into zygotes. *Dev. Growth Differ.* **56**, 122–129 (2014).

184. D. Mashiko *et al.*, Generation of mutant mice by pronuclear injection of circular plasmid expressing Cas9 and single guided RNA. *Sci. Rep.* **3**, 3355 (2013).

185. Y. Nakagawa *et al.*, Production of knockout mice by DNA microinjection of various CRISPR/Cas9 vectors into freeze-thawed fertilized oocytes. *BMC Biotechnol.* **15**, 33 (2015).

186. J. Mianné *et al.*, Analysing the outcome of CRISPR-aided genome editing in embryos: Screening, genotyping and quality control. *Methods* (2017), doi:10.1016/j.ymeth.2017.03.016.

187. B. Oh, S. Hwang, J. McLaughlin, D. Solter, B. B. Knowles, Timely translation during the mouse oocyte-to-embryo transition. *Development*. **127**, 3795–3803 (2000).

188. W. Fujii, A. Onuma, K. Sugiura, K. Naito, Efficient generation of genome-modified mice via offset-nicking by CRISPR/Cas system. *Biochem. Biophys. Res. Commun.* **445**, 791–794 (2014).

189. U. Mock, I. Hauber, B. Fehse, Digital PCR to assess gene-editing frequencies (GEF-dPCR) mediated by designer nucleases. *Nat. Protoc.* **11**, 598–615 (2016).

190. C. Kuscu, S. Arslan, R. Singh, J. Thorpe, M. Adli, Genome-wide analysis reveals characteristics of off-target sites bound by the Cas9 endonuclease. *Nat. Biotechnol.* **32**, 677–683 (2014).

191. X. Wu *et al.*, Genome-wide binding of the CRISPR endonuclease Cas9 in mammalian cells. *Nat. Biotechnol.* **32**, 670–676 (2014).

192. R. O. Goral, E. Leipold, E. Nematian-Ardestani, S. H. Heinemann, Heterologous expression of NaV1.9 chimeras in various cell systems. *Pflugers Arch. Eur. J. Physiol.* **467**, 2423–2435 (2015).

Index of Figures

Index of Plasmid maps

Index of Tables

Ehrenwörtliche Erklärung

Hiermit versichere ich,

(1) dass mir die Promotionsordnung der Fakultät bekannt ist,

(2) dass ich die vorliegende Dissertation selbständig angefertigt habe, und alle verwendeten Quellen, Hilfsmittel und persönlichen Informationen als solche gekennzeichnet habe,

(3) dass mich Prof. Dr. Ingo Kurth bei der Auswahl und Anfertigung des Materials sowie Manuskriptes unterstützt hat,

(4) dass ich weder die Hilfe eines Promotionsberaters in Anspruch genommen habe, noch andere Personen unmittelbare oder mittelbare geldwerte Leistungen von mir erhalten haben, die im Zusammenhang mit dem Inhalt der vorgelegten Dissertation stehen,

(5) dass ich die Dissertation noch nicht als Prüfungsarbeit für eine staatliche oder andere wissenschaftliche Prüfung eingereicht habe,

(6) dass ich zu keinem Zeitpunkt die gleiche, eine in wesentlichen Teilen ähnliche oder eine andere Abhandlung als Dissertation an einer anderen Hochschule eingereicht habe.